Hamilton Standard
DIVISION OF UNITED AIRCRAFT CORPORATION

LINEAR AND ANGULAR VIBRATION MEASUREMENT OF V/STOL AIRCRAFT

VOLUME I OF II

APRIL 1970

Prepared by: D. Isakson
Program Manager

Approved by: L. Manchi
Department Manager

Approved by: L. Sher
Technical Monitor
NASA/ERC

FINAL TECHNICAL REPORT
Contract No. NAS 12-2028

ELECTRONICS RESEARCH CENTER
NATIONAL AERONAUTICS AND SPACE ADMINISTRATION

TABLE OF CONTENTS

VOLUME I

VOLUME II

1.0 INTRODUCTION

1.1 Objective

The purpose of this program was to design, fabricate and demonstrate a system capable of measuring the linear and angular vibration environments in V/STOL aircraft. A measured environment was then processed through an error model of a strapdown inertial guidance system and the resulting system errors tabulated. The following sections present the results of this effort.

1.2 General Description

The vibration measurement system consists of four individual packages (see Figures 1.2-1 through 1.2-3): a sensor block, electronics unit, flight tape recorder, and a ground discriminator. Figure 1.2-4 presents a block diagram for the flight system. The mechanical details of the block and electronics unit are shown in Figures 1.2-5 and 1.2-6. The schematic diagram is shown in Figure 1.2-7.

The sensor block (approximately 6 x 6 x 11 inches) contains 12 inertial quality angular rate and linear acceleration sensors, heaters and thermostats for thermal control, and indicator lights to show when warmup is achieved. Three Systron Donner pendulous accelerometers, one Endevco crystal accelerometer triad, three Honeywell rate gyros, and three General Electric angular differentiating-integrating accelerometers comprise the sensors. The Systron Donners and rate gyros are grouped as the low frequency sensors, while the Endevcos and ADA's are grouped as high frequency sensors.

The sensor block is mounted in an environment. The sensor outputs are fed to the electronics unit. There they are conditioned, and the six low frequency sensors are multiplexed. This multiplex output is fed to one channel of the flight recorder. The six high frequency sensor outputs are multiplexed and fed to a second channel of the flight recorder. When playback is required, one channel of the tape is played through the discriminator allowing the six sensor outputs (high or low) to be observed. The tape is then rewound and the other channel played through the discriminator to obtain the second set of sensor outputs.

1.3 Summary

The Vibration Monitor Program had three main objectives, all of which were successfully attained. These were:

1. Design and fabricate the sensor package and associated electronics.

2. Measure the vibration characteristics of a helicopter.

3. Predict the performance of a strapdown inertial system operating in such an environment.

The vibration monitor, after design, build, and checkout was used to measure vibrations on several different flights. The flight tapes were reduced at HSSC with oscillograph plots delivered to ERC. Two flight conditions were selected for generation of power spectral density plots. These were at flight idle and in forward flight; the latter was then used in the prediction of strapdown IMU performance.

Table 1.3-1 summarizes the random vibration characteristics experienced during the forward flight conditions, while Table 1.3-2 presents the resulting dynamic errors which would result for a strapdown inertial system operating in this environment. These results were based on the HSSC LM/ASA strapdown system mated with a 50 Hz computer. The performance shown in Table 1.3-2 could easily be improved by compensating in the computer for the major error sources.

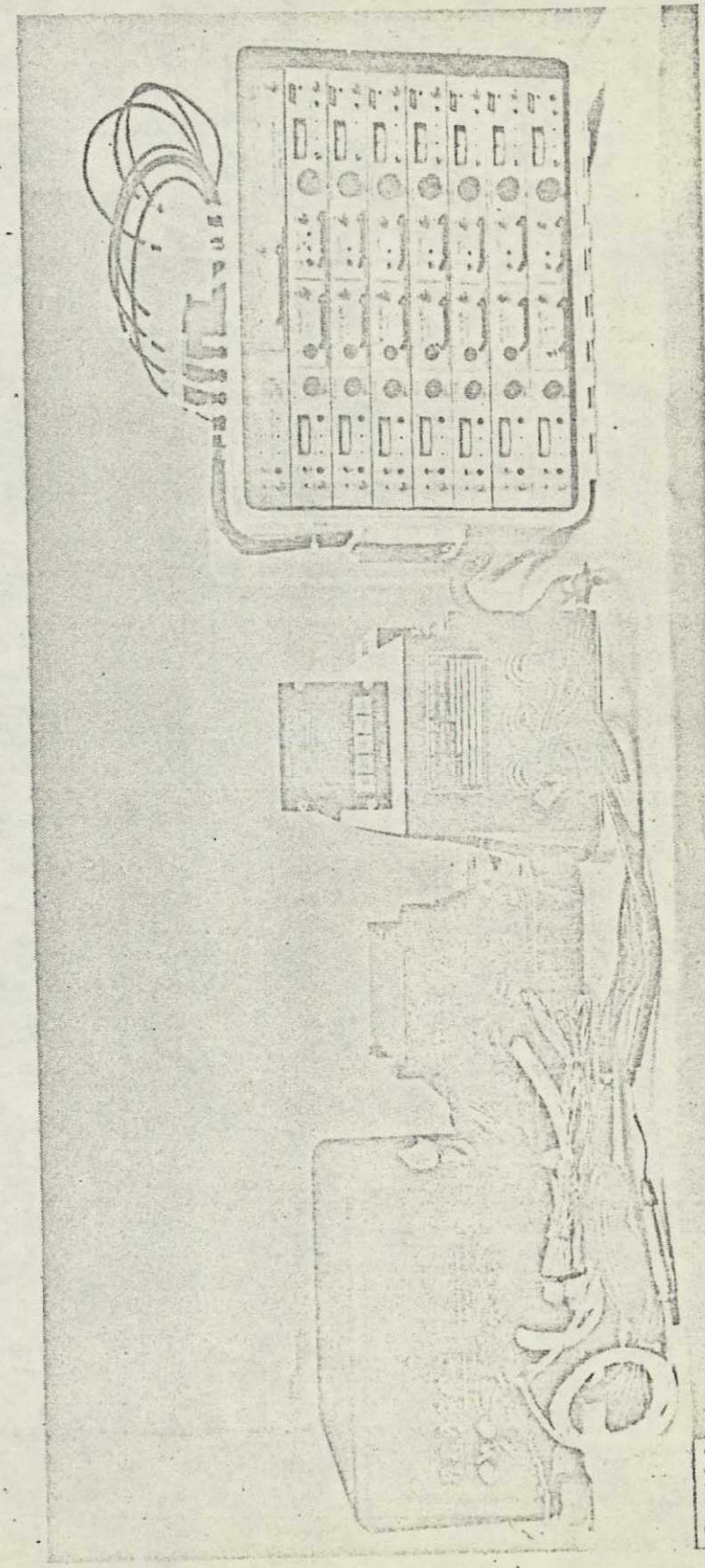

FIGURE 1.2-1.

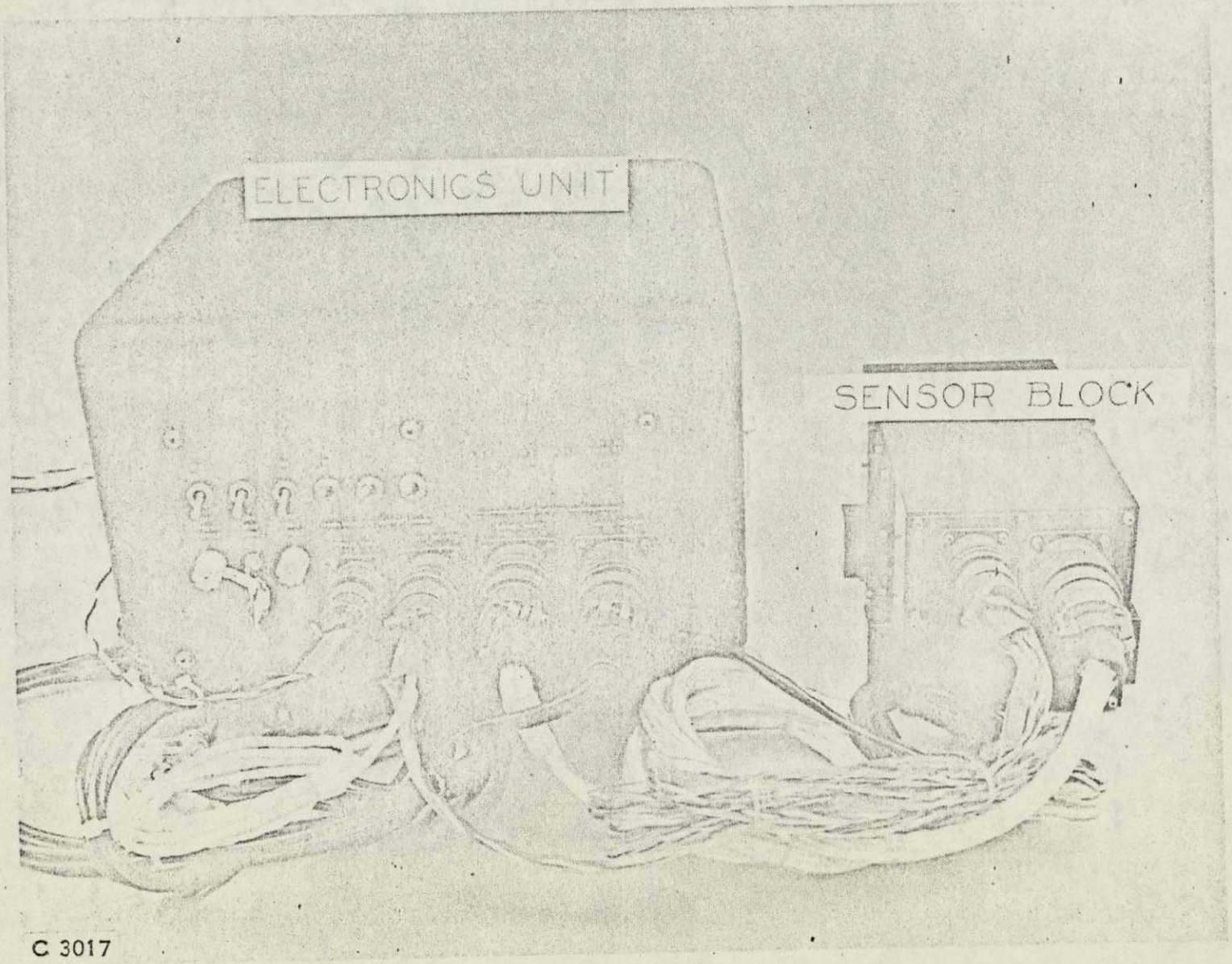

FIGURE 1.2–2.

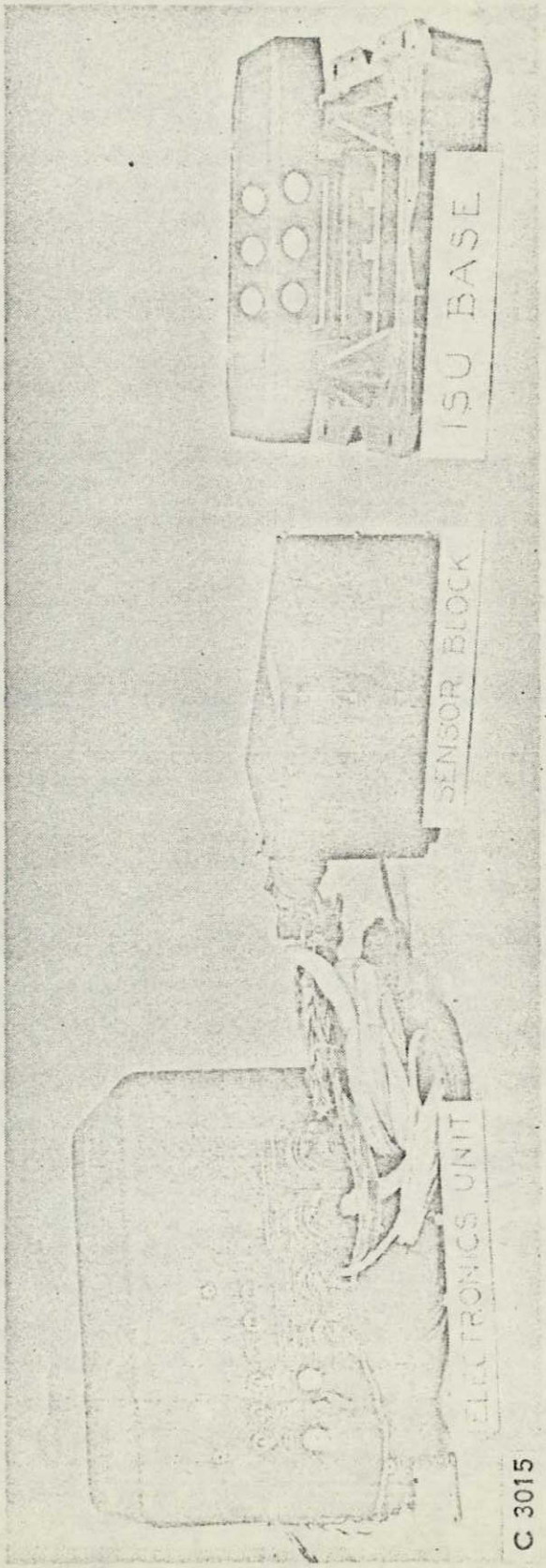

FIGURE 1.2–3.

Hamilton Standard
DIVISION OF UNITED AIRCRAFT CORPORATION
UA®

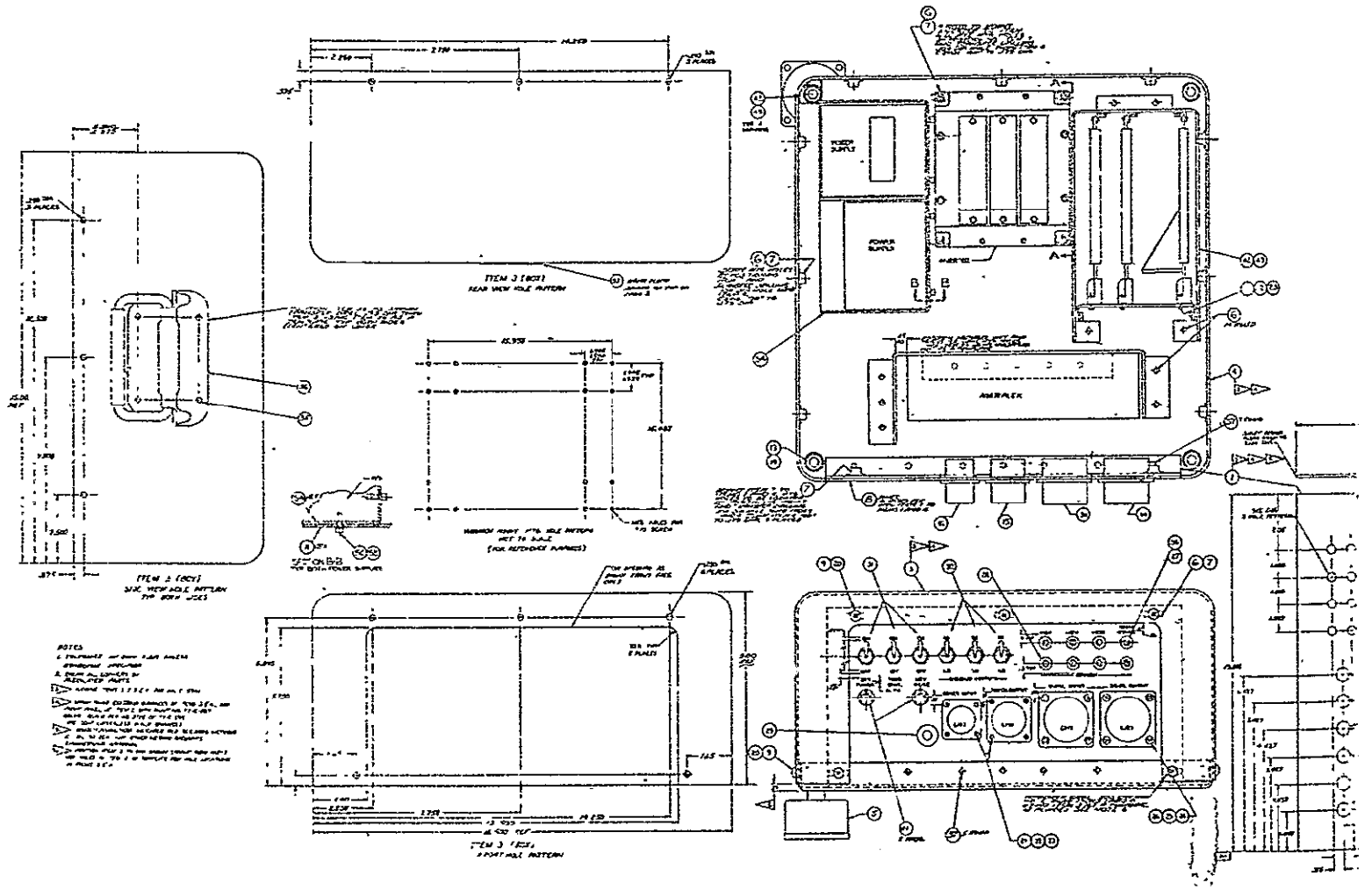

FOLDOUT FRAME

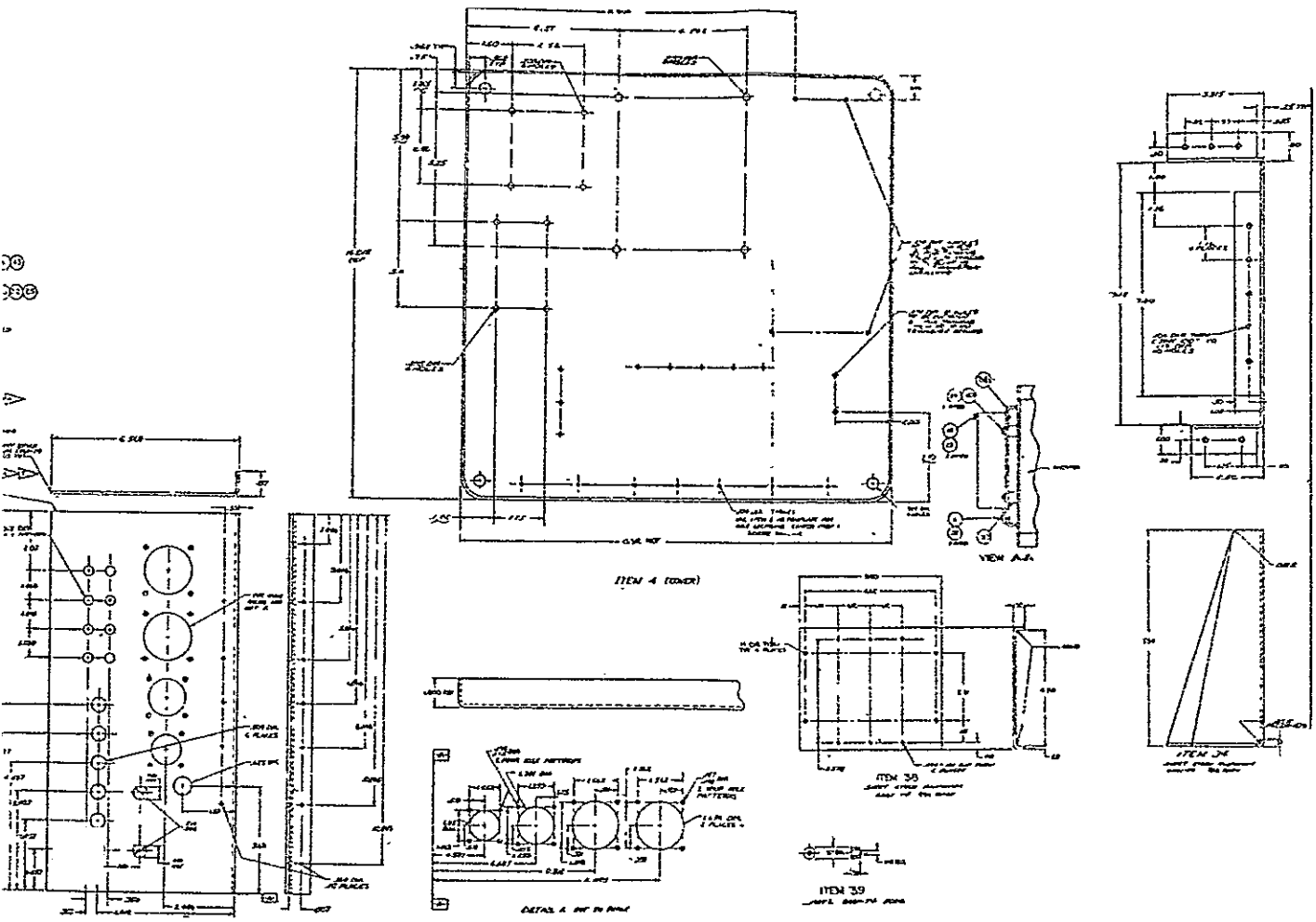

PHOTOGRAPHIC PAGE SCANNER NOT FILMED

FOLDOUT FRAME 2

Figure 1.2-6. V/STOL Electronics Unit

Hamilton Standard
DIVISION OF UNITED AIRCRAFT CORPORATION

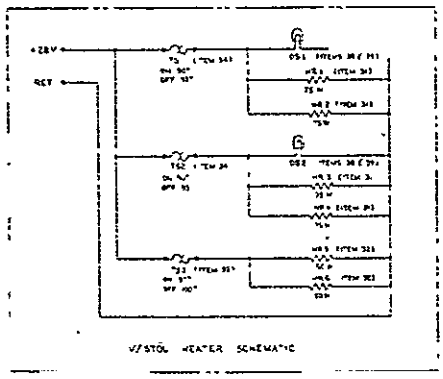

V/STOL HEATER SCHEMATIC

FOLDOUT FRAME

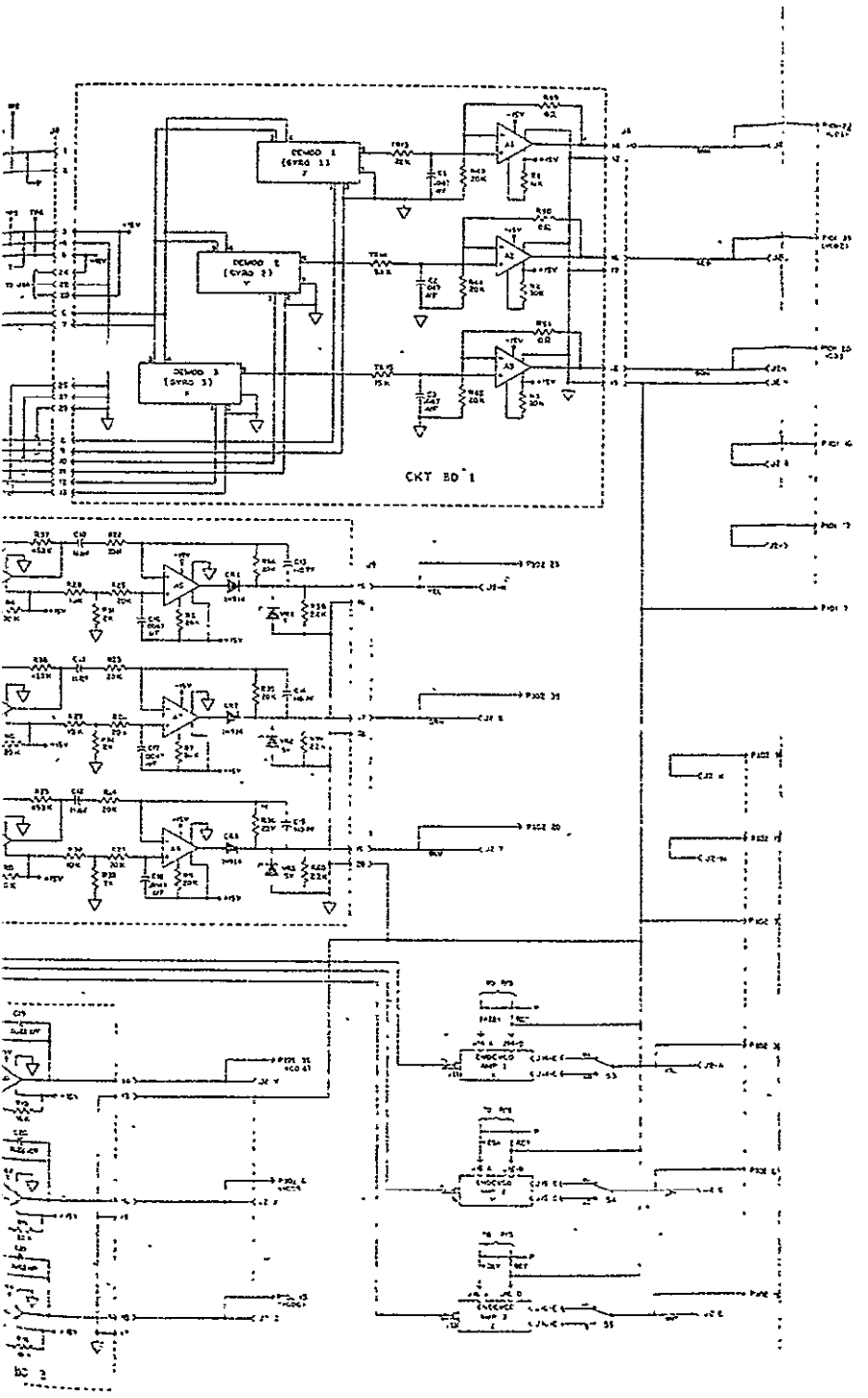

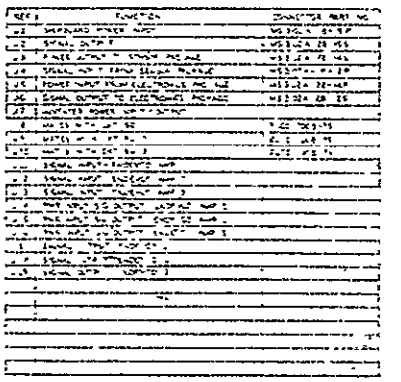

Figure 1.2-7. V/STOL Electronics Schematic

FOLDOUT FRAME 2

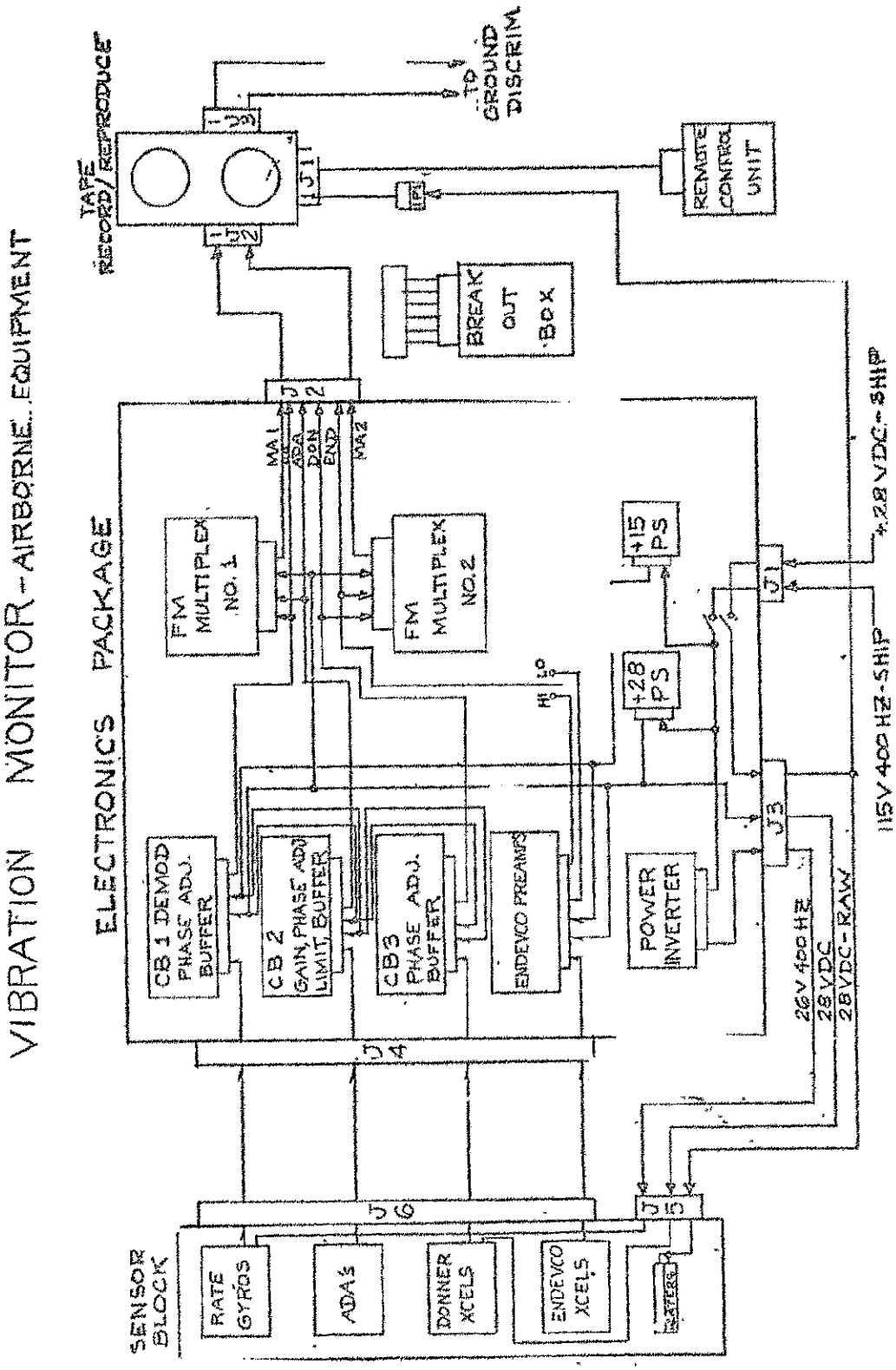
VIBRATION MONITOR - AIRBORNE EQUIPMENT
ELECTRONICS PACKAGE
TAPE RECORD/REPRODUCE
TO GROUND DISCRIM
REMOTE CONTROL UNIT
BREAK OUT BOX
J11
J1
J2
J3
J4
J5
J6
MA1
ADA
DON
END
MA2
FM MULTIPLEX NO. 1
FM MULTIPLEX NO. 2
+15 PS
+28 PS
HI
LO
CB 1 DEMOD PHASE ADJ. BUFFER
CB 2 GAIN PHASE ADJ LIMIT BUFFER
CB 3 PHASE ADJ. BUFFER
ENDEVCO PREAMPS
POWER INVERTER
+28 VDC - SHIP
115V 400 HZ - SHIP
26V 400 HZ
28VDC
28VDC - RAW
SENSOR BLOCK
RATE GYROS
ADAS
DONNER XCELS
ENDEVCO XCELS
HEATERS

Figure 1.2-4

TABLE 1.3-1

Summary of Vibration Characteristics

Channel	RMS Vibration Level	Significant Frequencies - Hz
X Angular	1.04 deg/sec	11, 16, 28
Y Angular	0.95 deg/sec	12, 27
Z Angular	0.52 deg/sec	15
X Linear	0.14 g	15, 28, 56, 94
Y Linear	0.13 g	13, 27, 100
Z Linear	0.26 g	13, 28, 50

TABLE 1.3-2

Summary of Strapdown IMU Dynamic Errors

	Range of Resulting Error	
Channel	Angular	Linear
X	0.11 to -0.19 deg/hr	-8.5 to -9.4 μg
Y	0.28 to -0.02 deg/hr	-4.2 to -4.9 μg
Z	0.15 to 0.00 deg/hr	4.1 to 1.6 μg

2.0 SYSTEM TEST

Each unit of the system (block, electronics, tape recorder) was subjected to environmental tests to qualify for flight. Also, calibrations before and after flight tests were made to determine the characteristics required for data analysis. This volume outlines the tests and summarizes the results. Detailed test results are presented in Volume II. The test equipment is shown in Figures 2.1-2.4.

Environmental Testing

The vibration environments applied to each axes of each unit were specified by MIL-STD-810B, in particular, Method 514, Paragraph 4.1, Proc. I, Part 1, Resonance Search and Method 514, Paragraph 4.2, Proc. II, Part 3, Random. No failures or malfunctions occurred during these tests. Temperature-Altitude tests were also run on the sensor block and electronics unit per MIL-STD-810B, Method 500, Procedure II.

2.2 System Calibration

The system was calibrated, both before and after flight test, by applying a known input at a discrete frequency along or about each axis of the sensor block and observing the output of the sensor of interest. The gain and phase characteristics of each of the twelve sensors were thus obtained. Tables 2.2-1 and 2.2-2 summarize the scale factor determinations for the pre and post flight calibrations. The frequency response curves can be found in Volume II.

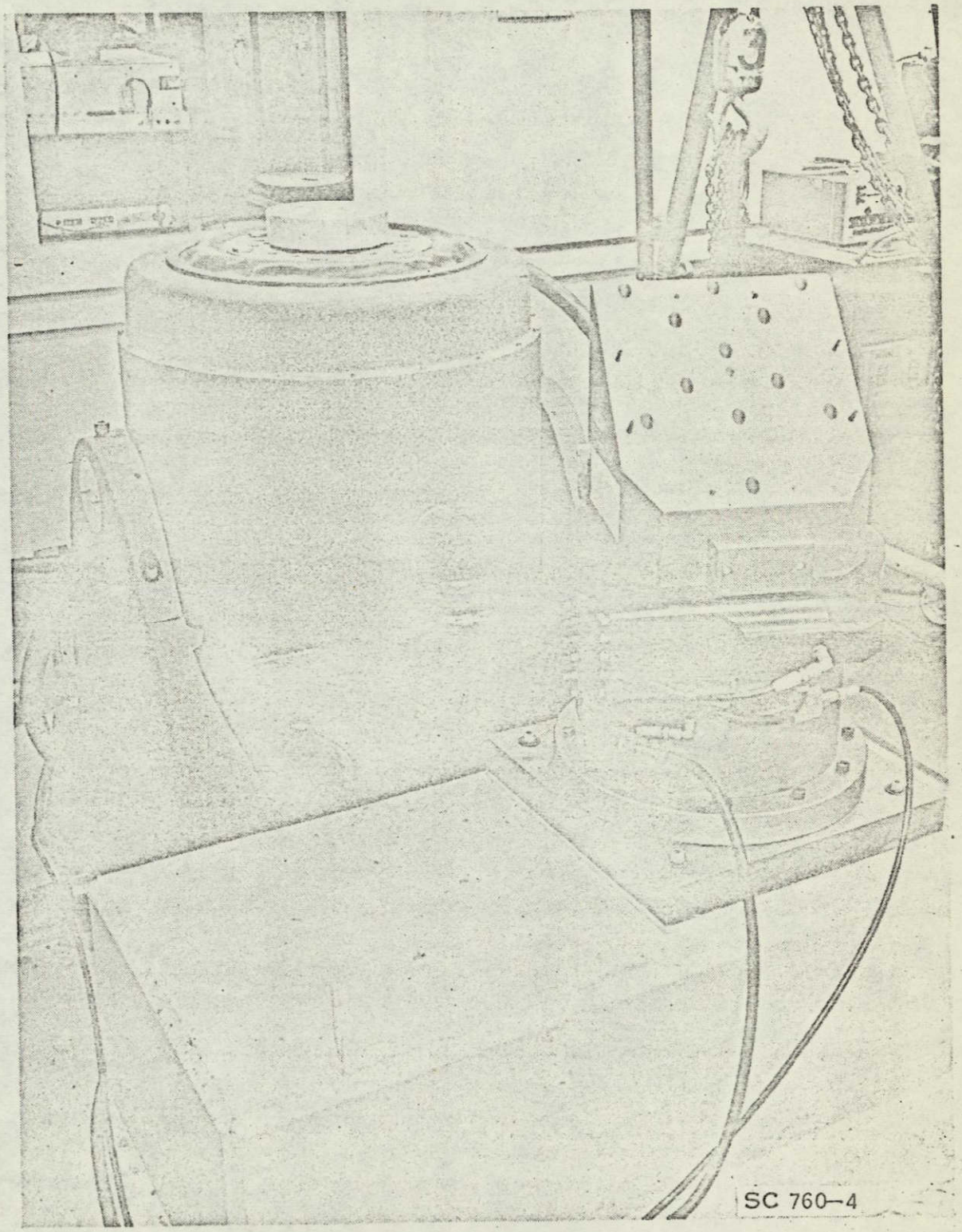

FIGURE 2.1. VERTICAL SHAKER

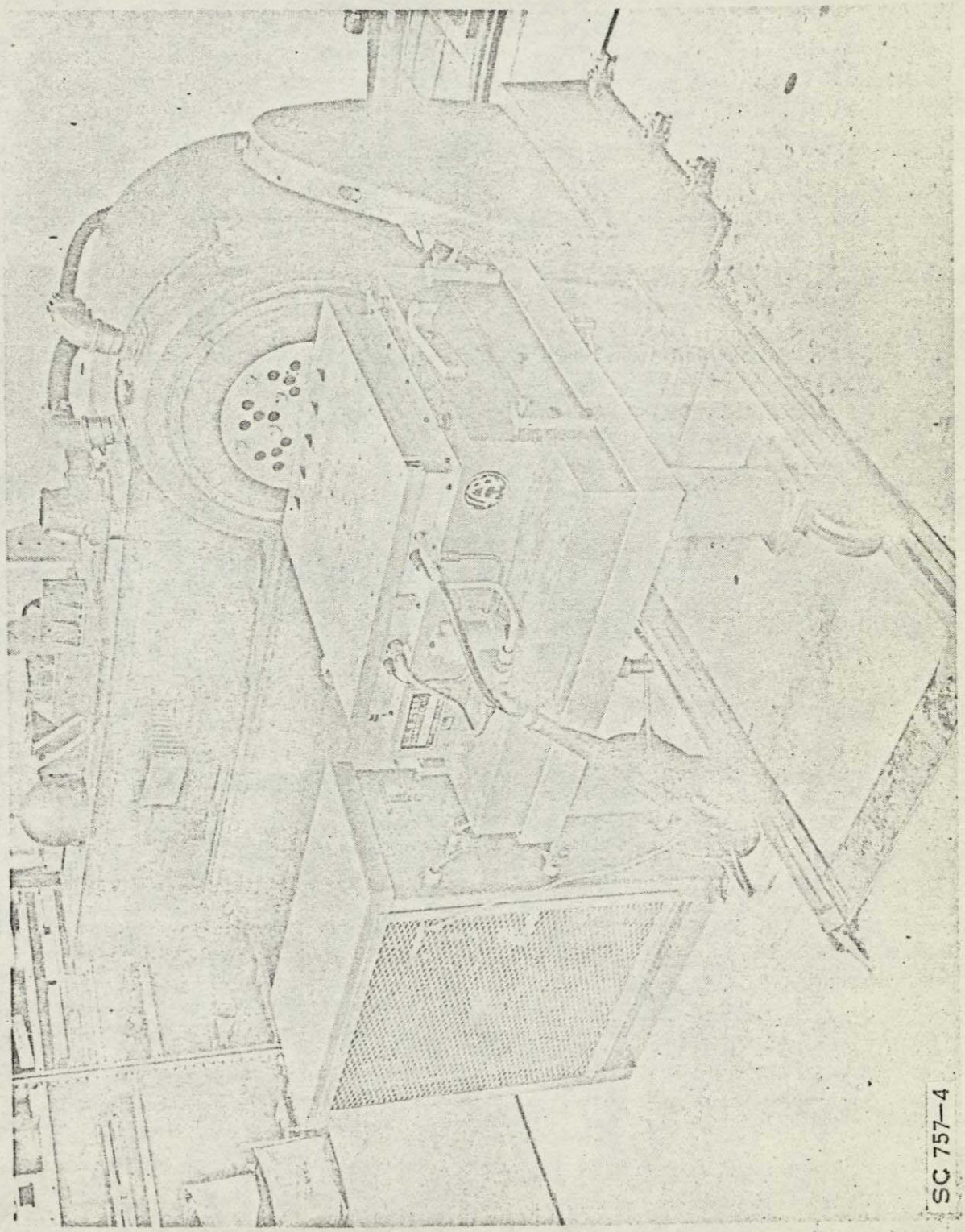

FIGURE 2.2. SLIP TABLE

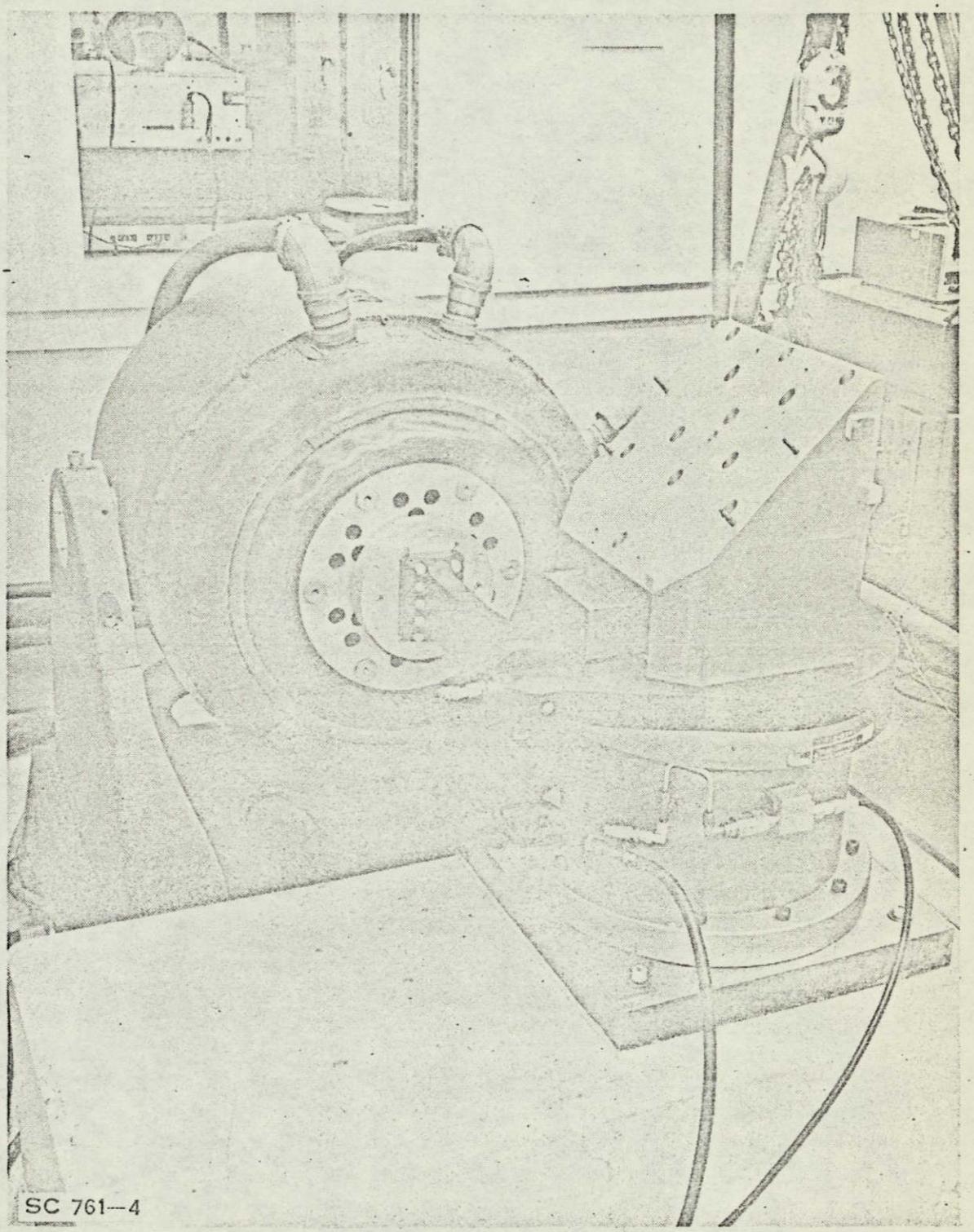

FIGURE 2.3. TEAM TABLE

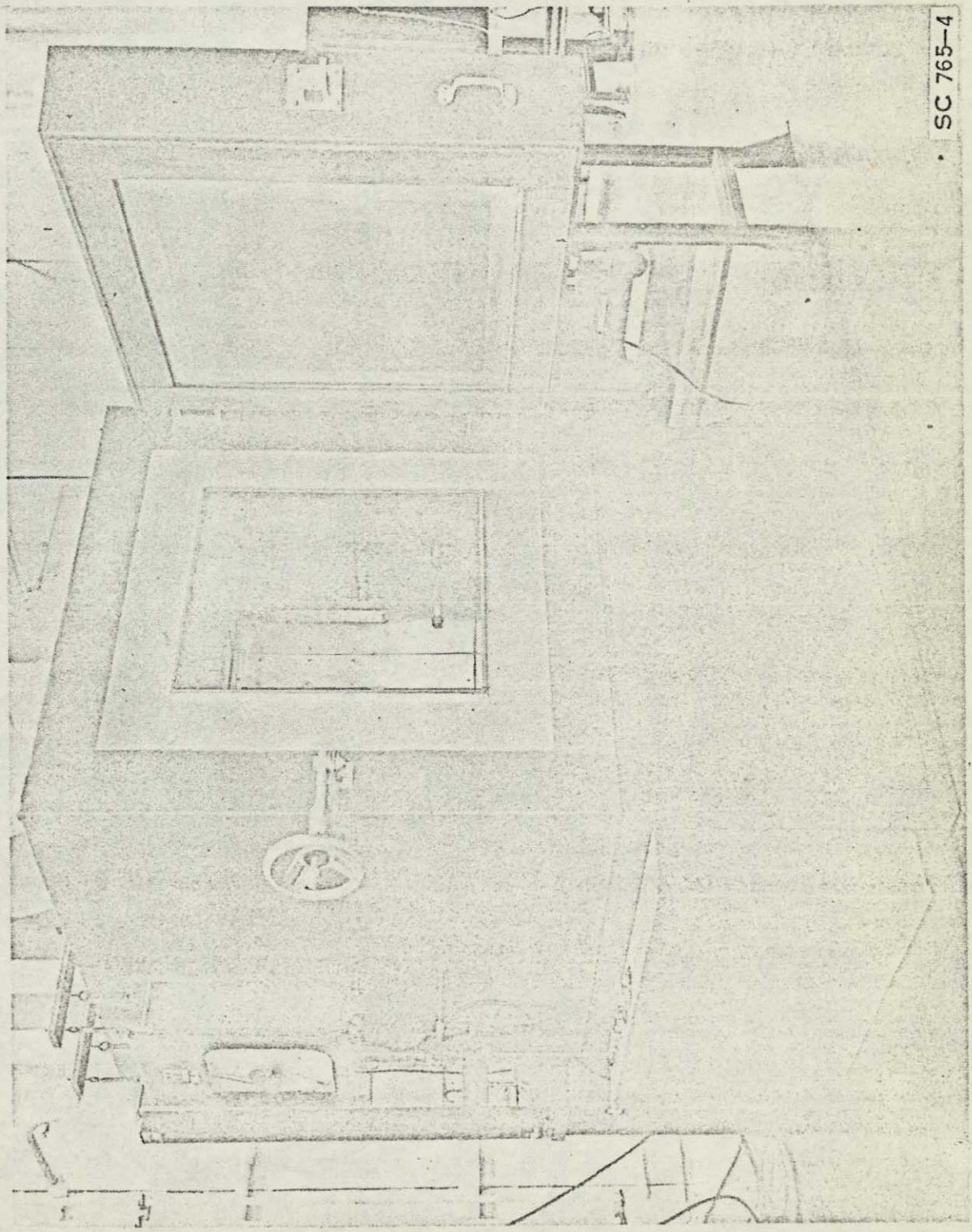

FIGURE 2.4. TEMPERATURE/ALTITUDE CHAMBER

TABLE 2.2-1

Pre-Flight Scale Factor Summary

	1st	2nd	Average
X Donner	1.09 VRMS/g	1.10 VRMS/g	1.10 VRMS/g
Y Donner	1.06 VRMS/g	0.98 VRMS/g	1.02 VRMS/g
Z Donner	1.21 VRMS/g		1.21 VRMS/g
X Endevco	2.07 VRMS/g	2.08 VRMS/g	2.08 VRMS/g
Y Endevco	2.72 VRMS/g	2.40 VRMS/g	2.56 VRMS/g
Z Endevco	2.39 VRMS/g		2.39 VRMS/g
X Gyro	0.19 VRMS/°/sec	0.19 VRMS/°/sec	0.19 VRMS/°/sec
Y Gyro	0.20 VRMS	0.17 VRMS	0.18 VRMS
Z Gyro	0.19 VRMS/°/sec		0.19 VRMS/°/sec
X ADA		0.73 VRMS/°/sec	0.73 VRMS/°/sec
Y ADA	0.89 VRMS/°/sec	0.80 VRMS/°/sec	0.84 VRMS/°/sec
Z ADA	0.80 VRMS/°/sec		0.80 VRMS/°/sec

TABLE 2.2-2

Post-Flight Calibration (10/13-14/69)

AXIS	GYRO	DONNER
X	0.25 V rms/°/sec, 0-Pk(1)	0.97 V rms/g, 0-Pk(3)
Y	0.18 V rms/°/sec, 0-Pk	0.74 V rms/g, 0-Pk
Z	0.19 V rms/°/sec, 0-Pk	1.05 V rms/g, 0-Pk

AXIS	ADA's		ENDEVCO
X	0.75 V rms/°/sec, 0-Pk(1)	0.46 V rms/°/sec, 0-Pk(2)	1.76 V rms/g, 0-Pk(3)
Y	0.89 V rms/°/sec, 0-Pk	0.55 V rms/°/sec, 0-Pk	1.99 V rms/g, 0-Pk
Z	0.84 V rms/°/sec, 0-Pk	0.53 V rms/°/sec, 0-Pk	2.23 V rms/g, 0-Pk

(1) Input = 5°/sec, 0-Pk @ 10 Hz

(2) Input = 1.5°/sec, 0-Pk @ 100 Hz

(3) Input = 0.5 g, 0-Pk @ 10 Hz

3.0 FLIGHT TEST

3.1 Description

The Vibration Measurement System was shipped to Langley Field, Virginia in July of 1969. From August 4 through August 8, 1969, a series of flights were made. The system was mounted on the YHC1 (CH 46) helicopter. The block was in the ISU fixture (Figure 1.2-1) so that its axes were Z down, X forward, and Y lateral. Three flights were made; the tape numbers, footage, flight phase, and comments are given in Table 3.1-1.

3.2 Test Results

The data were played back through a strip chart recorder for determining which sequences would be analyzed. The following sections will describe the analysis in detail. Figure 3.2-1 gives an example of what the playback of the raw data looked like. Table 3.2-1 summarizes the maximum environments seen during the tests.

Table 3.1-1
FLIGHT EVENTS

Flight No. 1 8/6/69

Tape No. 1	Tape Footage Start	Event	Stop	Notes
On Ground Power	0		30	
Engine starting to G. I.	30		200	
Ground idle to flight idle	200		270	
Boost/SAS check				
T.O. to Hover(SAS on)	400			
Lift off		460	590	
Trans to FWD, 60KN	590			
Approach to Hover			750	
T.O. to hover.(SAS off)	750		(800)	not sure if turned off
Trans to FWD	(800)		1010	
Square Pattern	1010			
(SAS on)			1130	
Square Pattern(SAS off)	1130		1230	
Level Flight(SAS on)	1240	1280- 15 KN		
		1330- 40		
		1360- 50		
		1390- 60		
		1400- 70		
		1430- 80		
		1500- 90		
		1550-100		
		1580-110		
		1610-115		
Deceleration to level flight	1710		1790	
Ascending (climb)	1790		1830	800 ft/min.
Descending	1830			
		1900 45 KN		500 ft/min
		1960		1000
			2000	(end)

Flight No. 2 8/7/69

On Ground Power	0		150
At T.O. RPM	150		
Ground Taxi		240	
Lift Off		320	
Fwd flight			430
Variables Stab. Syst.	430		
Checkout: Pitch		600	
Roll		620	
Yaw		650	
Collective		690	
Roll trim		750	
Plugboard Racetrack		820	

Table 3.1-1 (Cont.)

	Start	Event	Stop	Notes
Pattern			1170	
Computer Stab. System				
Engage & Hover	1170			
FWD Flight		1260		
Hover		1720		
Off			1740	
Centered Controls				
FWD Flight	1750			
Hover		2270		
Off			2280	
Tape No. 2				
Pulses in Control Actuators				
Longitudinal	0			
Lateral Pulses		30		75 knots
Yaw Pulses		60		75 knots
Longitudinal		170		45 knots
Lateral		200		"
Yaw		230		"
Computer Engaged-Level Flt.		290		
Left turn		450		15 KN
		690		30
		1130		60
Off			1250	
Engage/Desengage Transients				
Left lateral slip	1250			
Diseng		1290		
Right lateral		1340		
Dis		1400		
Engage		1480		
Pitching		1510		
Dis		1530		
Engage		1570		
Yawing		1590		
Dis		1610		
Yaw Kicks		1650		
Commence Descend		1660		
Touchdown		1690		
"		1720		
"		1740		
Touchdown & ground taxi		1790		
Stationary		1830		
Off			1860	

Table 3.1-1 (Cont.)

Flight No. 3 8/8/69

Tape No. 1	Start	Event	Stop	Notes
On Ground Pwr	0		150	
Ground Taxi	150		230	
Engage VSS	230			
Yaw Check		300		
Roll "		360		
FWD Flight		410		Race Track PTN
Off			730	
Record On	730			
Comp SS Engage		750		
FWD Flight				Race Track PTN
Decel		----------		
Hover				
Off		----------	1100	
Control Act Pulses				
Record On	1100			80 knots
Longitud		1130		"
Later		1170		"
Collect		1230		"
Yaw		1260		"
Off			1290	
Computer S.S.				
Level Flight	1290			75 KN
Left Bank 10°		1860		
20°		2070		
30°		2210		
Off			2260	

Tape No. 2				
Computer S.S. on	0			
Contr. Pulses				
Longitud		40		
Lateral		70		
Yaw		100		
Collective		160		
Left Bank 30°		210		45 knots
Right Bank 30°		270		
Descending		470		
" 800 F/M		500		
" 1100 "		550		
Off			660	
On	660			
Comp. S.S. Eng.		680		

Table 3.1-1 (Cont.)

Tape No. 2	Start	Event	Stop	Notes
Lateral Slip				
Diseng		770		
Yaw Manuever				
Diseng		860		
Snap into Heading Hold		1010		
Head Hold Off		1110		
Off			1350	
Landing Seq	1360			
Touchdown		1380		
"		1420		
"		1460		
Ground Taxi		1500		
Stationary & Power Down		1650		
Rotors Decel		1700		Large Oscill
Off			1760	

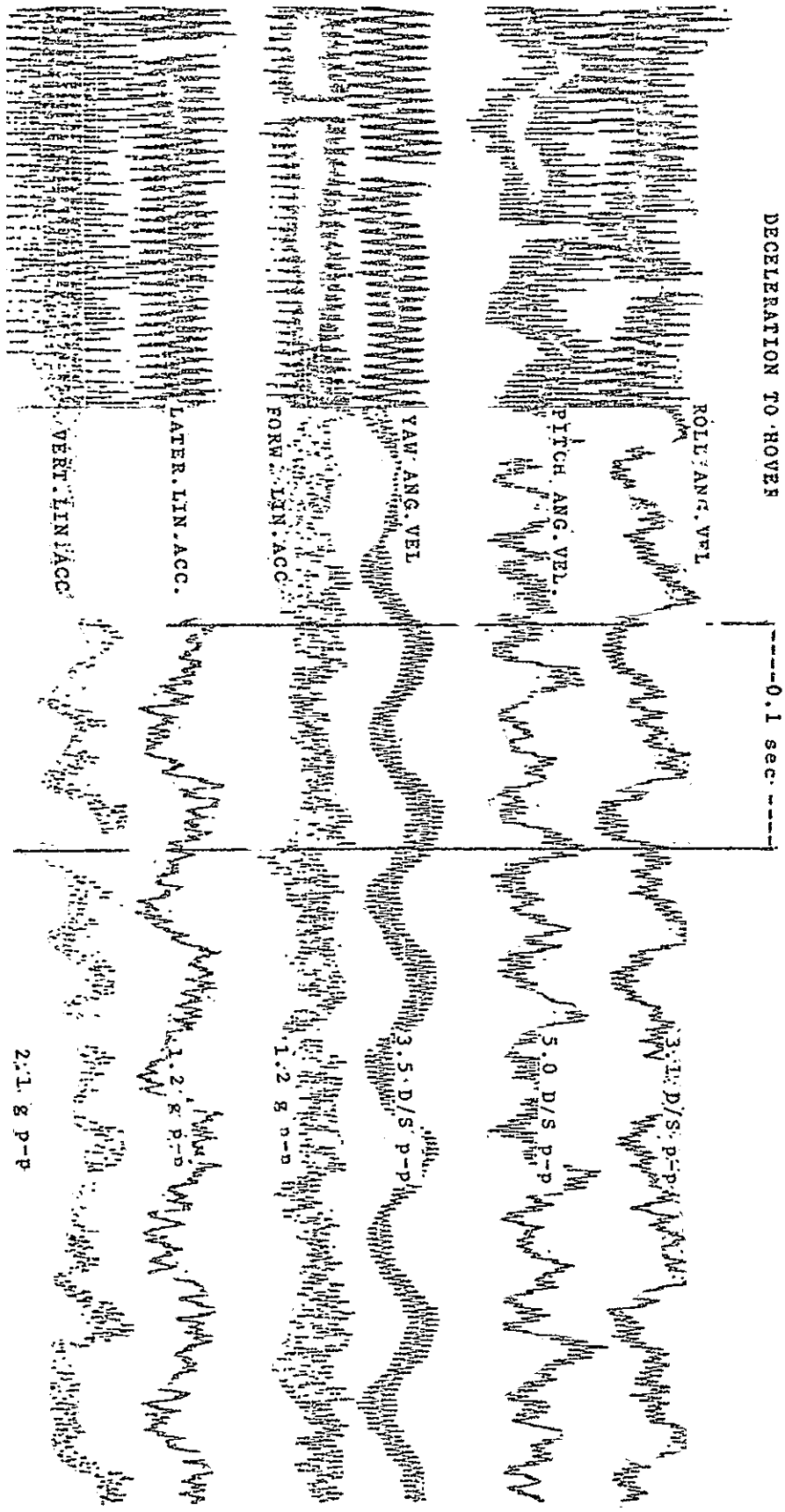
COMPUTER VSS
DECELERATION TO HOVER
ROLL ANG. VEL
PITCH ANG. VEL.
YAW ANG. VEL
FORW. LIN. ACC.
LATER. LIN. ACC.
VERT. LIN. ACC.
0.1 sec
3.1 D/S p-p
5.0 D/S p-p
3.5 D/S p-p
1.2 g n-n
1.2 g p-p
2.1 g p-p

Figure 3.2-1

TABLE 3.2-1

MAXIMUM INDICATED ENVIRONMENT-LOW FREQUENCY SENSORS

EVENT	Donner Linear Accelerometer			Rate Gyros		
	X Forward g's p-p	Y Lateral g's p-p	Z Vertical g's p-p	X Roll D/Sp-p	Y Pitch D/S p-p	Z Yaw D/S p-p
On Ground, Flight RPM, Boost System Checks	0.45	0.39	1.1	1.9	2.1	3.8
On Ground, Taxiing	1.3	1.5	2.0	7.5	10.6	7.5
Lift-Off To Hover	0.5	0.45	1.6	5.6	10.6	9.4
Transition to Forward Flight	0.5	0.45	1.6	22.6	15.	19.
Forward Flight with Manuevers deceleration to Hover	0.6	1.9	1.8	30.	28.	17.
Forward Flight, Manuevering, Control System Disengaging and Command Impulses	1.6	1.9	2.3	35.7	21.	26.
Touchdown	1.6	1.9	2.0	22.6	17.	11.3

TABLE 3.2-1 (Continued)
MAXIMUM INDICATED ENVIRONMENT - HIGH FREQUENCY SENSORS

EVENT	Endevco Accelerometers			ADA		
	X Forward g's p-p	Y Lateral g's p-p	Z Vertical g's p-p	X Roll D/S p-p	Y Pitch D/S p-p	Z Yaw D/S p-p
On Ground, Flight RPM, Boost System Checks	1.4	74	0.9	2.4	3.1	2.2
On Ground, Taxiing	1.4	0.9	1.5	4.9	5.7	1.8
Lift-Off to Hover	1.7	1.5	1.8	8.3	6.6	3.5
Transition to Forward Flight	1.4	1.5	1.9	5.8	5.3	3.5
Forward Flight, with Manuevers, and deceleration to Hover	1.7	1.3	1.6	6.3	7.0	3.5
orward Flight, Manuevering, Control System Disengaging and Command Impulses	1.5	1.2	1.9	9.2	6.1	3.5
Touchdown	1.4	1.8	2.2	17.8	7.9	3.9

4.0 DATA REDUCTION

4.1 Analog Data Reduction Procedure

The flight test data were reduced at HSSC by first generating individual analog tape loops from the flight tapes and then processing these to spectral density plots. Table 4.1-1 presents a summary of the 12 tape loops which were generated from flights 1 and 3, plus two additional tape loops taken while the system was operating in a serene HSSC laboratory environment. It was necessary to generate this number of tapes, since HSSC's record/playback equipment could maintain time synchronization between channels on only four of the seven channels.

The tape loop data were reduced using Spectral Dynamics equipment into the form of high and low frequency power spectral density plots (PSD's) and also high and low frequency Co and Quad spectral densities. The data analysis was such that 10% (200 DOF) statistical accuracy was always maintained from 0.75 to 2000 Hz; and that at most, 25% resolution (bandwidth/center frequency) was maintained from 6 to 2000 Hz.

Figure 4.1-1 shows the basic hardware block diagram for the data reduction equipment.

The actual hardware settings which were used for the analysis are presented in the following four tables:

Table 4.1-2	High Frequency PSD Settings
Table 4.1-3	Low Frequency PSD Settings
Table 4.1-4	High Frequency Co and Quad Settings
Table 4.1-5	Low Frequency Co and Quad Settings

TABLE 4.1-1

HSSC/ERC V/STOL TAPE LOOP DATA

Flight No.	Tape No.	Flight Tape Footage (Ft.)	HSSC Loop #	Type Sensors	HSSC Tape Channels/Sensor 1	3	5	7	HSSC Tape Length (Ft.)	Event
1	1	270-400	1	Low Freq.	Gx	Gy	Gz	Ax	30	Flt. Idle
1	1	"	2	Low Freq.	Ay	Az	Cx	Gy	"	"
1	1	"	3	Low Freq.	Gz	Ay	Az	Ax	"	"
1	1	"	4	High Freq.	Gx	Gy	Gz	Ax	"	"
1	1	"	5	High Freq.	Ay	Az	Gx	Gy	"	"
1	1	"	6	High Freq.	Gz	Ay	Az	Ax	"	"
3	1	880-1080	7	Low Freq.	Gx	Gy	Cz	Ax	46	Fwd.Flt./Desc./Hover
3	1	"	8	Low Freq.	Ay	Az	Gx	Gy	"	"
3	1	"	9	Low Freq.	Gz	Ay	Az	Ax	"	"
3	1	"	10	High Freq.	Gx	Gy	Gz	Ax	"	"
3	1	"	11	High Freq.	Gz	Ay	Az	Ax	"	"
3	1	"	12	High Freq.	Ay	Az	Gx	Gy	"	"
			13	Low Freq.	1 (Gz)	2(Gy)	3(Gx)	4(Az)	5(Ay) 6(Ax)	40	Noise Tape
			14	High Freq.	1 (Gx)	2(Gy)	3(Gz)	4(Ax)	5(Ay) 6(Az)	40	Noise Tape

HARDWARE IMPLEMENTATION FOR BOTH PSDs AND CO-QUAD SPECTRUMS

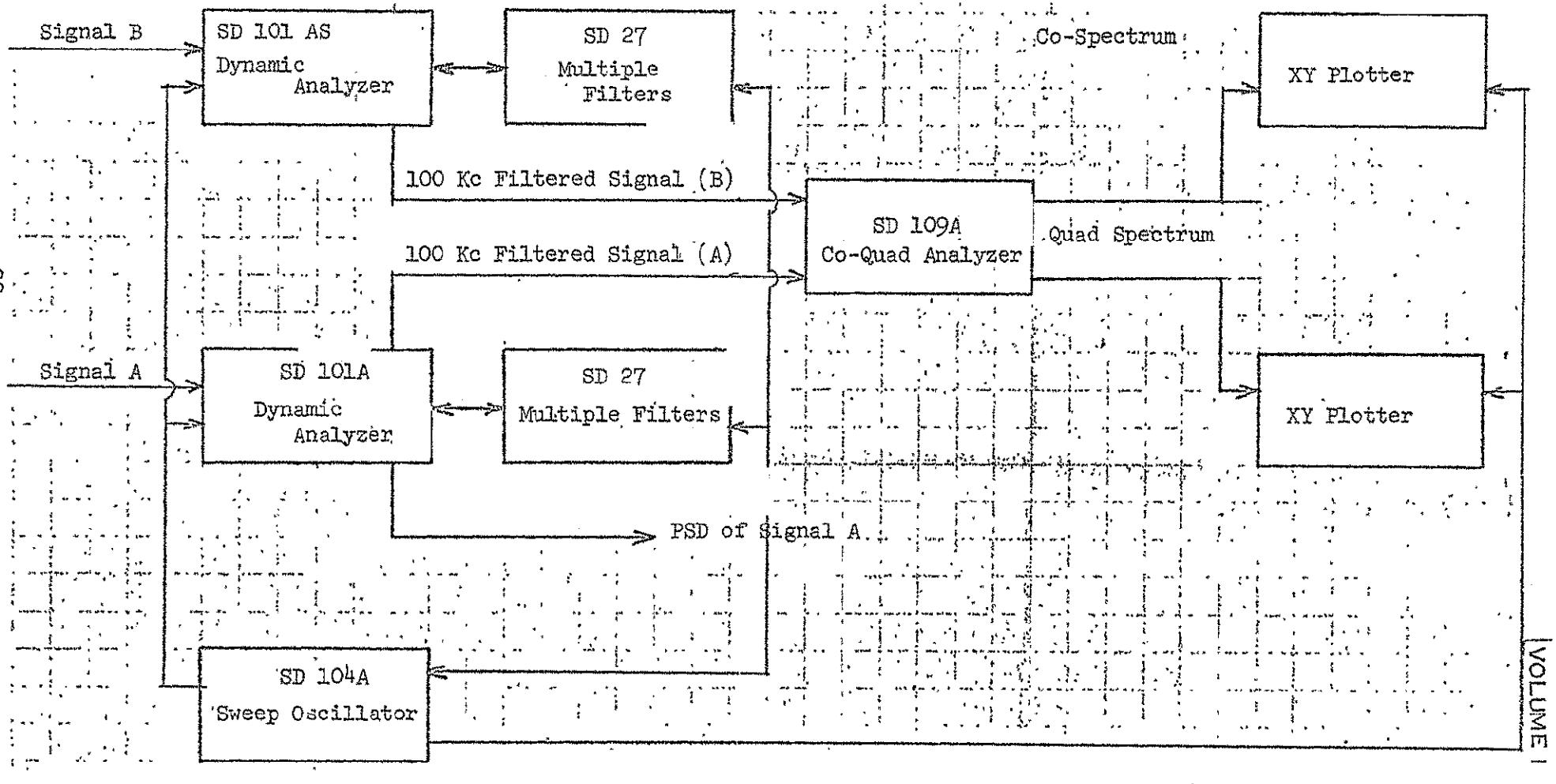

Figure 4.1-1

TABLE 4.1-2

HIGH FREQUENCY PSD SPECTRAL DYNAMICS HARDWARE SETTINGS (9-8-69)

Filter #	Filter Cal.	Bandwidth (Hz)	Averaging Time (sec.)	Sweep Rate (Hz/sec.)	Frequency Range (Hz)	Sweep Time (sec.)
1	7.00	5	10.0 (400 uf - J3)	.125 (SD104A)	10-40	240
2	4.96	10	5.0	.50	40-80	80
3	3.52	20	2.5	2.0	80-200	60
4	2.21	50	1.0	6.25	200- 500	32
5	1.57	100	.5	25.0	500-2000	64
					Total	476

Range Setting	=	1.0 V rms	SD101A
Multiplier	=	1.0	SD101A
Multiplier (A)	=	1.0	SD104A
Multiplier (B)	=	1.0	SD104A

TABLE 4.1-2 cont'd)

HIGH FREQUENCY PSD PLOTTER CALIBRATION

With the following Hardware Settings:

1. RANGE and MULTIPLIER in CAL position,
2. Lowest Filter (5 Hz Bandwidth),

the X-Y plotters should be set as follows:

a. For Endevco Accelerometers - Y axis = .012 $(g)^2/Hz$,

b. For ADAs - Y axis = .10 $(deg./sec.)^2/Hz$,

c. X axis setting is on 3 cycle Log/Log Paper at 10-100, 100-1000, and 10000 -- 10000 Hz decades.

TABLE 4.1-2 (cont'd)

HIGH FREQUENCY PSD X-Y PLOTTER CALIBRATION

Axis		ADA's	Endevco
X		✓.73 (V rms/°/sec.$_{pk}$)	✓ 2.07 (V rms/g_{o-pk})
Y		✓.81 "	✓ 2.46 "
Z		✓.80 "	✓2.40 "
Average	=	.78 "	2.31 "
Average	=	1.11 (V_{pk}/°/sec.$_{pk}$)	3.27 (V_{pk}/g_{pk})
With Range	=	1 V rms and Multiplier = 1 :	
F. S.	=	.90 °/sec.	.306 g
CAL. (5 Hz BW)	=	.100 (°/sec.$_{rms}$)^2/Hz	.012 (g_{rms})^2/Hz

TABLE 4.1-3

LOW FREQUENCY PSD SPECTRAL DYNAMICS HARDWARE SETTINGS

Filter #	Filter Cal.	Bandwidth (Hz)	Averaging Time (Sec.)	Sweep Rate (Hz/sec.)	Frequency Range	Sweep Time
1	7.0	1.5	33.0 (1500 uf-J3)	.0113	75-20	1711

Range Setting	1.0 Vrms	SD101A
Multiplier	1.0	
Multiplier (A)	.01	SD104A
Multiplier (B)	1	
Sweep Rate	1.12	

TABLE 4.1-3 (Cont'd)

LOW FREQUENCY PSD PLOTTER CALIBRATION

With the following hardware settings:

1. RANGE and MULTIPLIER in CAL position
2. Lowest filter (1.5 Hz Bandwidth)

the X-Y plotters should be set as follows:

a. For Donner accelerometers - Y axis = .163 $(g_{rms})^2/Hz$

b. For Honeywell gyros - Y axis = 6.15 $(°/sec._{rms})^2/Hz$

c. X axis setting is a 3-cycle Log/Log paper at .1-1; 1-10, and 10-100 Hz decades.

TABLE 4.1-3 (cont'd)

LOW FREQUENCY PSD X-Y PLOTTER CALIBRATION

Axis		Gyro	Donner
X		✓ 192 Vrms/°/sec.$_{o\text{-}pk}$	✓ 1.09 Vrms/$g_{o\text{-}pk}$
Y		✓ 165 "	✓ 1.06 "
Z		✓ .194 "	✓ 1.24 "
Average	=	.184 "	1.13 "
Average	=	.261 V_{pk}/°/sec.$_{pk}$	1.60 V_{pk}/ $g_{.pk}$
With: Range	= 1 Vrms		
Multiplier	= 1		
F.S.	=	3.83 °/sec.	.626 g
Cal. (1.5 Hz BW)	=	6.15 (°/sec.$_{rms}$)^2/Hz	.163 (g_{rms})^2 Hz

TABLE 4.1-4

HIGH FREQUENCY CO-QUAD SPECTRAL DYNAMICS HARDWARE SETTINGS

1. SD101A, SD101AS, SD104A, and SD27

Filter #	Filter Cal.	Bandwidth (Hz)	Sweep Rate (Hz/sec.)	Frequency Range (Hz)	Sweep Time (sec.)
1	7.00	5	.125	10 - 40	240
2	4.96	10	.50	40 - 80	80
3	3.52	20	2.0	80 - 200	60
4	2.21	50	6.25	200 - 500	48
5	1.57	100	25.0	500 - 2000	60
				Total	488

Range Setting = 1 V rms } SD101A, SD101AS
Multiplier = 1
Multiplier (A) = 1.0 } SD104A
Multiplier (B) = 1.0

2. SD 109A

Channel A	Channel B
Input = 1/0 V rms/db	Input = 1/0 V rms/db.
Averaging Time (sec.) = 10.0	Averaging Time (sec.) = 10.0

TABLE 4.1-4 (cont'd)

HIGH FREQUENCY CO-QUAD PLOTTER CALIBRATION

With the Following Hardware Settings:

1. SD101A, SD101AS RANGE and MULTIPLIER in CAL position,
2. Filtered 100 K Hz signals to SD109A,
3. Lowest filter bandwidth on each (5 Hz),
4. Both SD109A inputs at 1/0 V rms/db,

the X-Y Plotter Calibration Point will be:

a. For Endevco-Endevco accelerometer combination Y axis = .0094 $(g\ rms)^2/Hz$.

b. For ADA-ADA Combination Y axis = .081 $(deg./sec._{rms})^2/Hz$.

c. For Endevco-ADA Combination Y axis = .028 $(g\ rms\ deg./sec._{rms})/Hz$.

d. X axis setting is on 3 cycle semilog paper at

10-100, 100-1000, and 1000-10000 Hz decades.

TABLE 4.1-4 (cont'd)

HIGH FREQUENCY CO-QUAD PLOTTER CALIBRATION

Average Scale Factors: ADA - 1.11 (V pk./°/sec. pk.)
Endevco - 3.27 (V pk./g pk.)

With RANGE on SD101A and SD101AS = 1 V rms
and Inputs to SD109A = 1/0 V rms/db on both channels.

Full Scale = .9 °/sec. for ADA
= .306 g for Endevco

CAL (5 hz BW): ADA-ADA = .081 (°/sec. rms)^2/Hz
Endevco-Endevco = .0094 (g rms)^2/Hz
ADA-Endevco = .028 (g rms °/sec. rms)/Hz

ABLE 4.1-5

LOW FREQUENCY CO-QUAD SPECTRAL DYNAMICS HARDWARE SETTINGS

1. AD101A, SD101AS and SD104

Filter #	Filter Cal.	Bandwidth (Hz)	Sweep Rate (Hz/sec.)	Frequency Range (Hz)	Sweep Time (sec.)
1	7.0	1.5	.0113	.75-20	1711

Range Setting = 1 Vrms
Multiplier = 1
} SD101A, SD101AS

Multiplier (A) = .01
Multiplier (B) = .1
Sweep Rate = 1.12
} SD104A

2. SD109A

Channel A

Input = 1/0 V rms/db.

Average Time = 10 sec. on Front Panel plus 250 uf capacitor on CO function (J3)

(Total averaging time = .33 sec.)

Channel B

Input = 1/0 V rms/db.

Average Time = 10 sec. on Front Panel plus 250 uf capacitor on Quad Function (J4)

TABLE 4.1-5(cont'd)

LOW FREQUENCY CO-QUAD PLOTTER CALIBRATION

With the following hardware settings:

1. SD101A, SD101AS RANGE and MULTIPLIER in CAL. positions,
2. Filtered 100 K Hz signals to SD109A,
3. Lowest filter bandwidth on each (1.5 Hz),
4. Both SD109A inputs at 1/0 V rms/db,

the X-Y plotter calibration point will be:

a. For Donner-Donner Accelerometer combination Y axis = .130 $(g\ rms)^2/Hz$,

b. For Honeywell-Honeywell gyro combination Y axis = 4.90 $(deg./sec._{rms})^2$ Hz,

c. For Donner-Honeywell combination axis = .797 $(g_{rms}\ deg./sec._{rms})/Hz$,

d. X axis setting is a 3-cycle semilog paper at:
.1-1, 1-10, and 10-100 Hz decades.

TABLE 4.1-5 (cont'd)

LOW FREQUENCY CO-QUAD PLOTTER CALIBRATION DERIVATION

Average Scale Factors: Honeywell - .261 ($V_{pk}/^{o}/sec._{pk}$)

Donner - 1.60 $V_{pk}/^{o}g_{pk}$)

With RANGE on SD101A and SD101AS = 1 V rms

and Inputs to SD109A = 1/0 V_{rms}/db on both channels.

Full Scale = 3.83°/sec. for Honeywell

= .626 g for Donner

CAL. (1.5 Hz BW) = Honeywell - Honeywell = 4.90 $(deg./sec._{rms})^2/Hz$

Donner-Donner = .130 $(g_{rms})^2/Hz$

Honeywell-Donner = .797 $(gr_{ms}\ deg./sec._{rms})/Hz$

4.2 Uncompensated Test Results

The individual PSD's and CSD's are presented in Volume II. Here we will merely summarize the test data. Tables 4.2-1 through 4.2-3 present the total RMS vibration level for Flight 1, Flight 3, and noise tapes, respectively.

TABLE 4.2-1

Test Results - Flight: 1
Tape 1
Date: 8-6-69
Tape Ft: 270-460
Event: Flight Idle

HSSC Loop	Channel	Sensor	Frequency Range	RMS Voltage	Scale Factor	RMS Vibration Level	(Vol II) PSD Plot Figure
1	1	Gx	Low	.10	0.271 V/°/sec	0.37°/sec	B-1
1	3	Gy	Low	.09	0.233 V/°/sec	0.39°/sec	B-2
1	5	Gz	Low	.08	0.272 V/°/sec	0.29°/sec	B-3
1	7	Ax	Low	.08	1.54 V/g	0.05 g	B-4
3	3	Ay	Low	.08	1.50 V/g	0.05 g	B-5
3	5	Az	Low	.13	1.76 V/g	0.07 g	B-6
4	1	Gx	High	.35	1.03 V/°/sec	0.34°/sec	B-7
4	3	Gy	High	.30	1.15 V/°/sec	0.26°/sec	B-8
4	5	Gz	High	.17	1.13 V/°/sec	0.15°/sec	B-9
6	7	Ax	High	.30	2.93 V/g	0.10 g	B-10
6	3	Ay	High	.30	3.48 V/g	0.09 g	B-11
6	5	Az	High	.29	3.40 V/g	0.09 g	B-12

TABLE 4.2-2

Test Results - Flight: 3
Tape: 1
Date: 8-8-69
Event: Fwd Flt/Desc Hover

HSSC Loop	Channel	Sensor	Frequency Range	RMS Voltage	Scale Factor	RMS Vibration Level
7	1	Gx	Low	0.15	0.271 V/°/sec	0.55°/sec
7	3	Gy	Low	0.17	0.233 V/°/sec	0.73°/sec
7	5	Gz	Low	0.10	0.272 V/°/sec	0.37°/sec
7	7	Ax	Low	0.10	1.54 V/g	0.06 g
9	5	Ay	Low	0.12	1.50 V/g	0.08 g
9	3	Az	Low	0.32	1.76 V/g	0.18 g
10	1	Gx	High	0.50	1.03 V/°/sec	0.49°/sec
10	3	Gy	High	0.70	1.15 V/°/sec	0.61°/sec
10	5	Gz	High	0.45	1.13 V/°/sec	0.40°/sec
11	7	Ax	High	0.41	2.93 V/g	0.14 g
11	3	Ay	High	0.38	3.48 V/g	0.11 g
11	5	Az	High	0.83	3.40 V/g	0.24 g

TABLE 4.2-3

Test Results - Noise Tape

HSSC Loop	Channel	Sensor	Frequency Range	RMS Voltage	Scale Factor	RMS Vibration Level	(Vol II) PSD Plot Figure
13	3	Gx	Low	0.078	0.271 V/°/sec	0.29°/sec	3-25
13	2	Gy	Low	0.090	0.233 V/°/sec	0.39°/sec	3-26
13	1	Gz	Low	0.079	0.272 V/°/sec	0.29°/sec	3-27
13	6	Ax	Low	0.060	1.54 V/g	0.04 g	3-28
13	5	Ay	Low	0.057	1.50 V/g	0.04 g	3-29
13	4	Az	Low	0.059	1.76 V/g	0.03 g	3-30
14	1	Gx	High	0.075	1.03 V/°/sec	0.07°/sec	3-31
14	2	Gy	High	0.083	1.15 V/°/sec	0.07°/sec	3-32
14	3	Gz	High	0.074	1.13 V/°/sec	0.07°/sec	3-33
14	4	Az	High	0.051	2.93 V/g	0.02 g	3-34
14	5	Ay	High	0.064	3.48 V/g	0.02 g	3-35
14	6	Az	High	0.074	3.50 V/g	0.02 g	3-36

Compensated Test Results

The analog test results from flight 3/tape 1 were reprocessed in order to take into account the effects of the Vibration Monitor frequency response characteristics of the 12 sensor channels. This was accomplished by transcribing the analog plots onto punched cards, and then digitally compensating each channel as a function of frequency. The transfer functions, which were used in the compensation, are presented in the following figures:

Figure	Sensor Channel
4.3-1	X Donner
4.3-2	Y Donner
4.3-3	Z Donner
4.3-4	X Gyro
4.3-5	Y Gyro
4.3-6	Z Gyro
4.3-7	X Endevco
4.3-8	Y Endevco
4.3-9	Z Endevco
4.3-10	X ADA
4.3-11	Y ADA
4.3-12	Z ADA

The dark lines on each figure were based on both the pre and post-flight calibration data. It is noted here that the ADA's were assumed to have a flat frequency response. Even though the calibration data indicate significant resonances, these are believed to be associated with the Team Angular Vibration Table, and not the Vibration Monitor.

Table 4.3-1 presents the final table of figures for the reconstructed environments. These are presented in Figures 4.3-13 through 4.3-48. These composite spectral plots were generated using the low frequency sensors up to 10 Hz and the high frequency sensors from 10 to 2000 Hz. Figure 4.3-49 summarizes the total data reduction procedure.

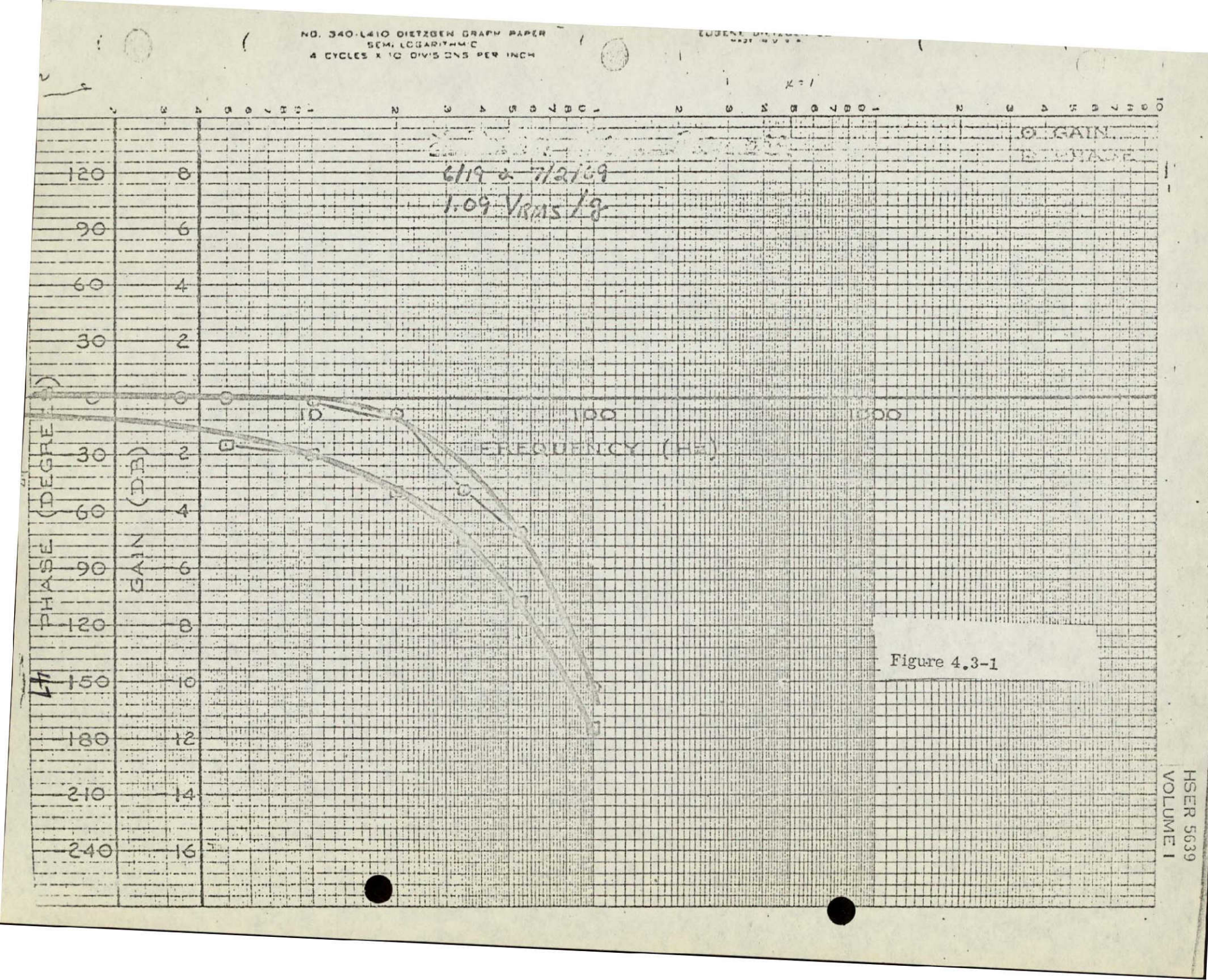
NO. 340-L410 DIETZGEN GRAPH PAPER
SEMI-LOGARITHMIC
4 CYCLES X 10 DIVISIONS PER INCH
6/19 & 7/2/69
1.09 VRMS I/P
PHASE (DEGREES)
GAIN (DB)
FREQUENCY (HZ)
10
100
1000
120
90
60
30
0
30
60
90
120
150
180
210
240
8
6
4
2
0
2
4
6
8
10
12
14
16

Figure 4.3-1

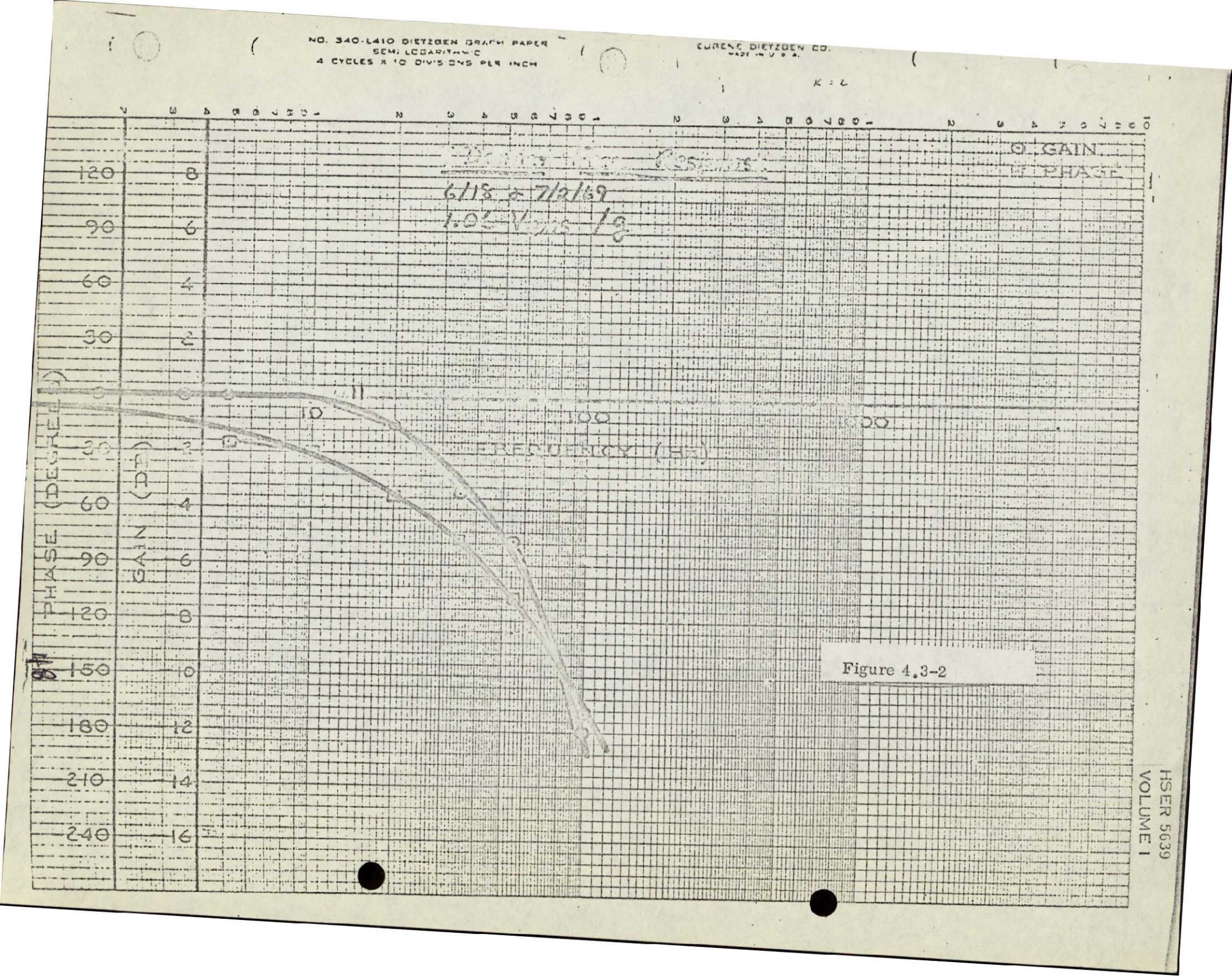
NO. 340-L410 DIETZGEN GRAPH PAPER
SEMI-LOGARITHMIC
4 CYCLES X 10 DIVISIONS PER INCH
EUGENE DIETZGEN CO.
K = 2
GAIN
PHASE
6/18 & 7/2/69
1.0 Vrms Ig
PHASE (DEGREES)
GAIN (DB)
FREQUENCY (HZ)
10
100
120
90
60
30
0
-30
-60
-90
-120
-150
-180
-210
-240
8
6
4
2
0
-2
-4
-6
-8
-10
-12
-14
-16

Figure 4.3-2

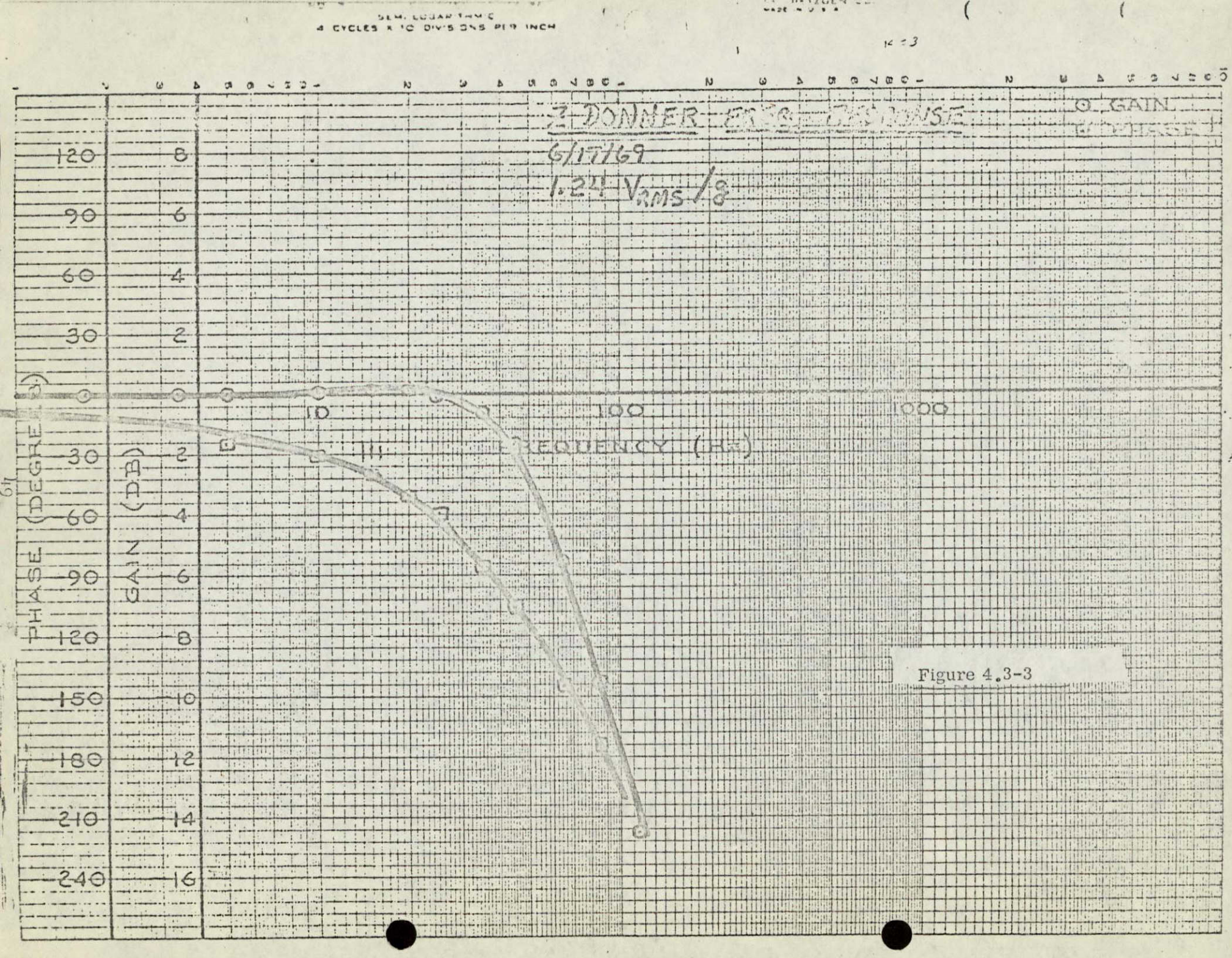
SEMI-LOGARITHMIC
4 CYCLES X 10 DIVISIONS PER INCH
K=3
DONNER ERB RESPONSE
6/11/69
1.24 VRMS/8
GAIN
PHASE
PHASE (DEGREES)
GAIN (DB)
10
100
1000
FREQUENCY (HZ)
120
90
60
30
0
30
60
90
120
150
180
210
240
8
6
4
2
0
2
4
6
8
10
12
14
16

Figure 4.3-3

K=4

X Gyro Frequency Response

SF = 0.5 to 1.5 Vdc @ 7.5 Hz

6/23 & 7/2/69

GAIN

PHASE (DEGREES)

GAIN (DB)

10

100

1000

FREQUENCY (HZ)

120 8
90 6
60 4
30 2
30 2
60 4
90 6
100 12
210 14
240 16

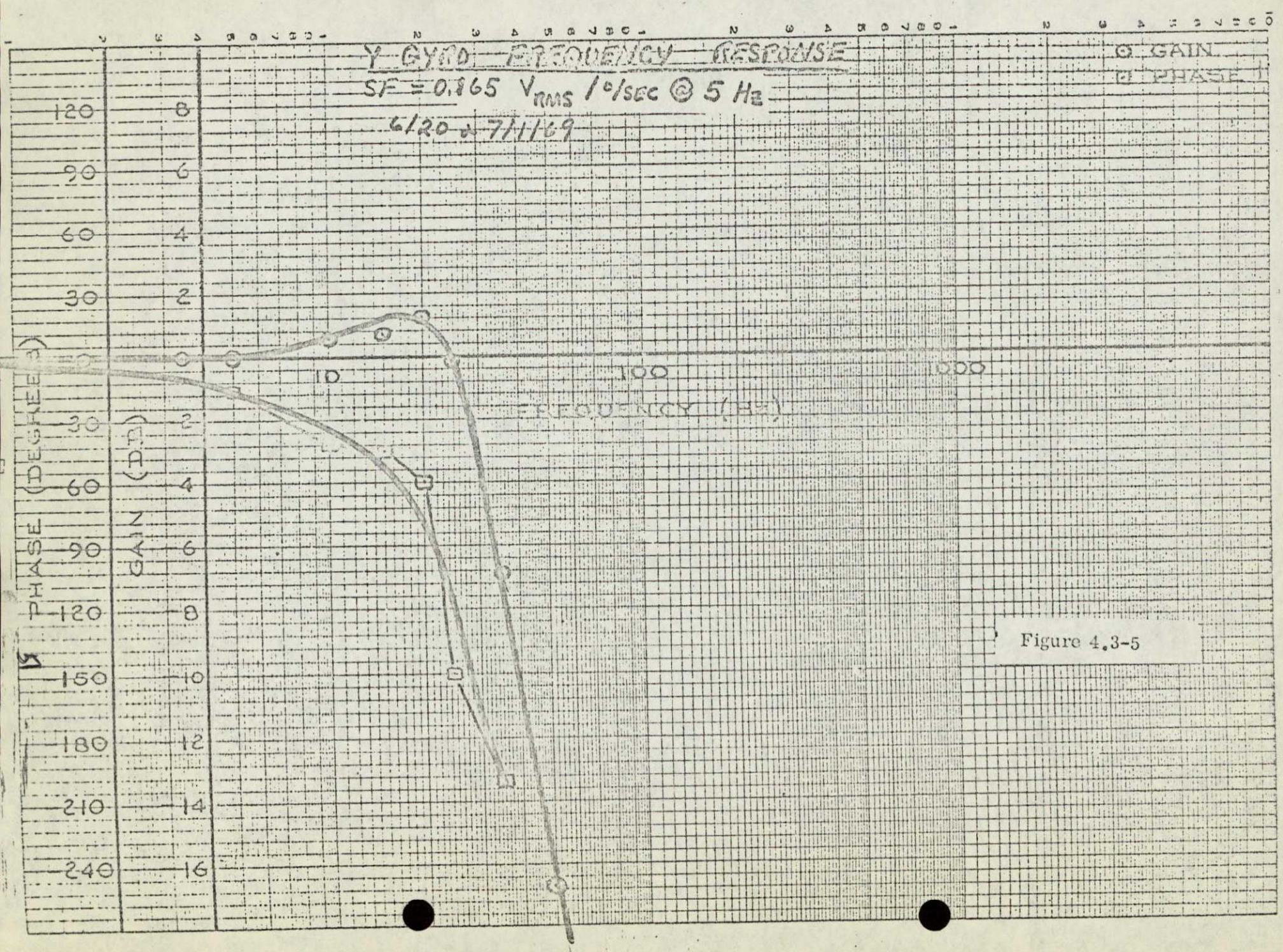

Figure 4.3-5

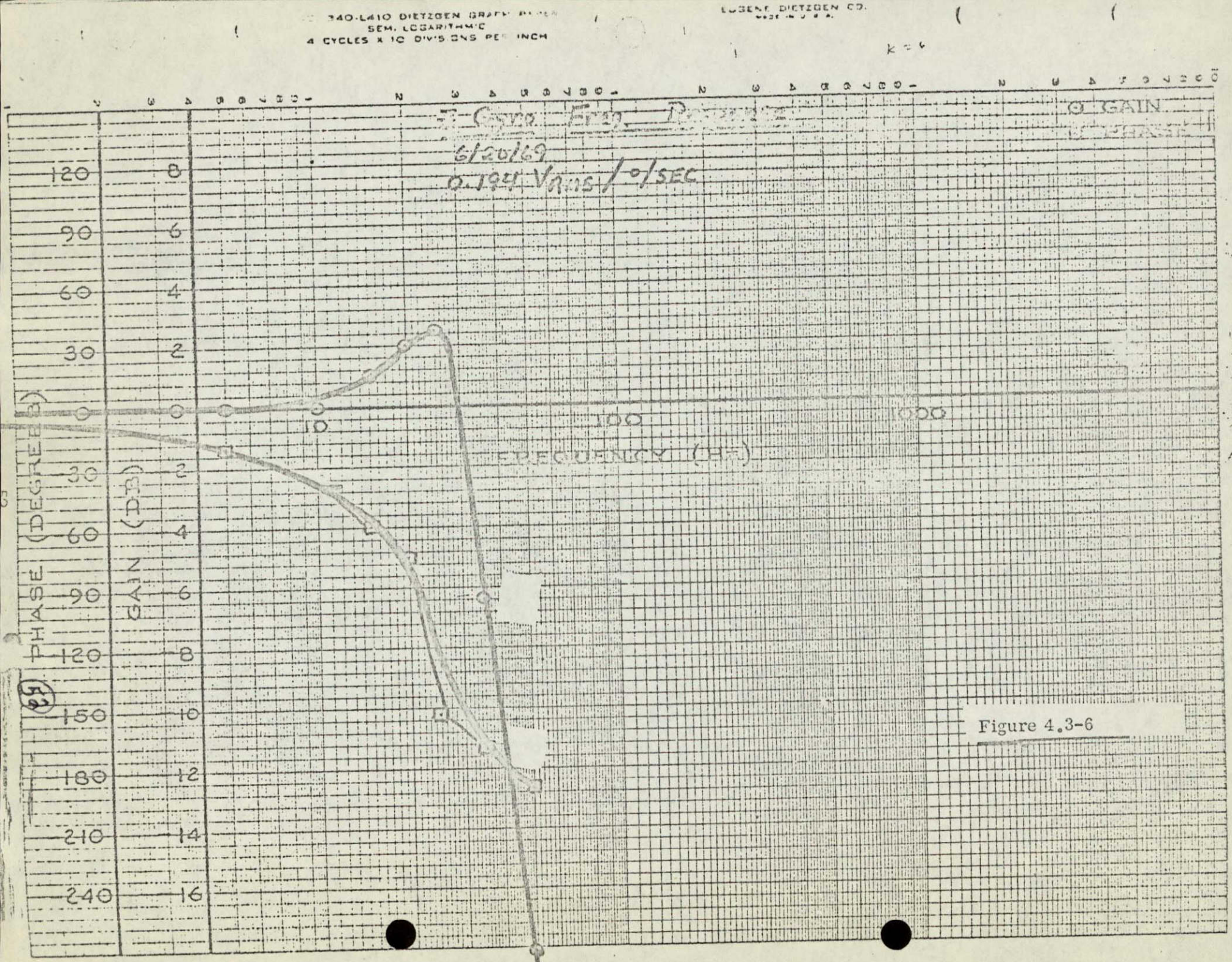
340-L410 DIETZGEN GRAPH PAPER
SEMI-LOGARITHMIC
4 CYCLES X 10 DIVISIONS PER INCH
EUGENE DIETZGEN CO.
k = 6
GAIN
PHASE
6/20/69
0.194 VOLTS / °/SEC
10
100
1000
FREQUENCY (HZ)
PHASE (DEGREES)
GAIN (DB)
120
90
60
30
0
30
60
90
120
150
180
210
240
8
6
4
2
0
2
4
6
8
10
12
14
16

Figure 4.3-6

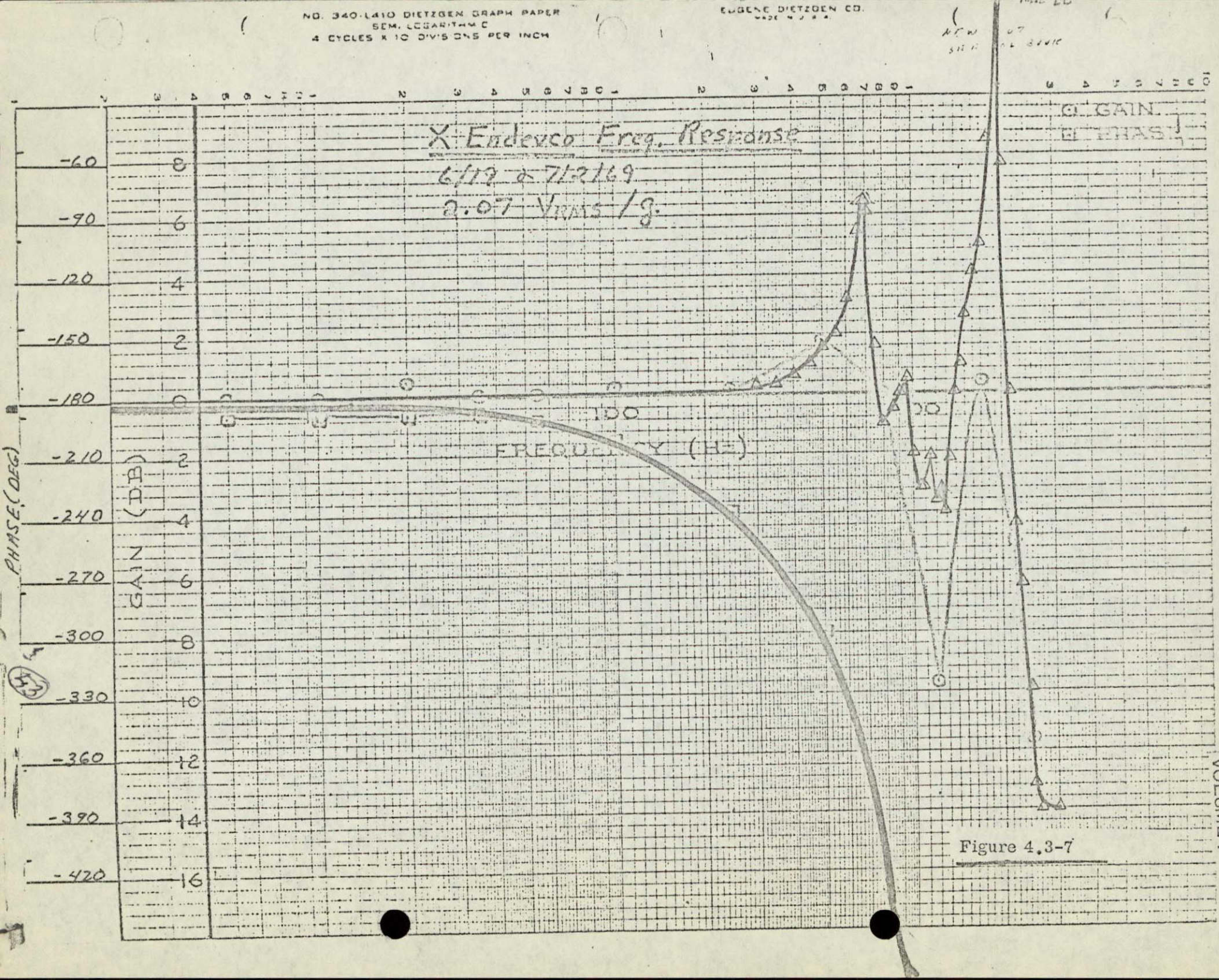
NO. 340-L410 DIETZGEN GRAPH PAPER
SEMI-LOGARITHMIC
4 CYCLES X 10 DIVISIONS PER INCH
EUGENE DIETZGEN CO.
X Endevco Freq. Response
6/12 & 7/2/69
2.07 Vrms / g
PHASE (DEG)
GAIN (DB)
FREQUENCY (HZ)
-60
-90
-120
-150
-180
-210
-240
-270
-300
-330
-360
-390
-420
8
6
4
2
0
2
4
6
8
10
12
14
16
GAIN
PHASE

Figure 4.3-7

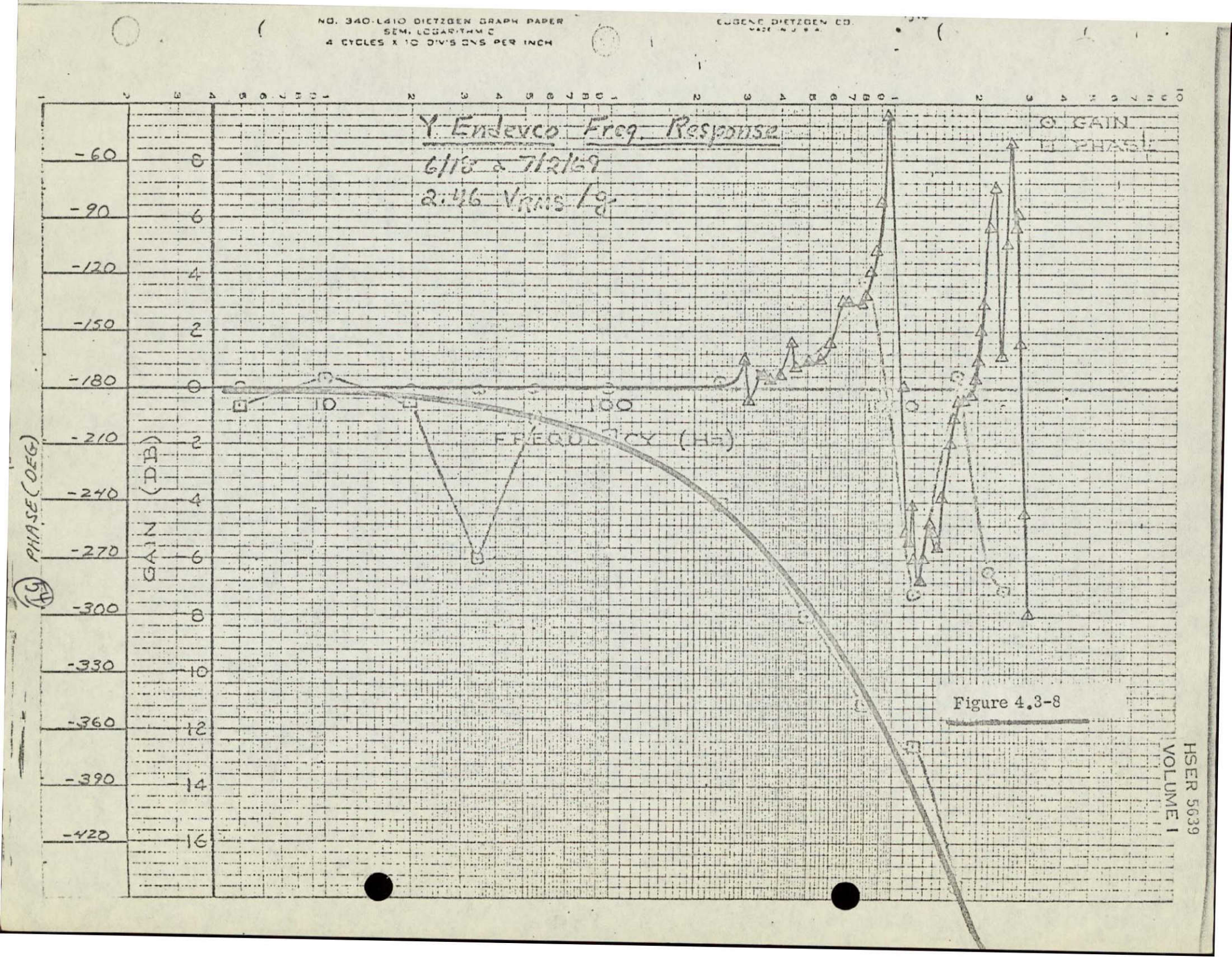
NO. 340-L410 DIETZGEN GRAPH PAPER
SEMI-LOGARITHMIC
4 CYCLES X 10 DIVISIONS PER INCH
EUGENE DIETZGEN CO.
Y Endevco Freq Response
6/15 & 7/2/69
2.46 Vrms Ig
GAIN
PHASE
-60
-90
-120
-150
-180
-210
-240
-270
-300
-330
-360
-390
-420
8
6
4
2
0
2
4
6
8
10
12
14
16
10
100
FREQUENCY (Hz)
PHASE (DEG)
GAIN (DB)

Figure 4.3-8

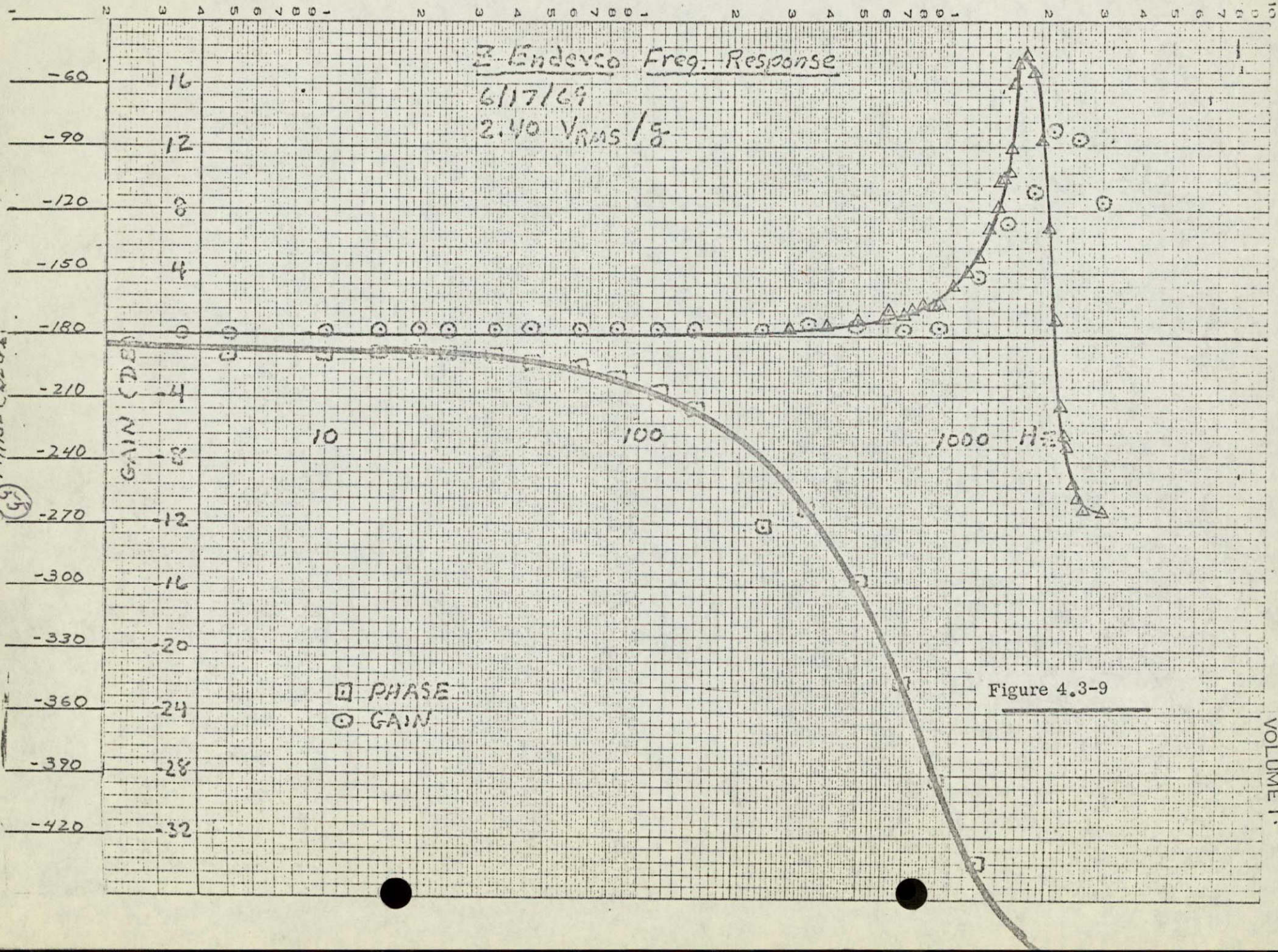

Figure 4.3-9

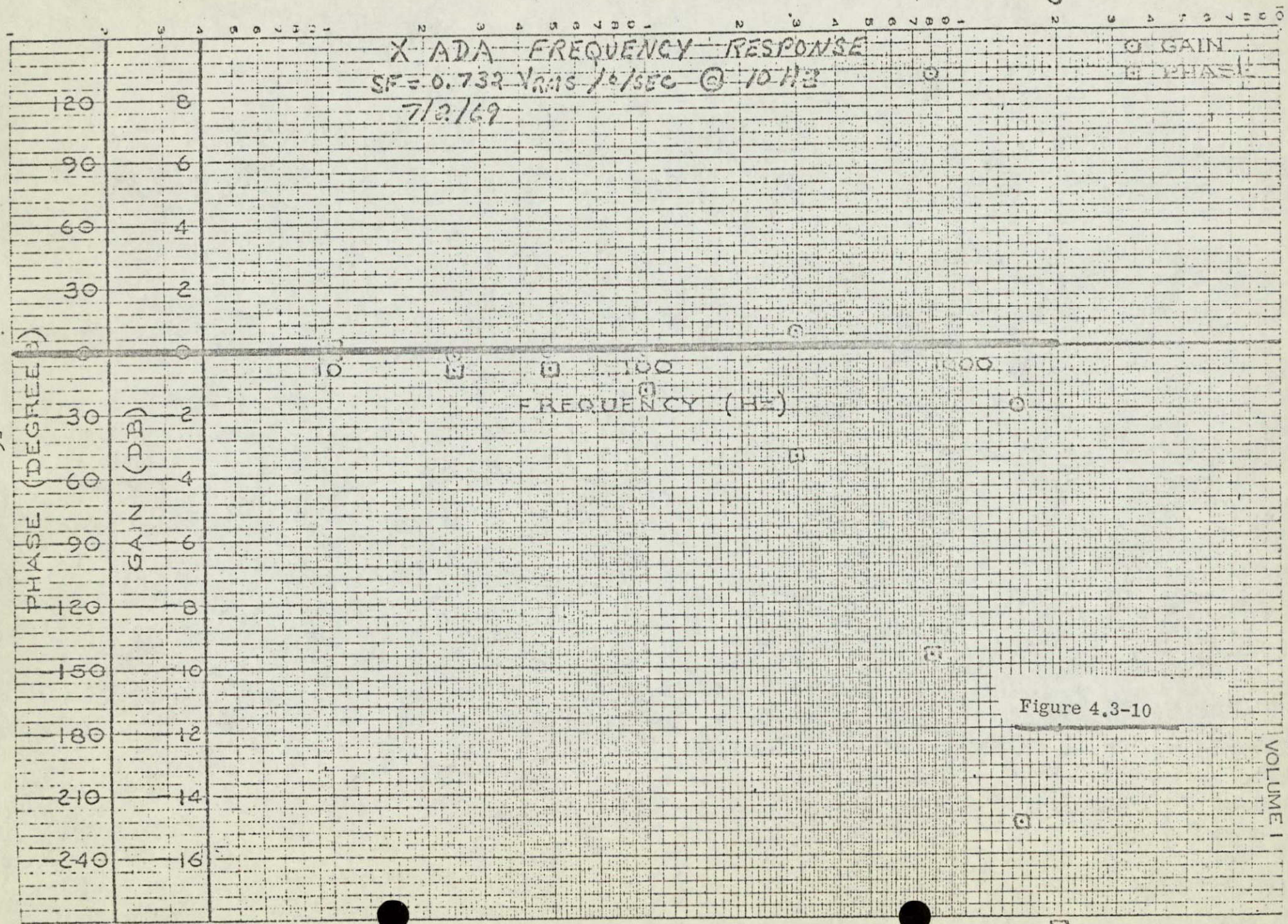
X ADA FREQUENCY RESPONSE
SF = 0.732 VRMS / 6/SEC @ 10 HZ
7/2/69
GAIN
PHASE
PHASE (DEGREES)
GAIN (DB)
120
90
60
30
30
60
90
120
150
180
210
240
8
6
4
2
2
4
6
8
10
12
14
16
10
100
1000
FREQUENCY (HZ)

Figure 4.3-10

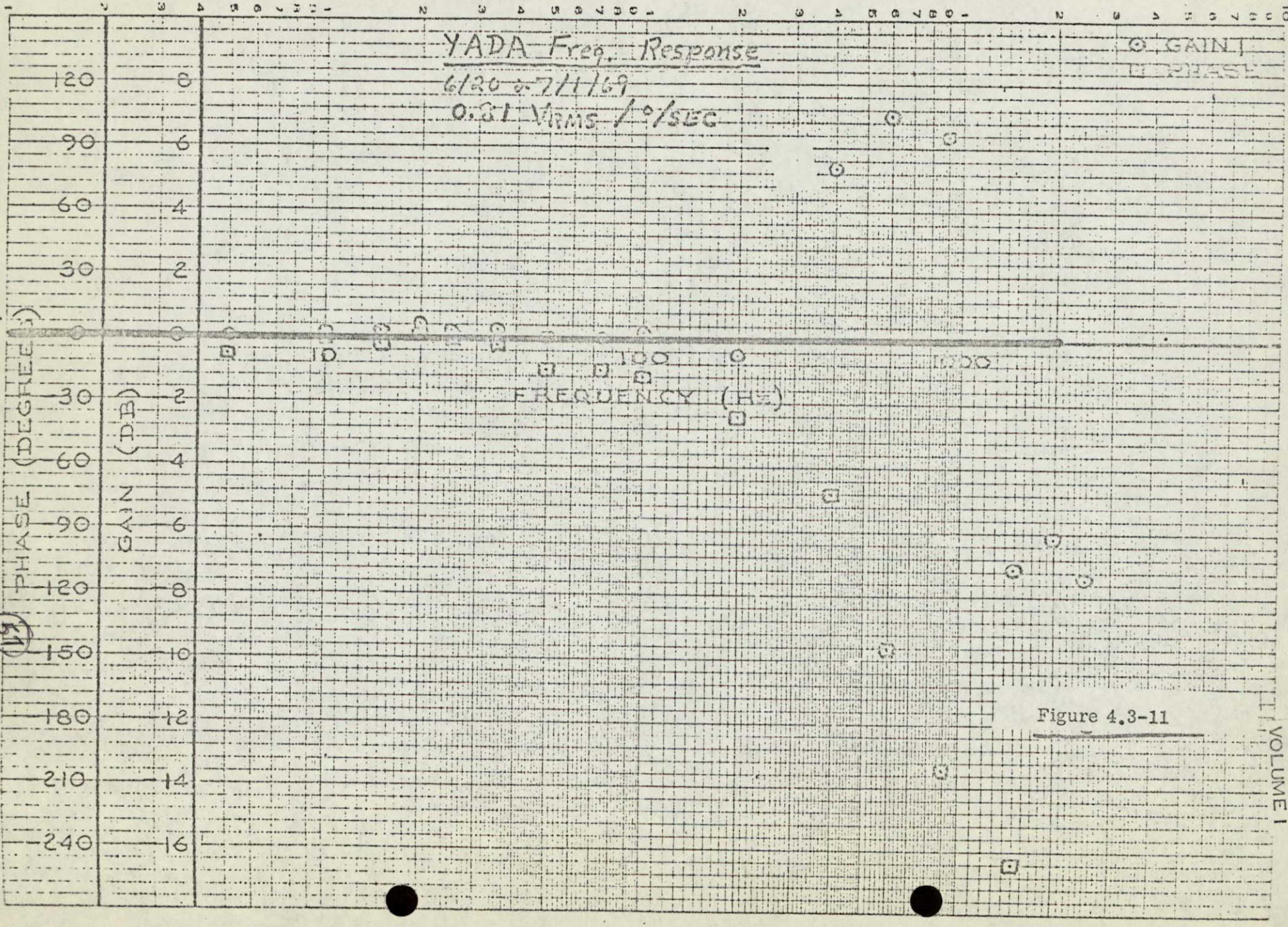

Figure 4.3-11

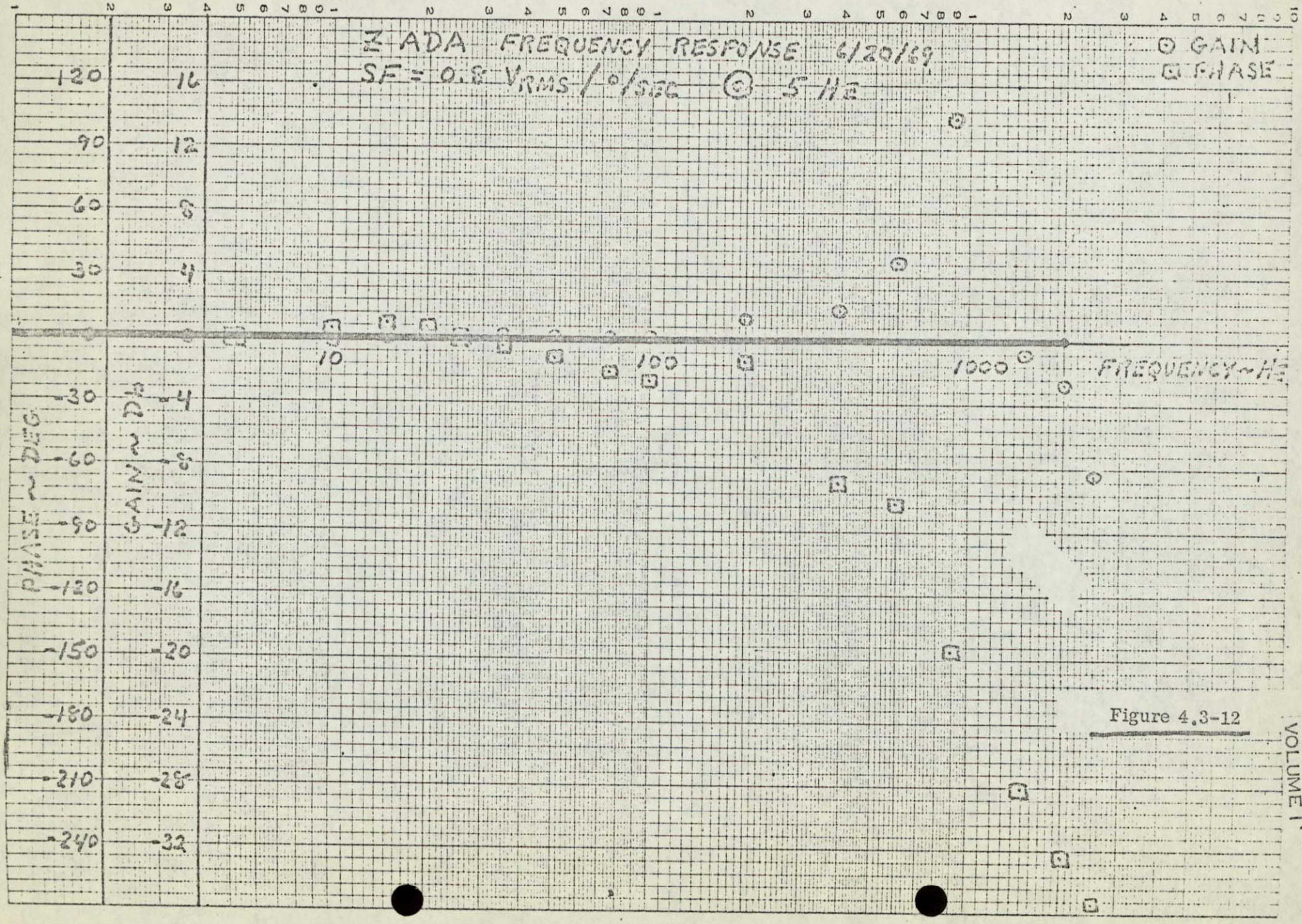

Figure 4.3-12

Hamilton Standard DIVISION OF UNITED AIRCRAFT CORPORATION

TABLE 4.3-1

Table of Figures For
Reconstructed Total Environments

ENVIRONMENTS	CO-SPECTRUM	QUAD-SPECTRUM
Ax - Ax	4.3-13	
Ay - Ay	4.3-14	
Az - Az	4.3-15	
Gx - Gx	4.3-16	
Gy - Gy	4.3-17	
Gz - Gz	4.3-18	
Ax - Ay	4.3-19	4.3-20
Ax - Az	4.3-21	4.3-22
Ay - Az	4.3-23	4.3-24
Gx - Gy	4.3-25	4.3-26
Gx - Gz	4.3-27	4.3-28
Gy - Gz	4.3-29	4.3-30
Ax - Gx	4.3-31	4.3-32
Ax - Gy	4.3-33	4.3-34
Ax - Gz	4.3-35	4.3-36
Ay - Gx	4.3-37	4.3-38
Ay - Gy	4.3-39	4.3-40
Ay - Gz	4.3-41	4.3-42
Az - Gx	4.3-43	4.3-44
Az - Gy	4.3-45	4.3-46
Az - Gz	4.3-47	4.3-48

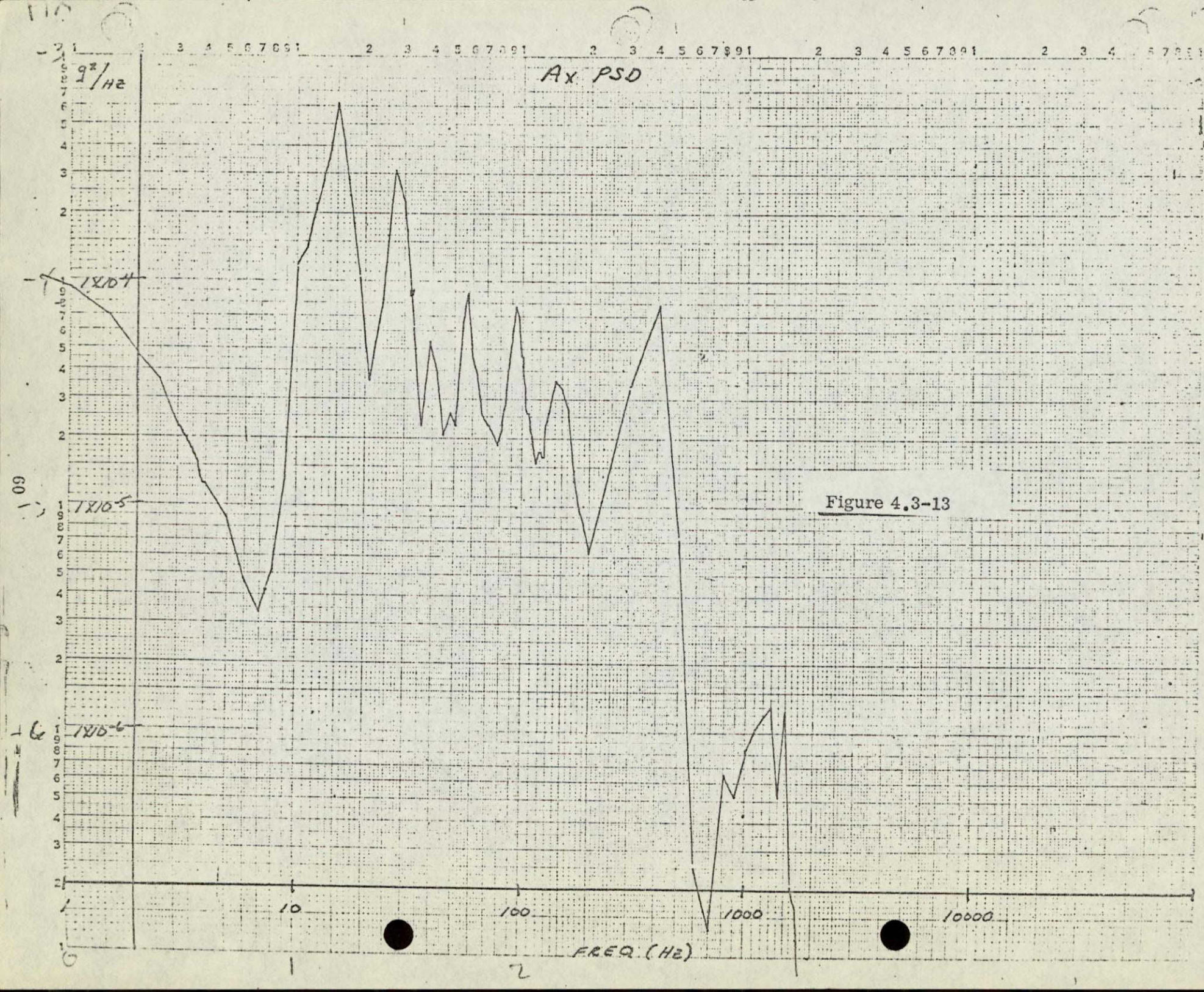

Figure 4.3-13

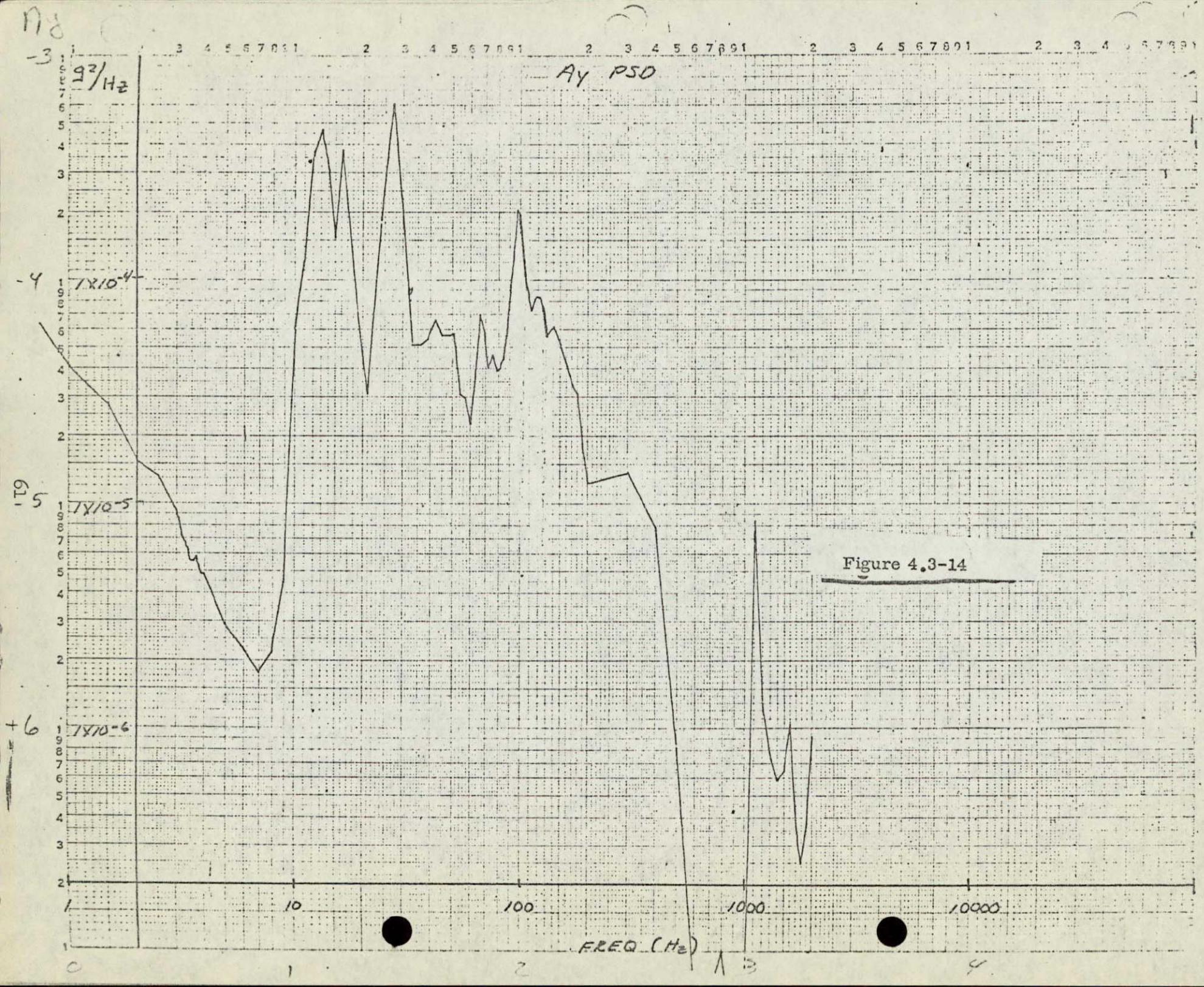

Figure 4.3-14

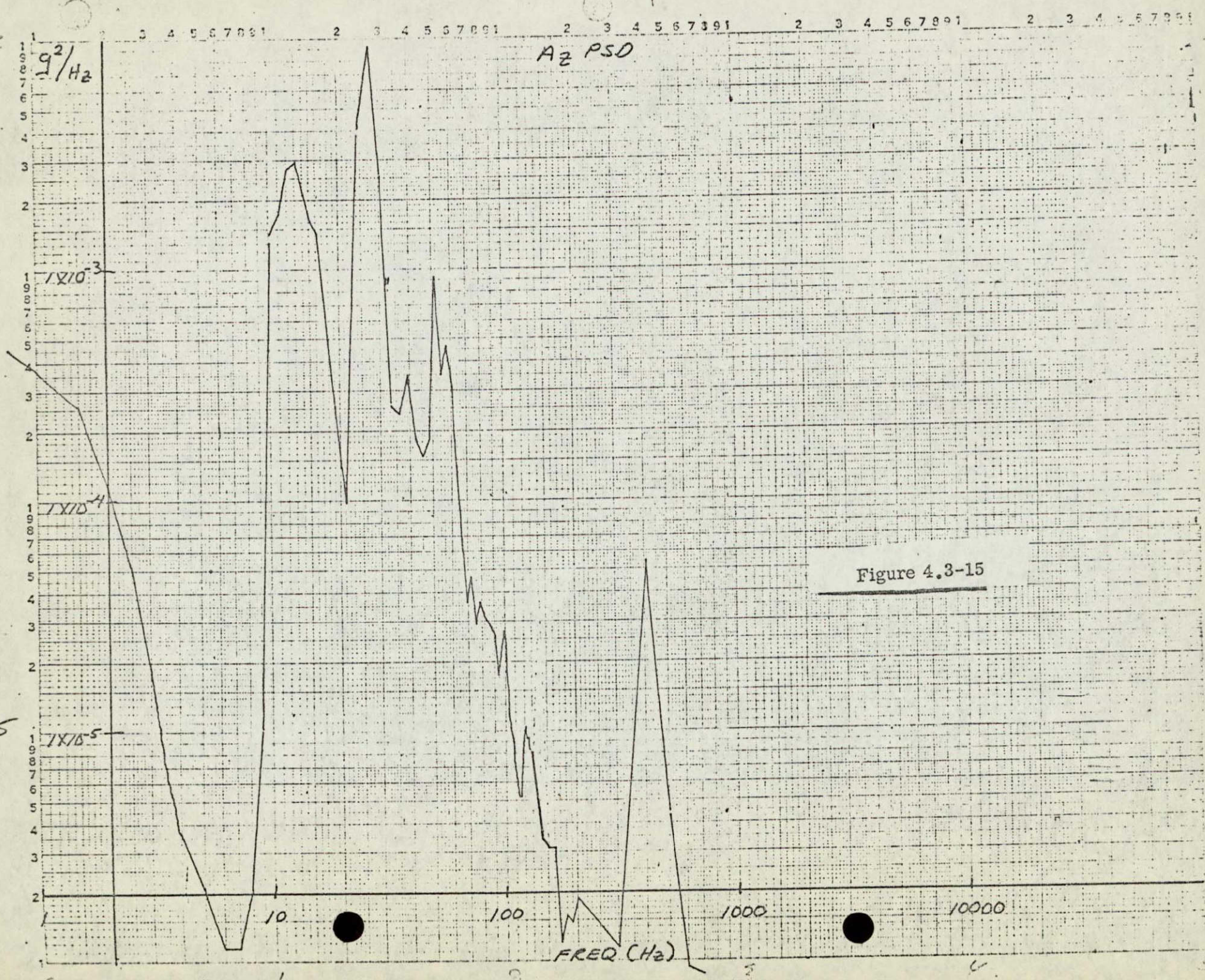

Figure 4.3-15

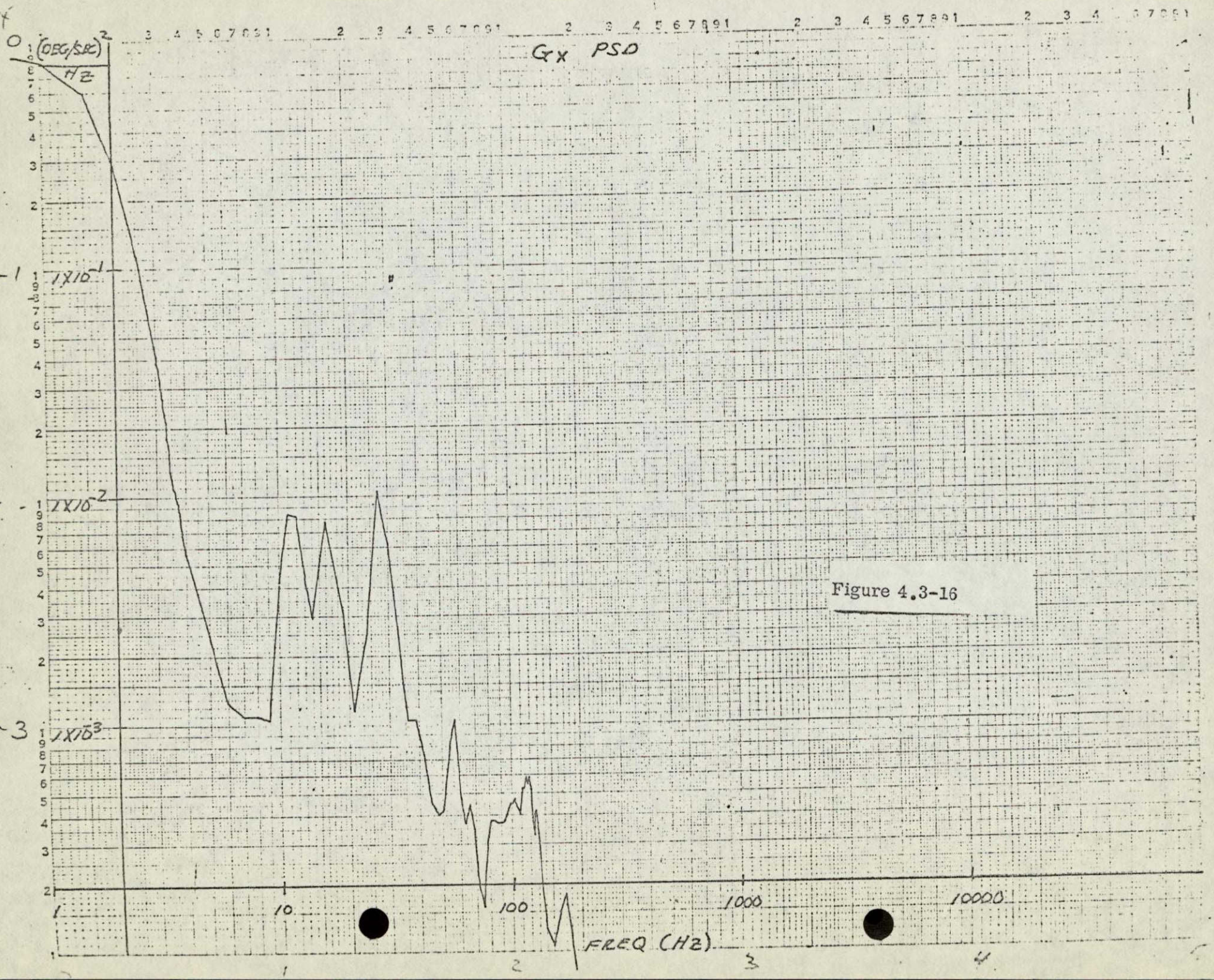

Figure 4.3-16

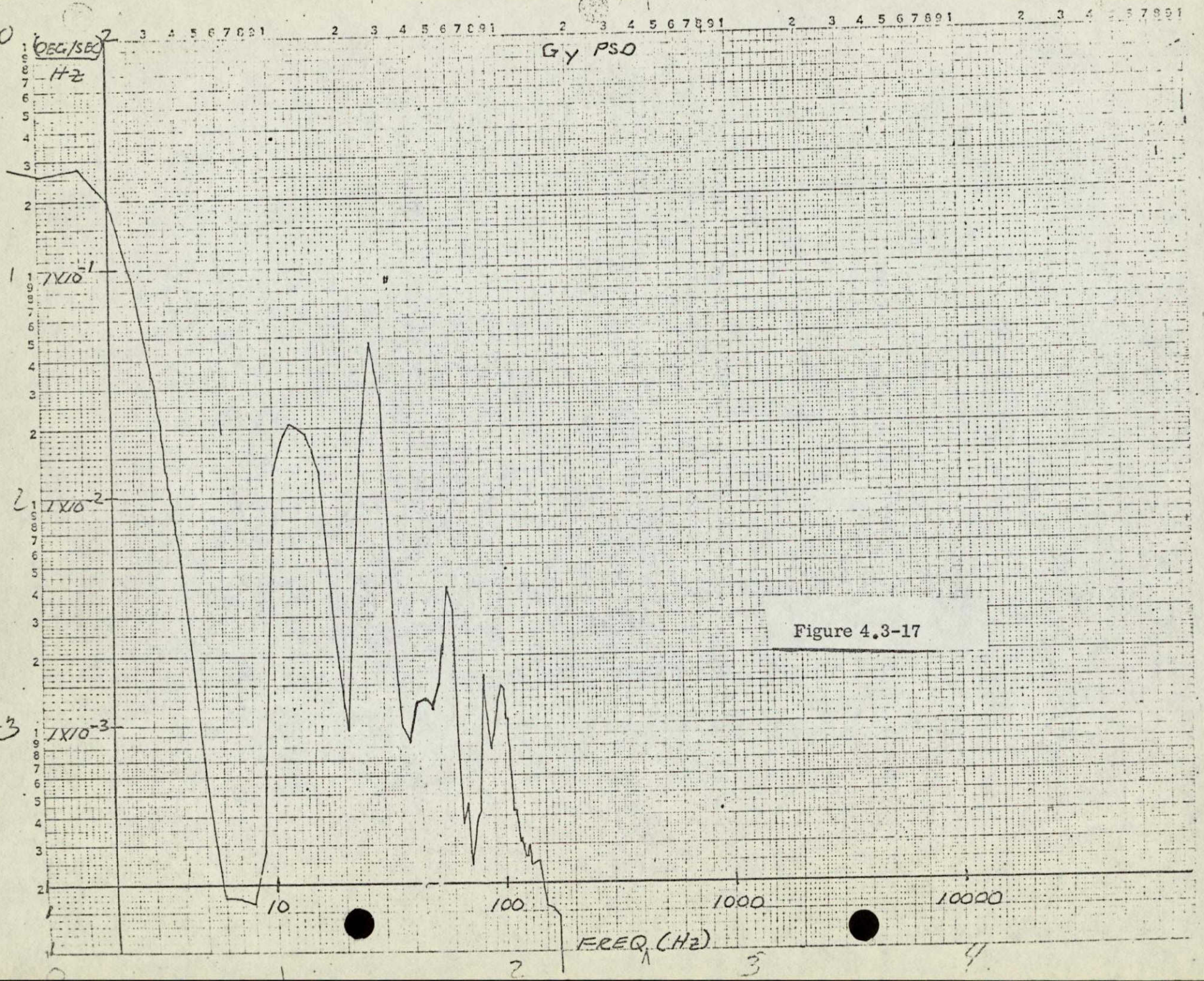

Figure 4.3-17

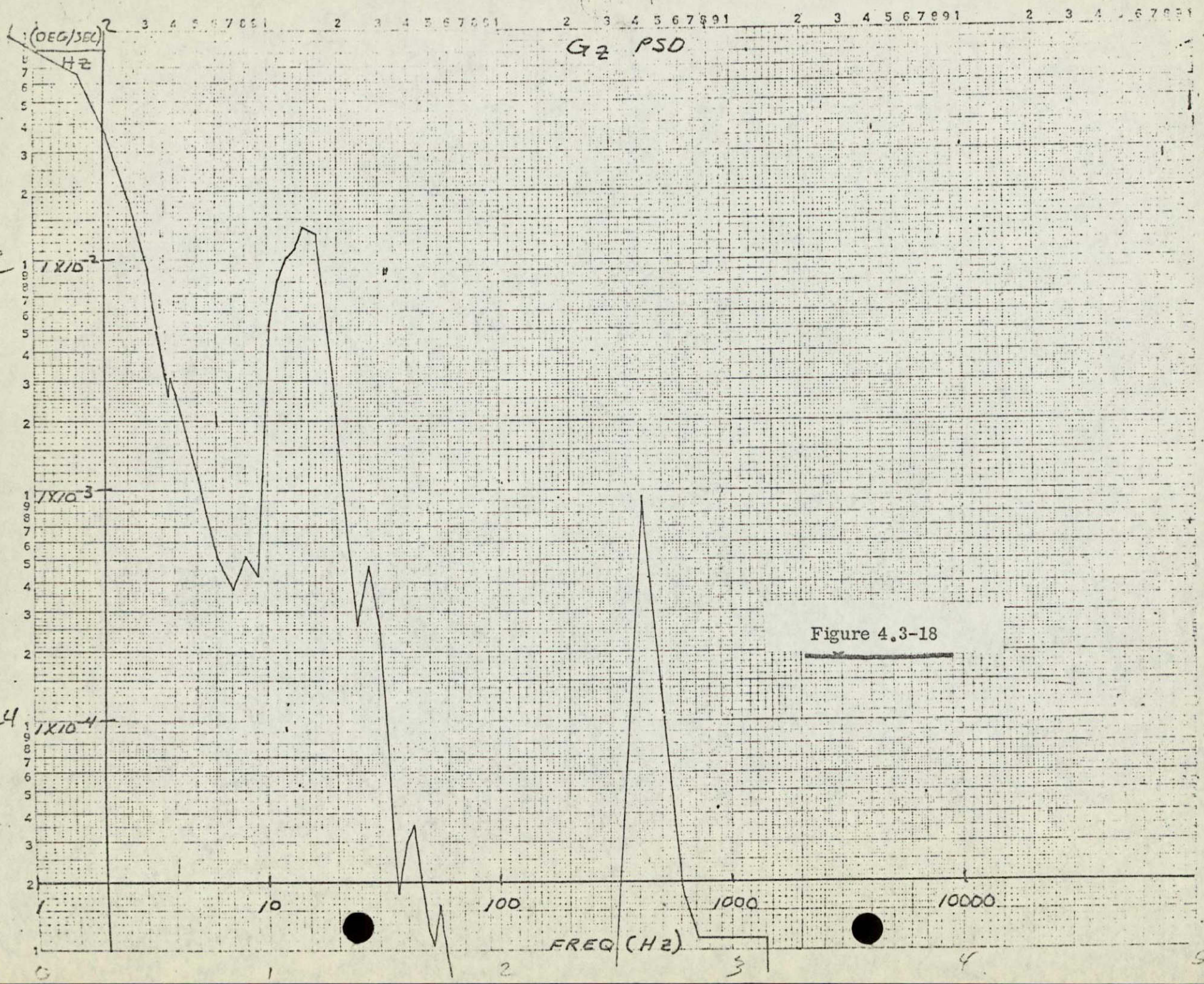
G2 PSD
(DEG/SEC)2
HZ
1X10-2
1X10-3
1X10-4
1
10
100
1000
10000
FREQ (HZ)

Figure 4.3-18

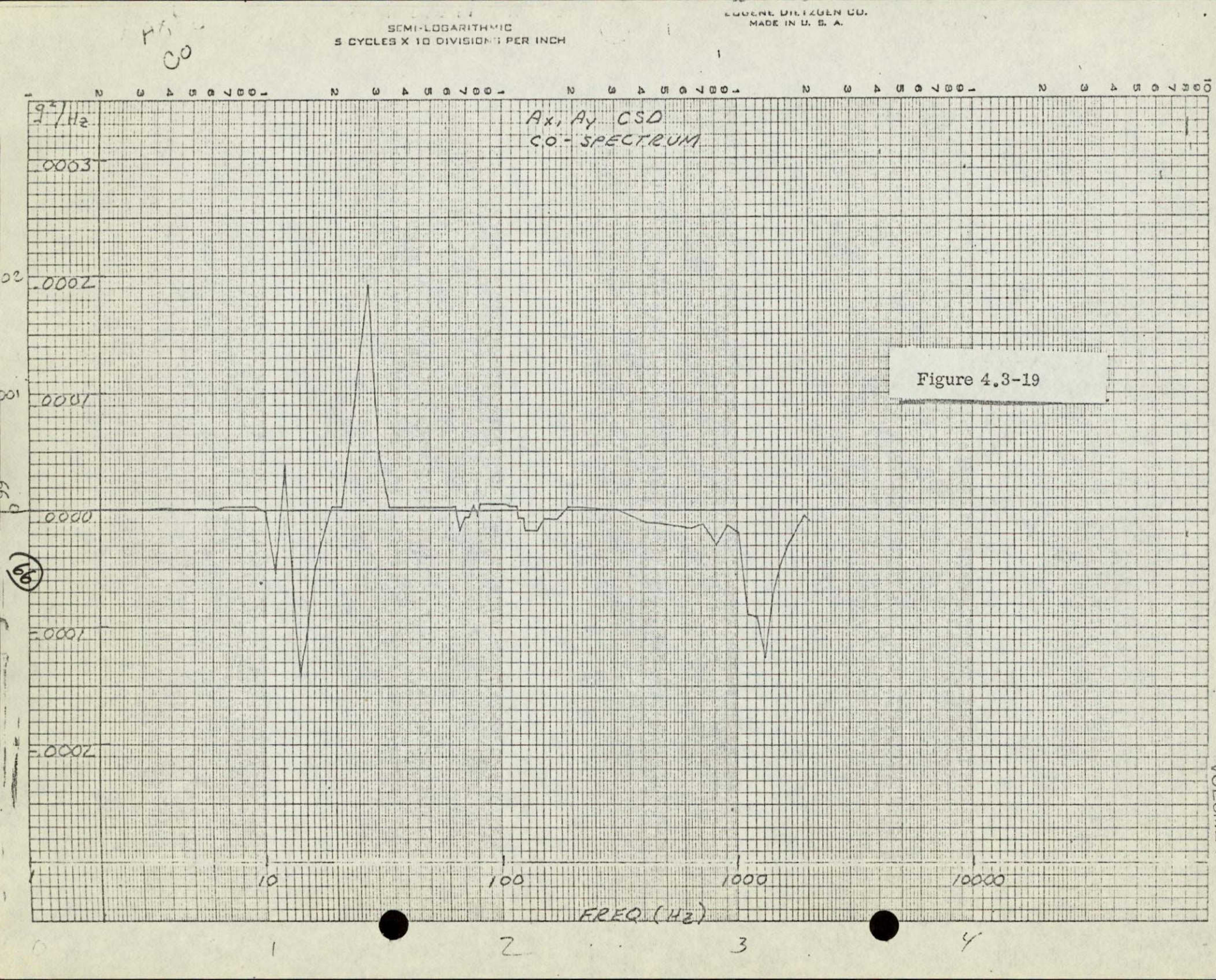
SEMI-LOGARITHMIC
5 CYCLES X 10 DIVISIONS PER INCH
EUGENE DIETZGEN CO.
MADE IN U. S. A.
CO
g²/Hz
Ax, Ay CSD
CO-SPECTRUM
.0003
.0002
.0001
.0000
-.0001
-.0002
10
100
1000
10000
FREQ (Hz)
1
2
3
4

Figure 4.3-19

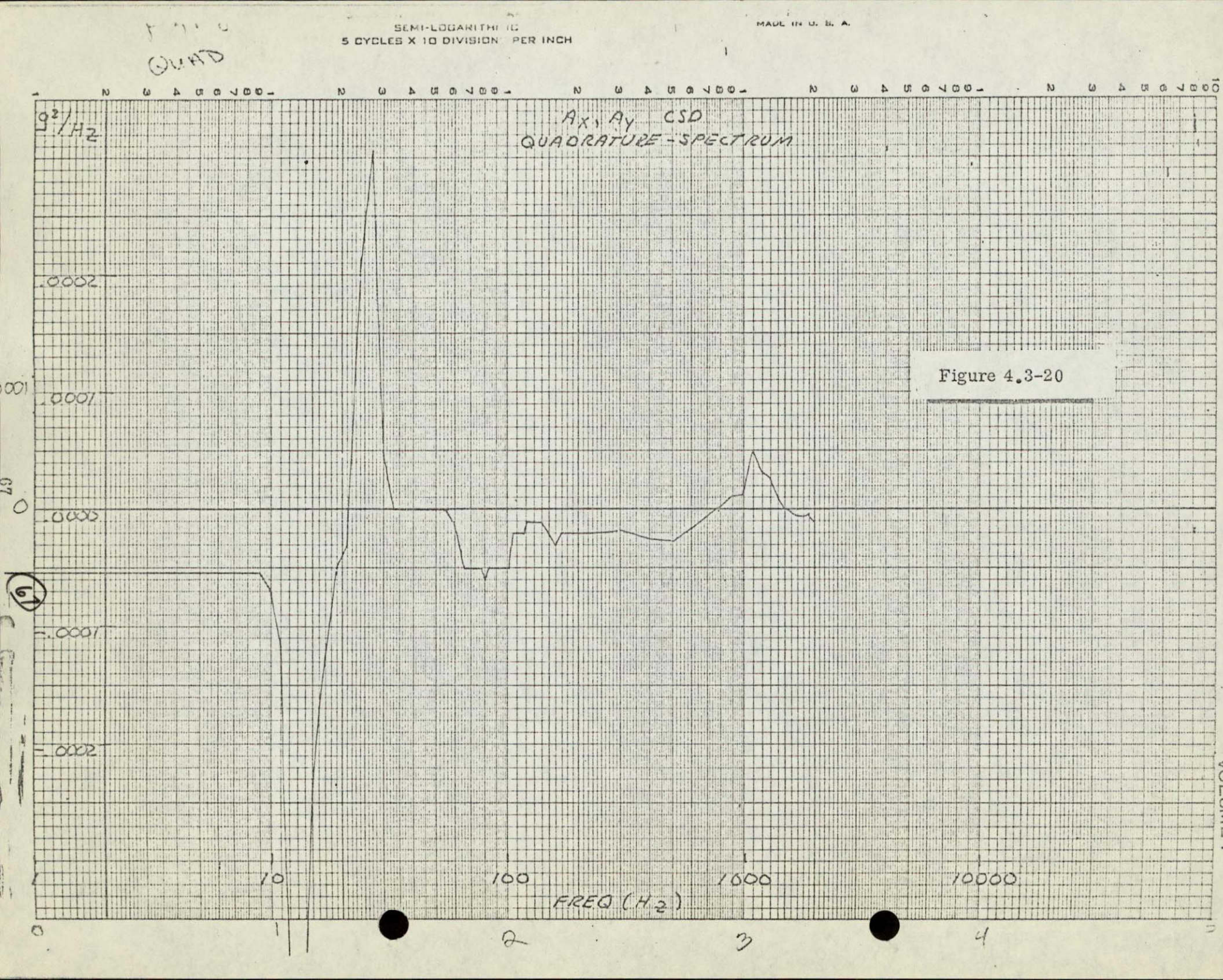
SEMI-LOGARITHMIC
5 CYCLES X 10 DIVISION PER INCH
MADE IN U. S. A.
QUAD
g^2/Hz
A_X, A_Y CSD
QUADRATURE-SPECTRUM
.0002
.0001
.0000
-.0001
-.0002
10
100
1000
10000
FREQ (Hz)
0
1
2
3
4

Figure 4.3-20

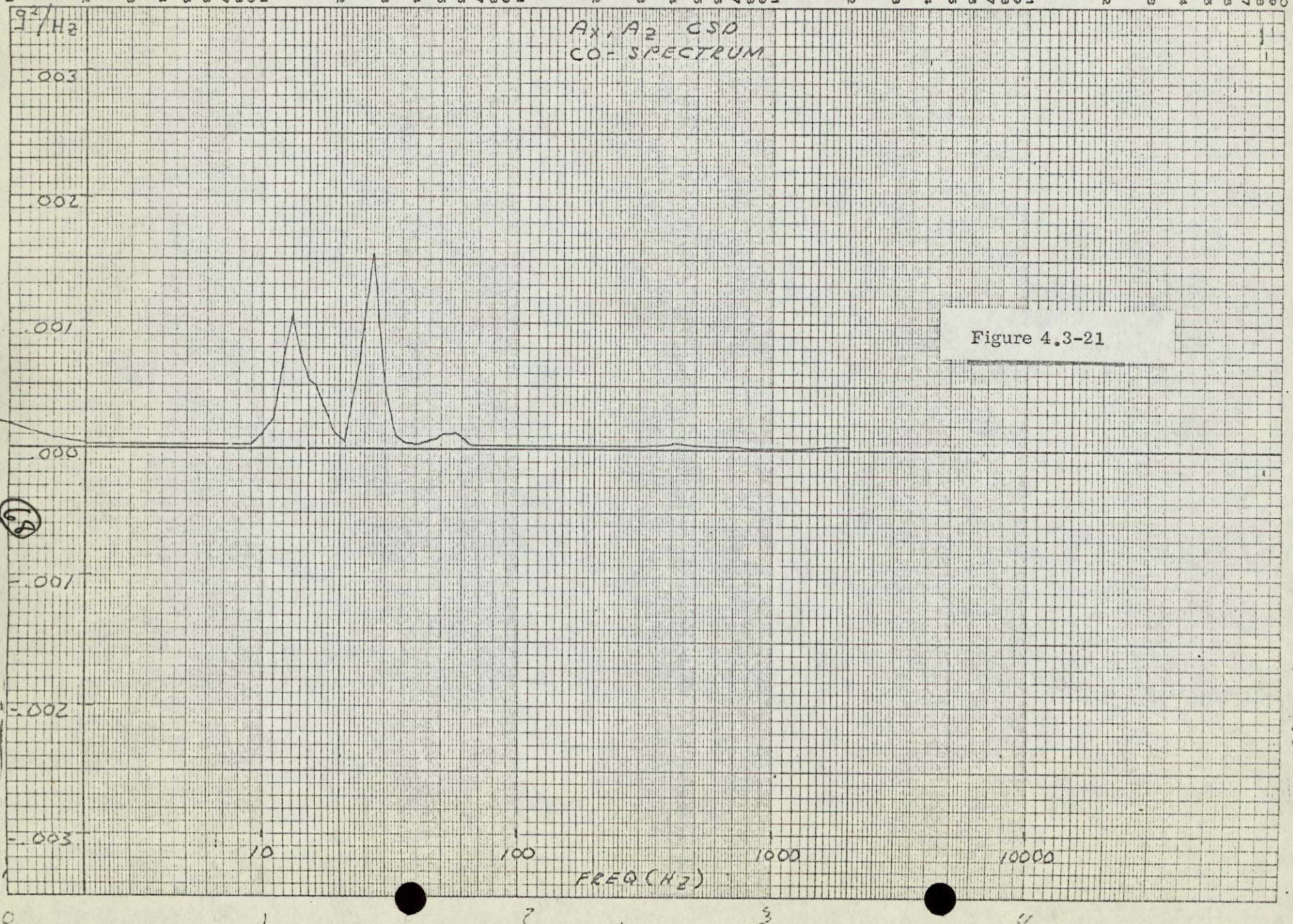

Figure 4.3-21

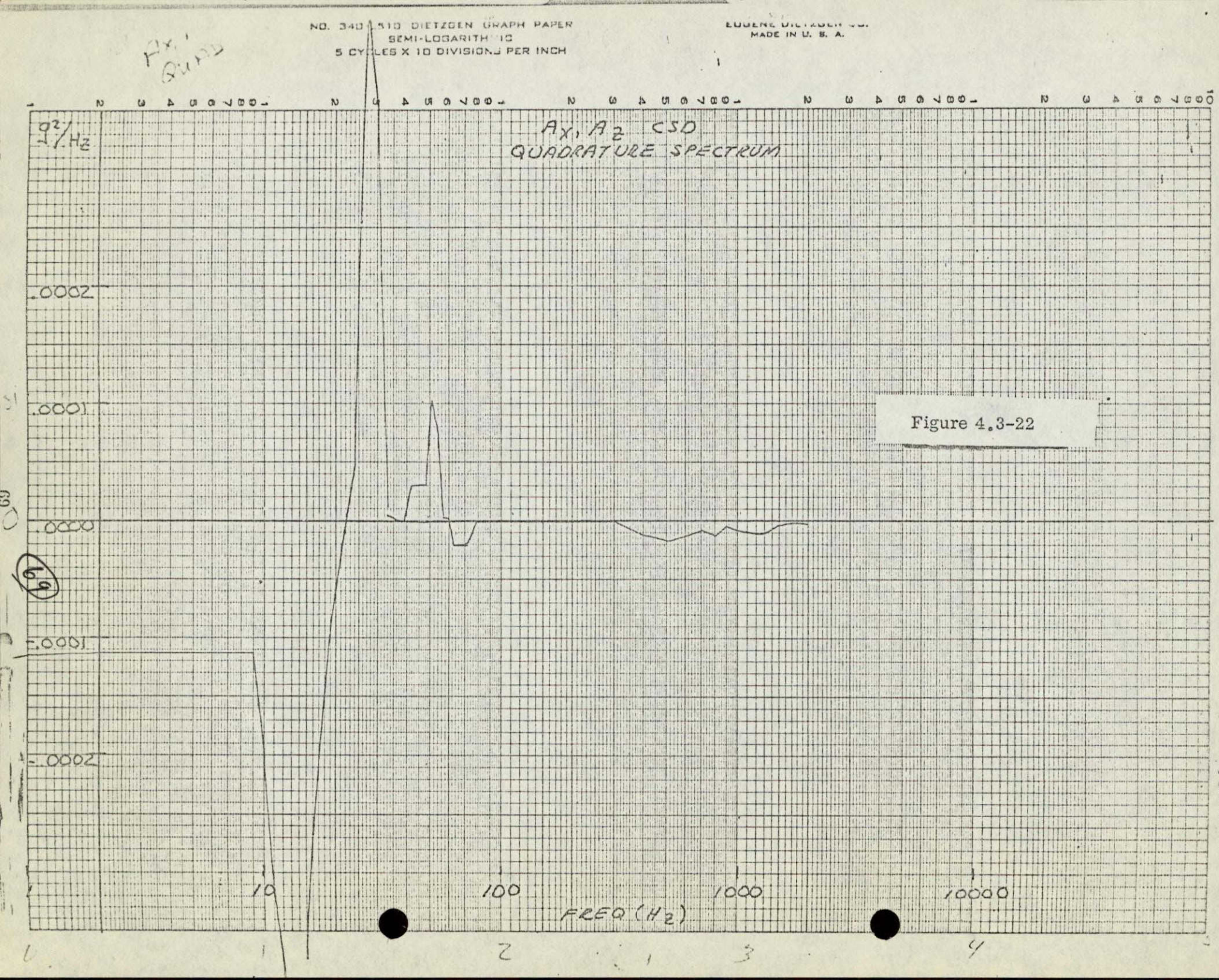
NO. 340 - 310 DIETZGEN GRAPH PAPER
SEMI-LOGARITHMIC
5 CYCLES X 10 DIVISIONS PER INCH
EUGENE DIETZGEN CO.
MADE IN U. S. A.
A_X, A_Z CSD
QUADRATURE SPECTRUM
g^2/Hz
.0002
.0001
.0000
-.0001
-.0002
10
100
1000
10000
FREQ (H_z)

Figure 4.3-22

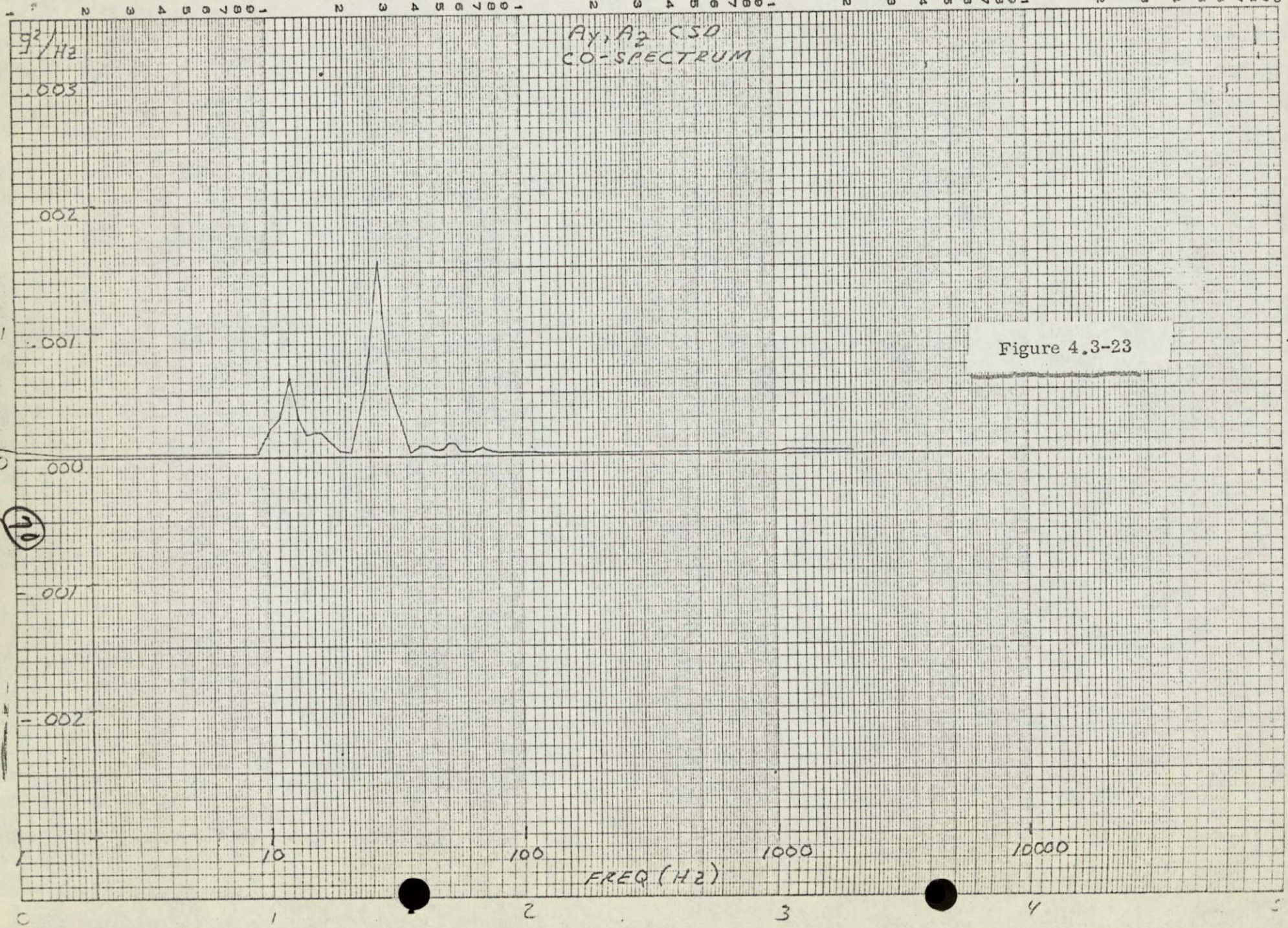

Figure 4.3-23

NO. 340-L510 DIETZGEN GRAPH PAPER
SEMI-LOGARITHMIC
5 CYCLES X 10 DIVISIONS PER INCH

EUGENE DIETZGEN CO.
MADE IN U. S. A.

AY, AZ QUAD

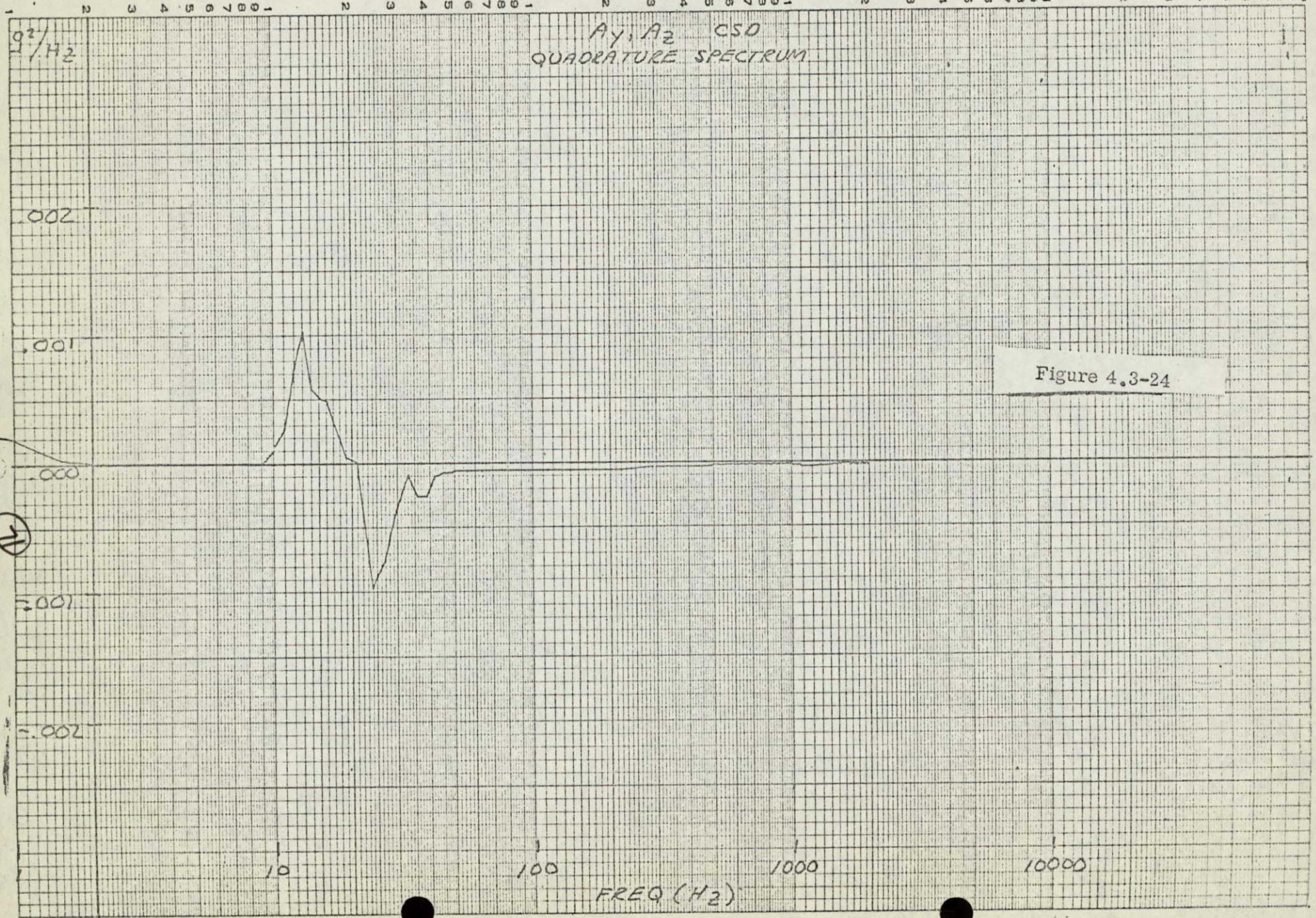

Figure 4.3-24

Gx, Gy
CO

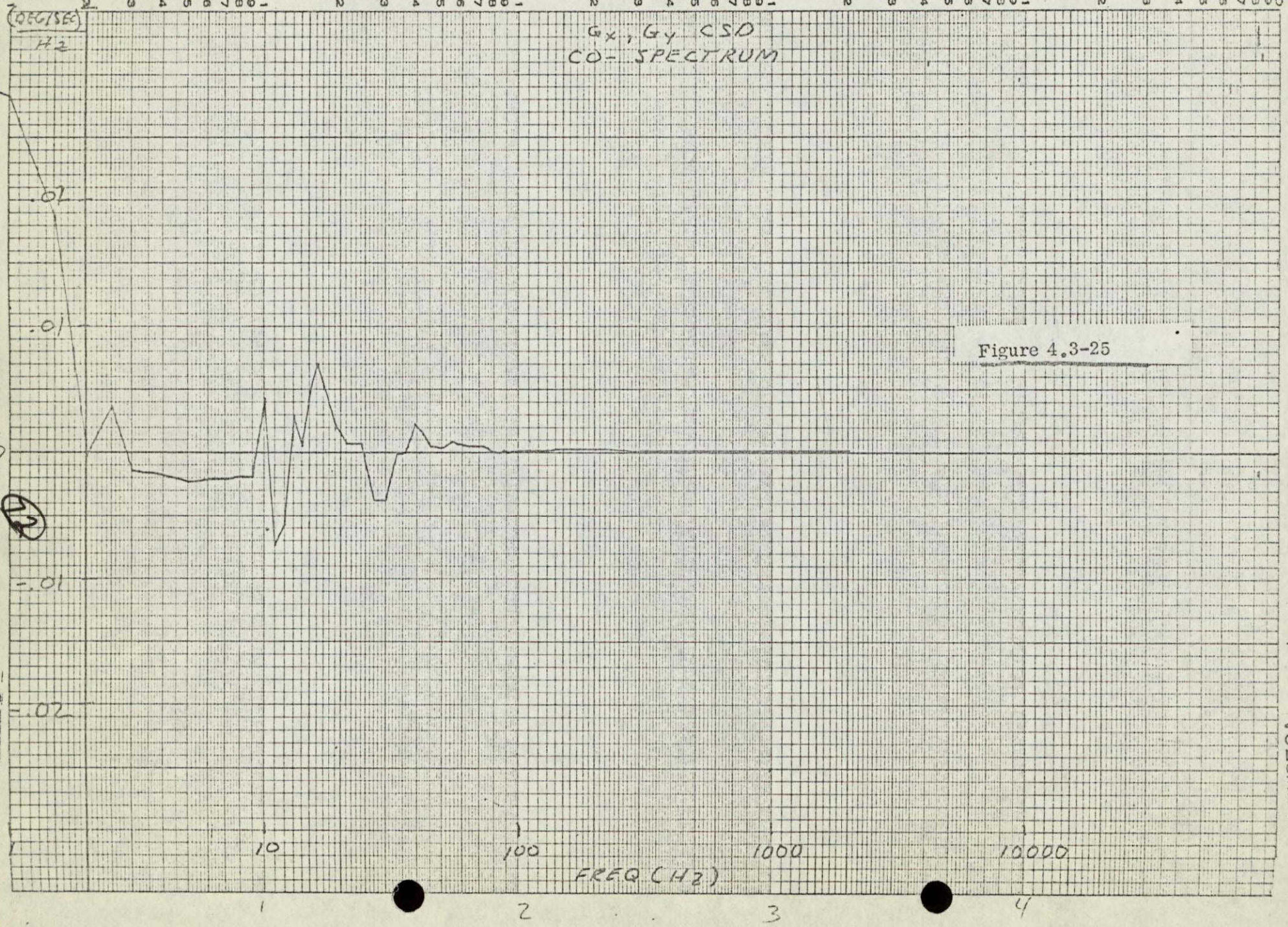

Figure 4.3-25

6x, 6y QUAD

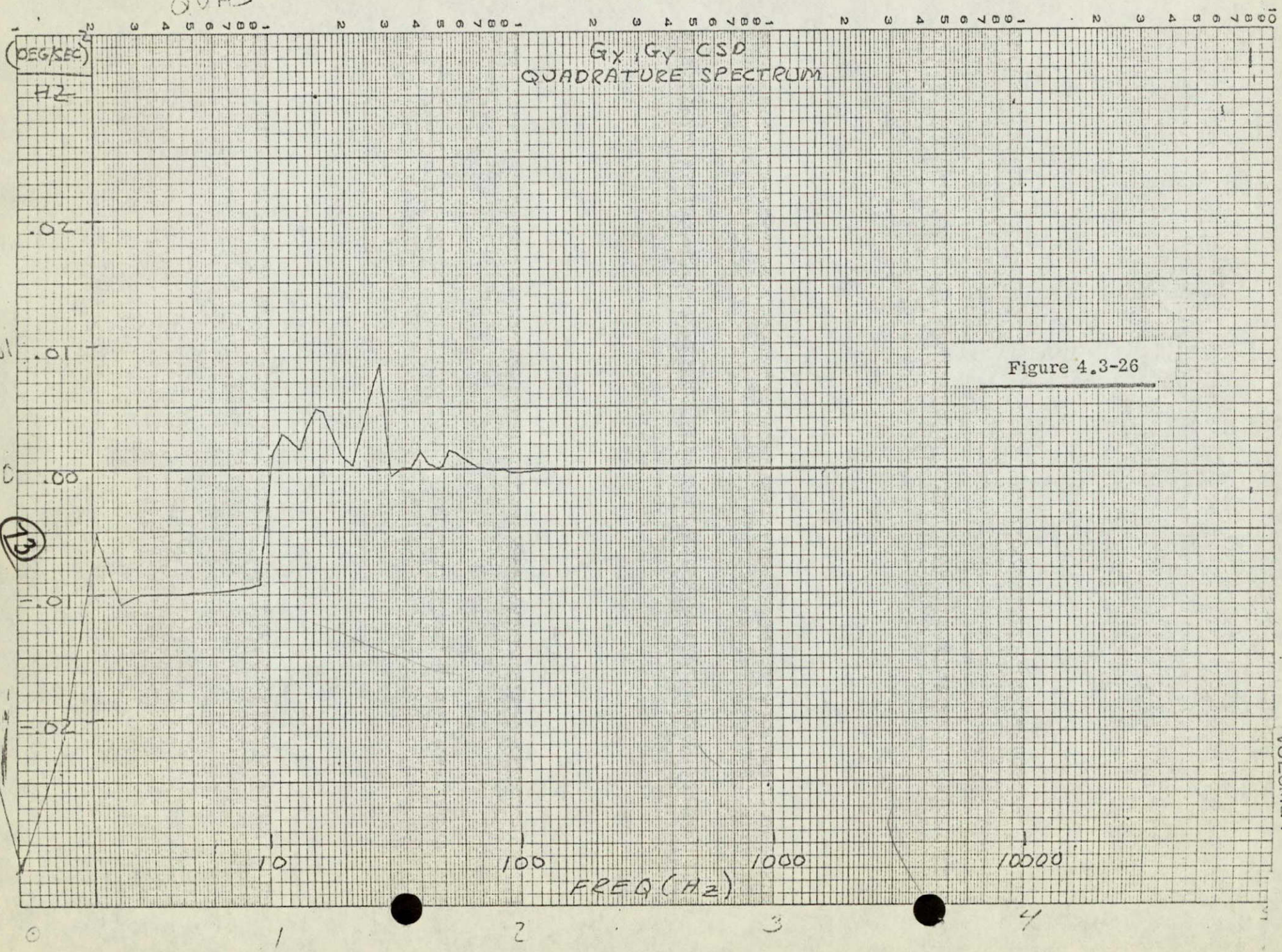

Figure 4.3-26

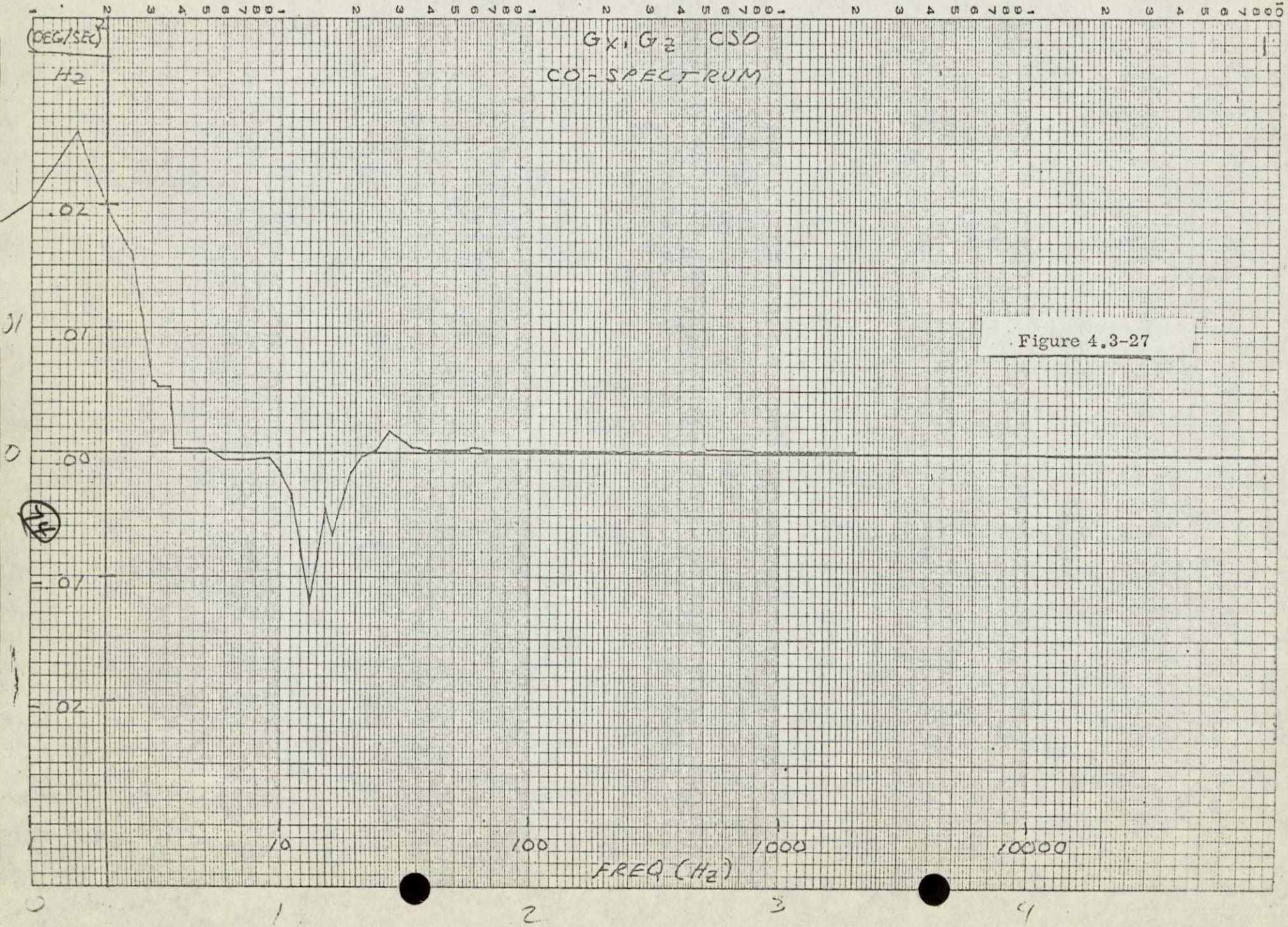

Figure 4.3-27

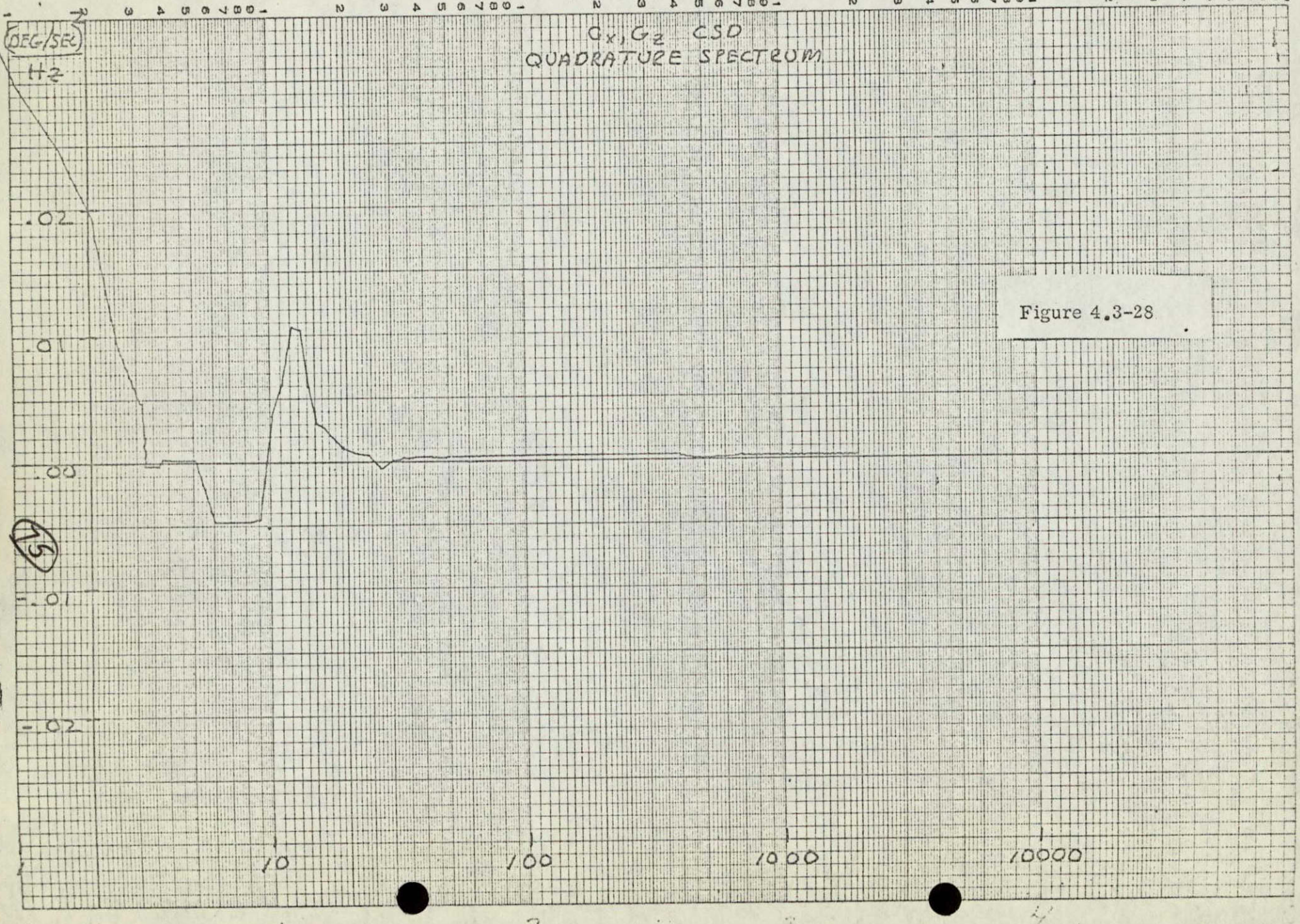

Figure 4.3-28

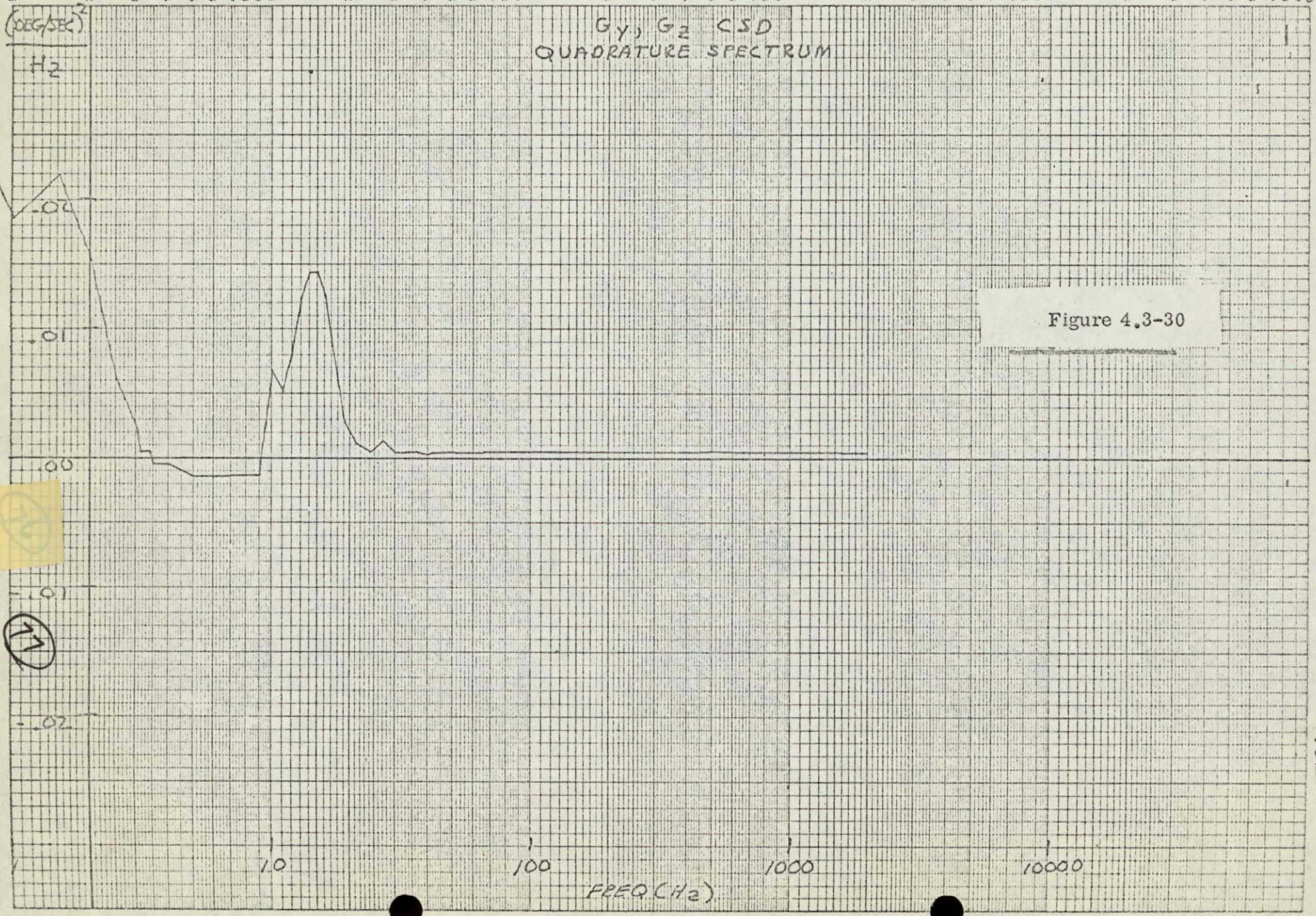

Figure 4.3-30

Ax, Gx
CO

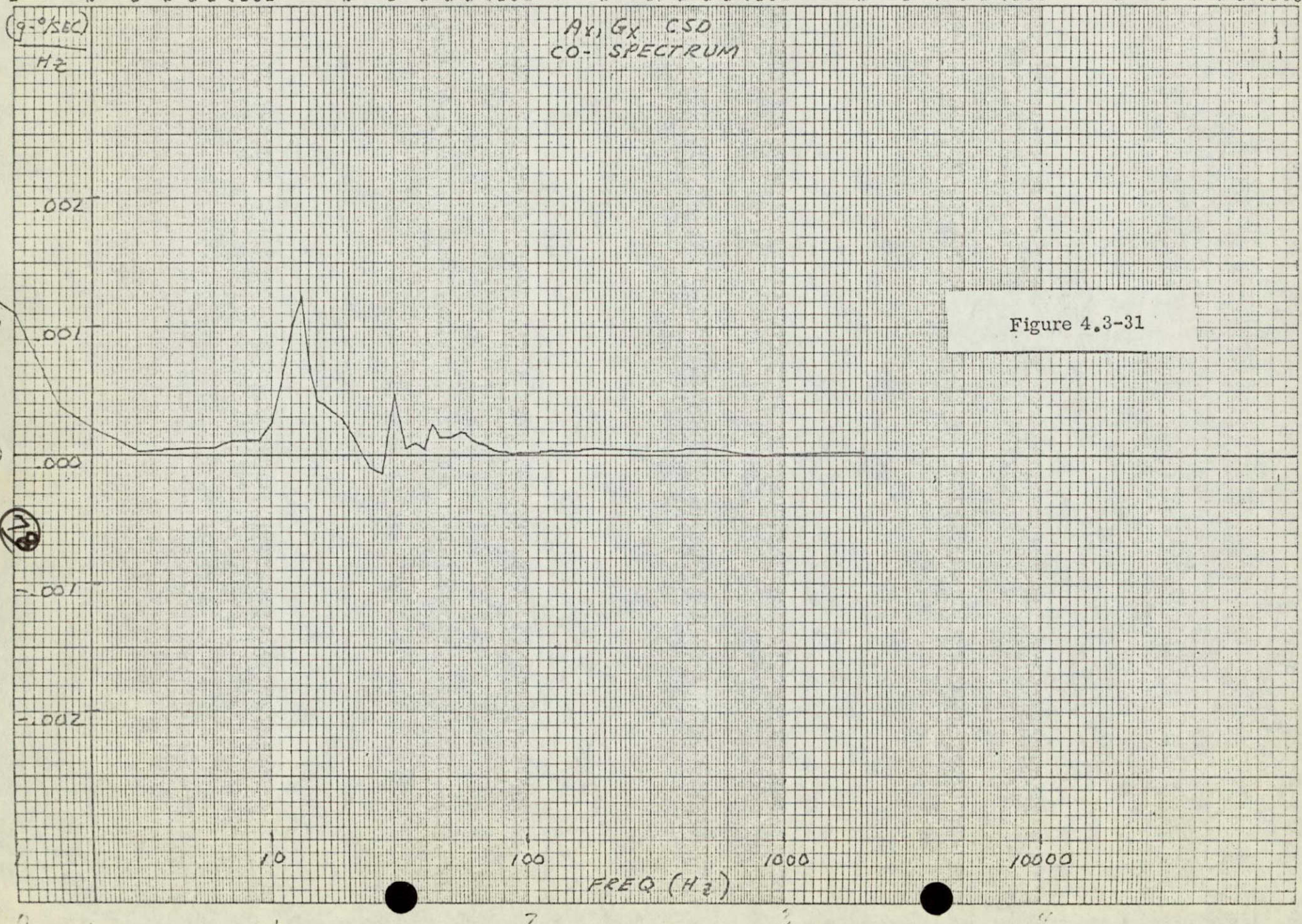

Figure 4.3-31

AX, GX QUAD

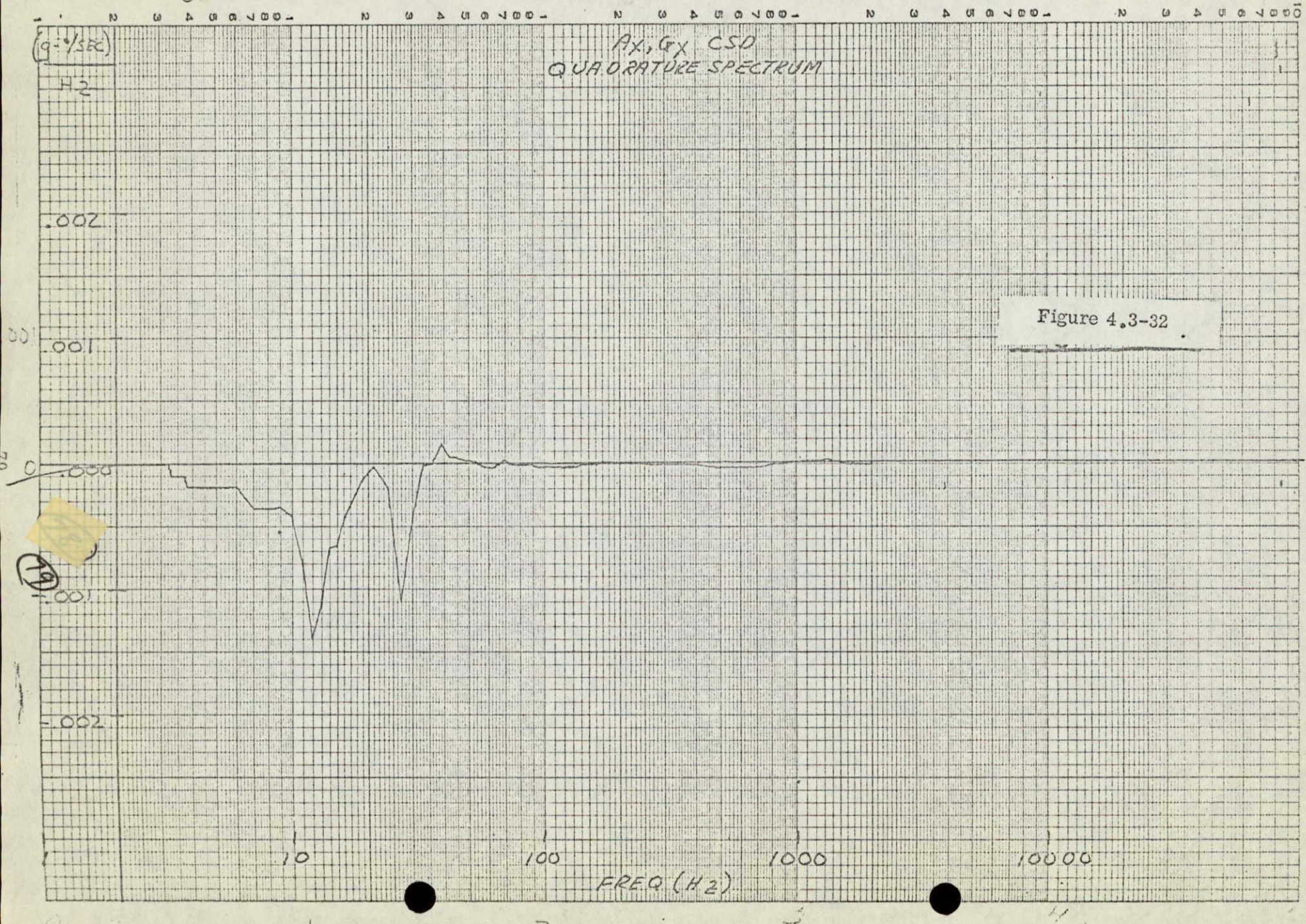

Figure 4.3-32

Ax, Gy
CO

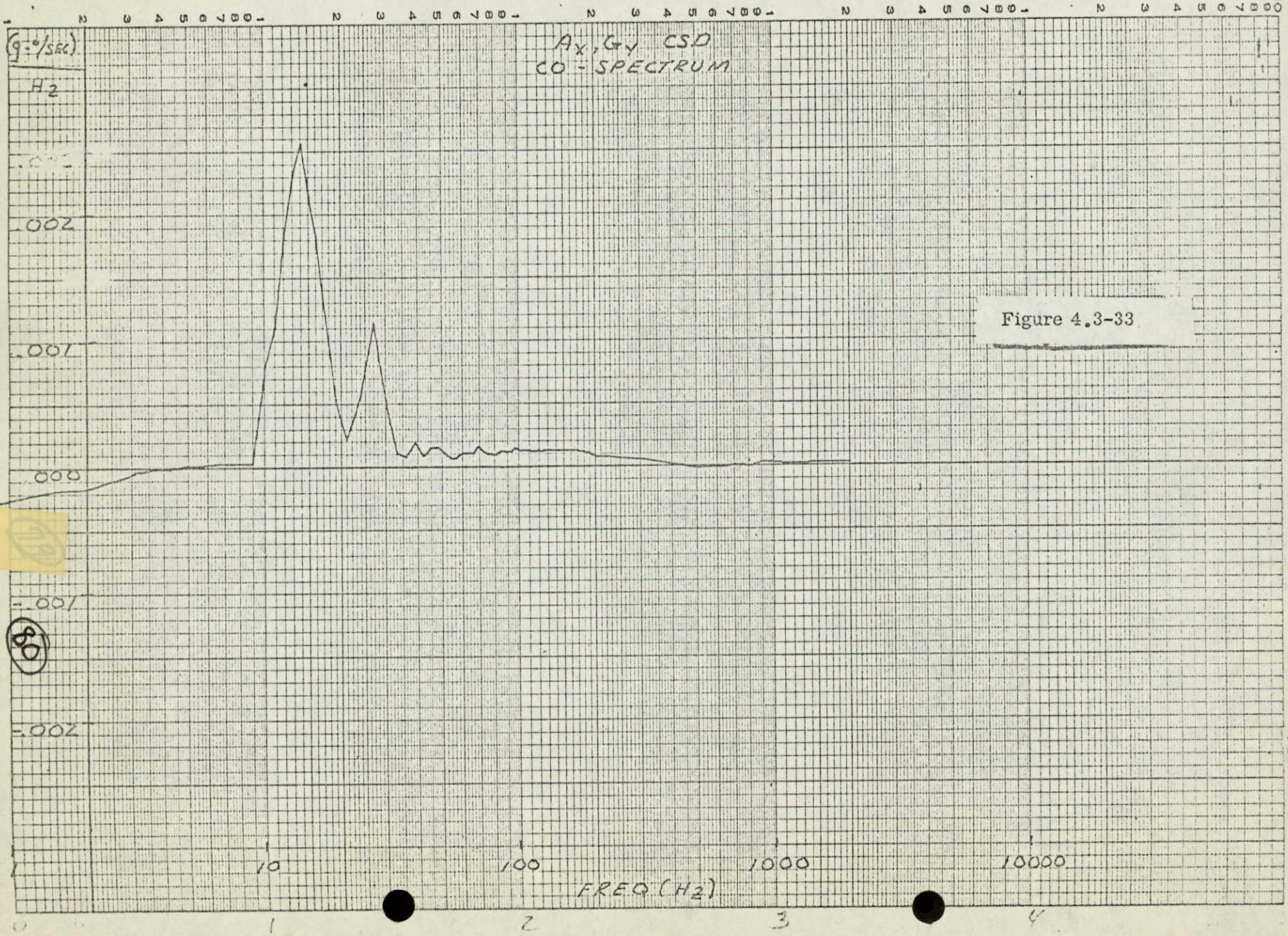

Figure 4.3-33

Ax, Gy
QUAD

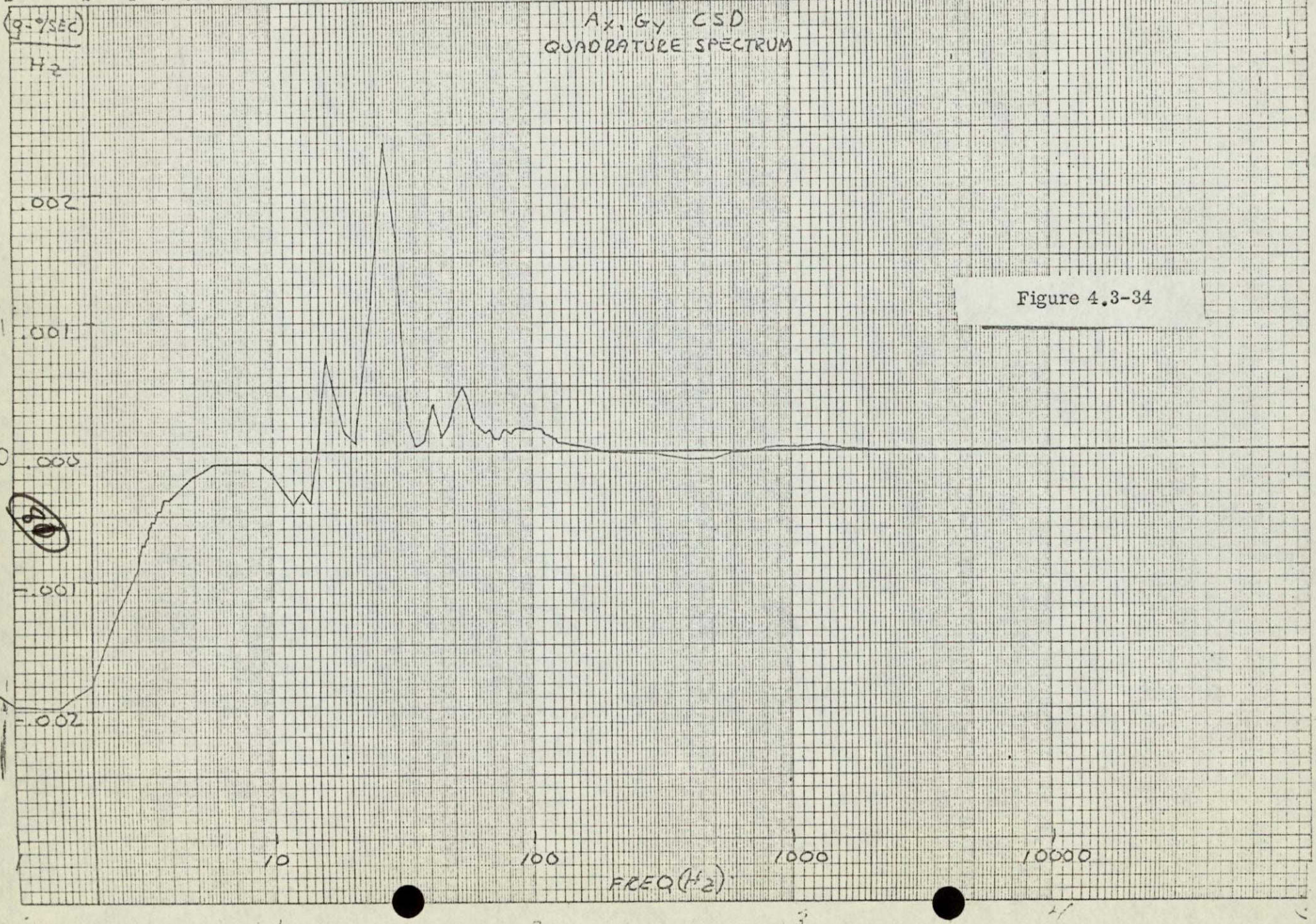

Figure 4.3-34

Ax, Gz
CO

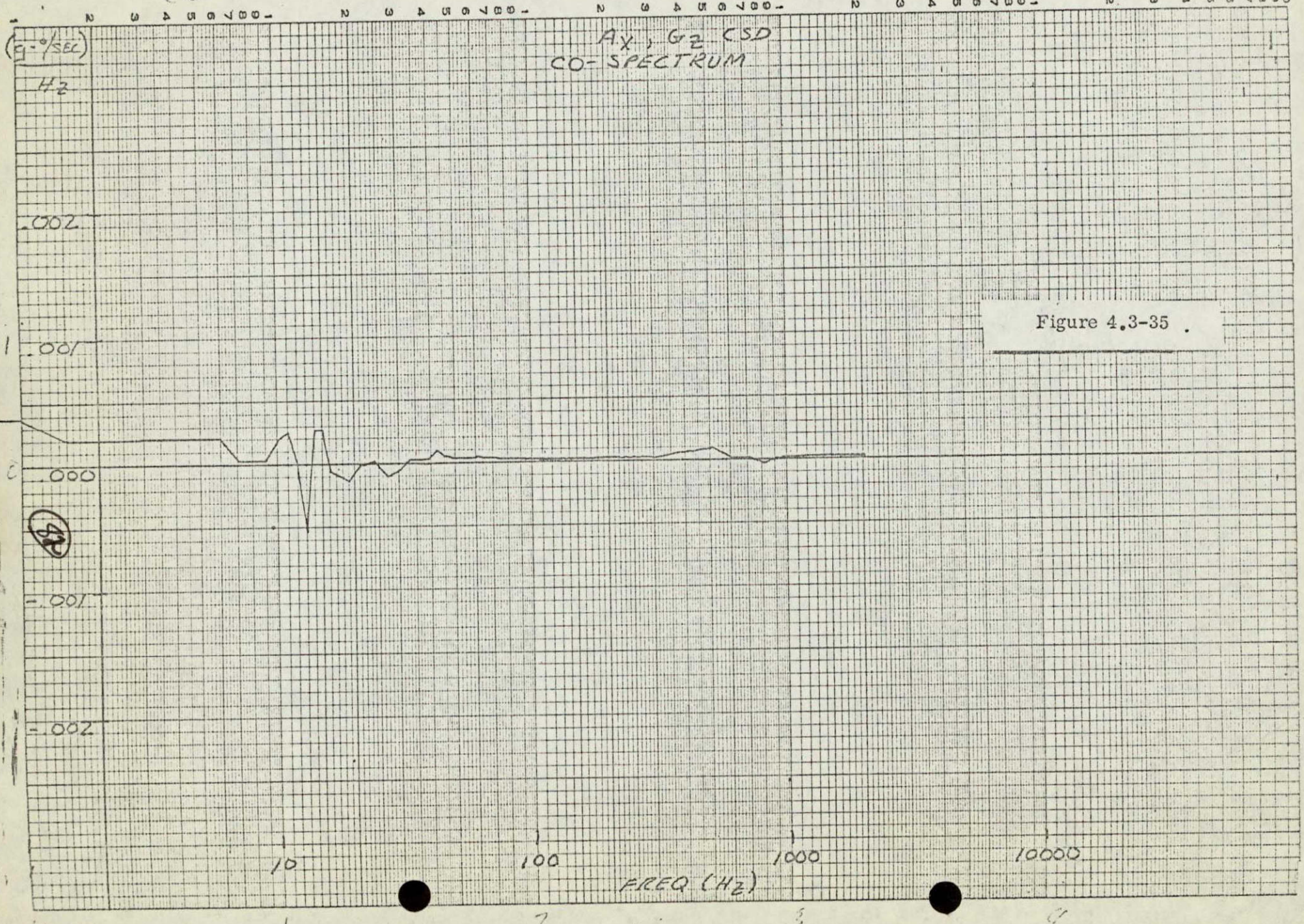

Figure 4.3-35

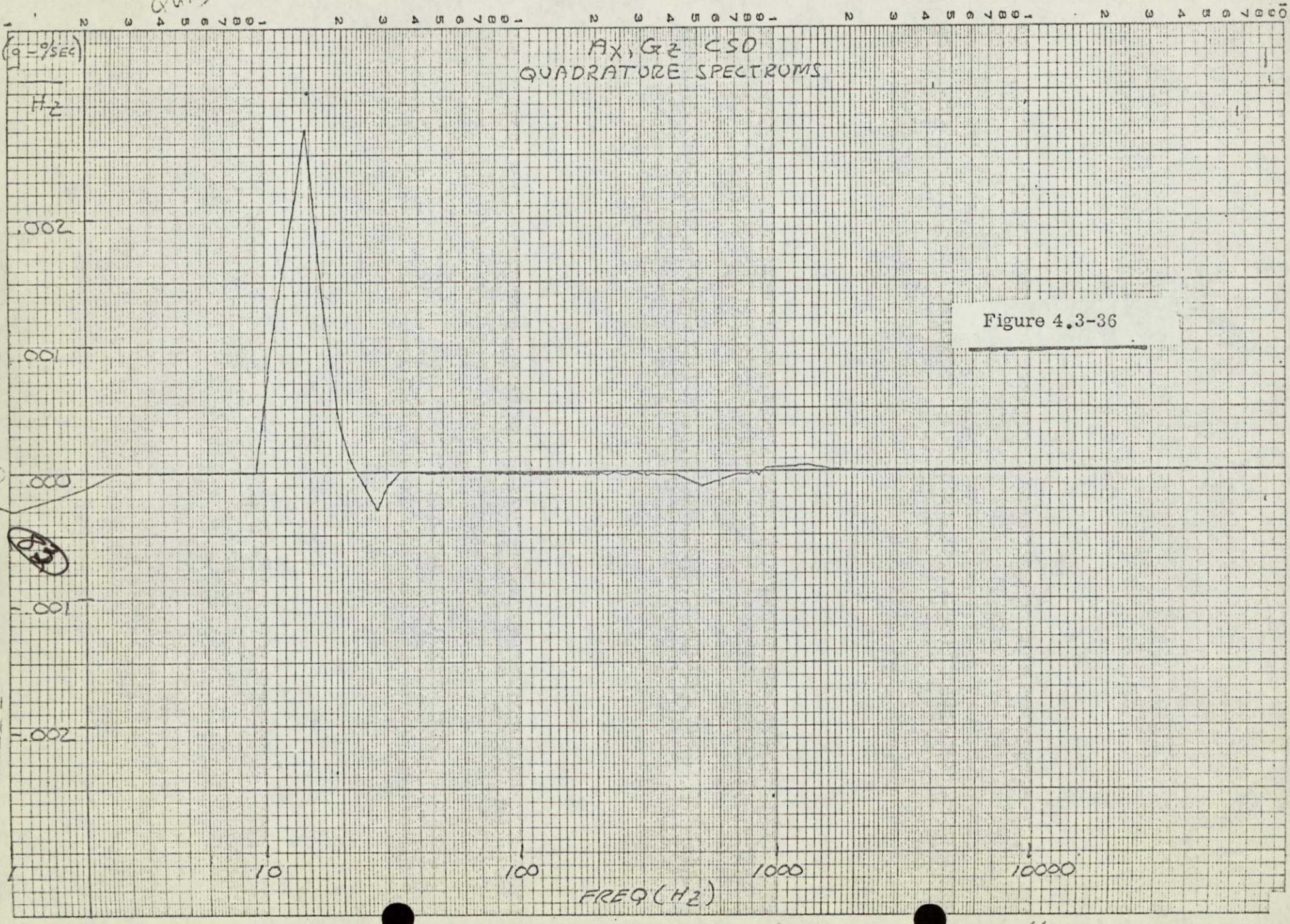

Figure 4.3-36

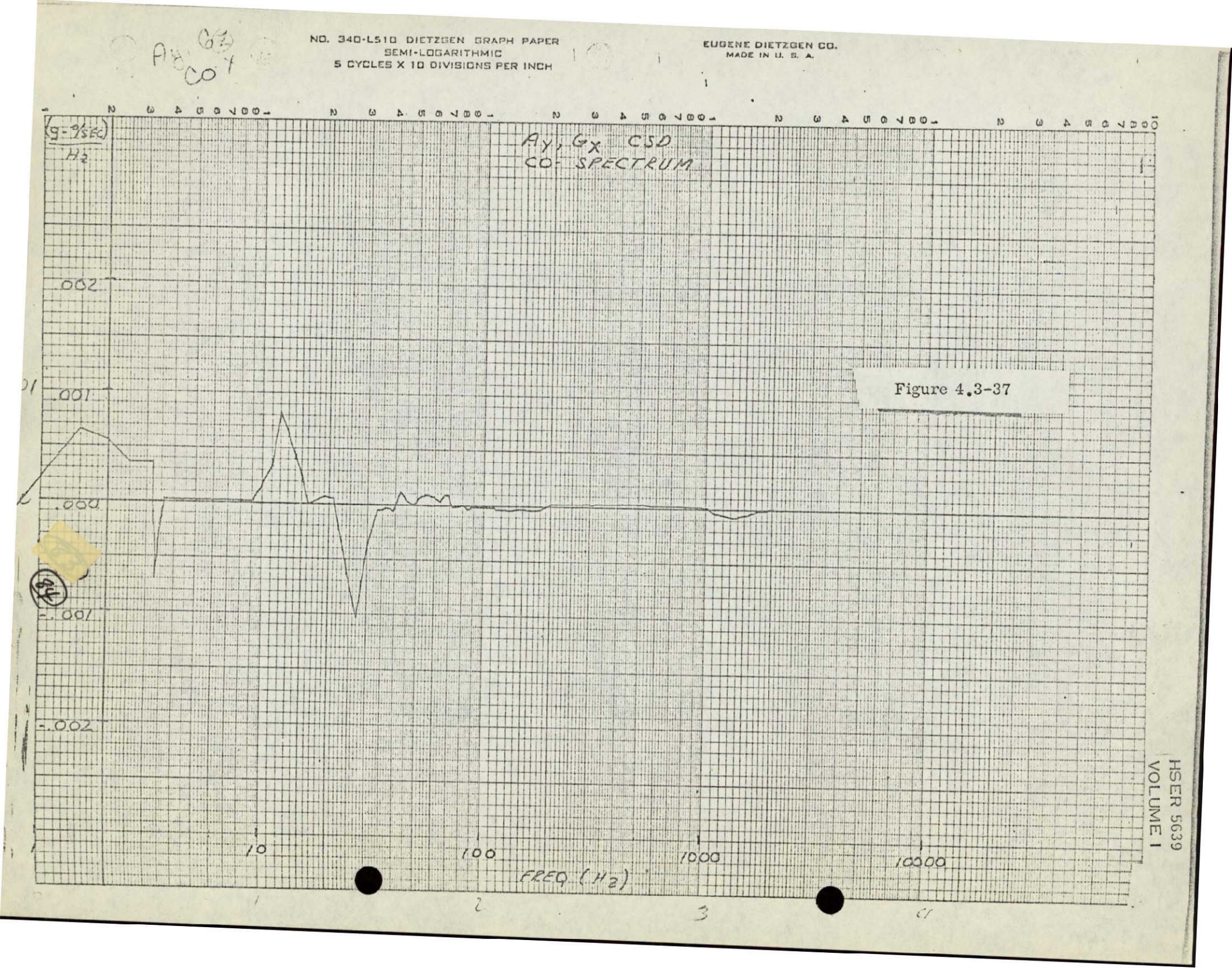
NO. 340-L510 DIETZGEN GRAPH PAPER
SEMI-LOGARITHMIC
5 CYCLES X 10 DIVISIONS PER INCH
EUGENE DIETZGEN CO.
MADE IN U. S. A.
Ay, Gx CSD
CO- SPECTRUM
(g-%SEC)
H2
.002
.001
.000
-.001
-.002
10
100
1000
10000
FREQ (H2)

Figure 4.3-37

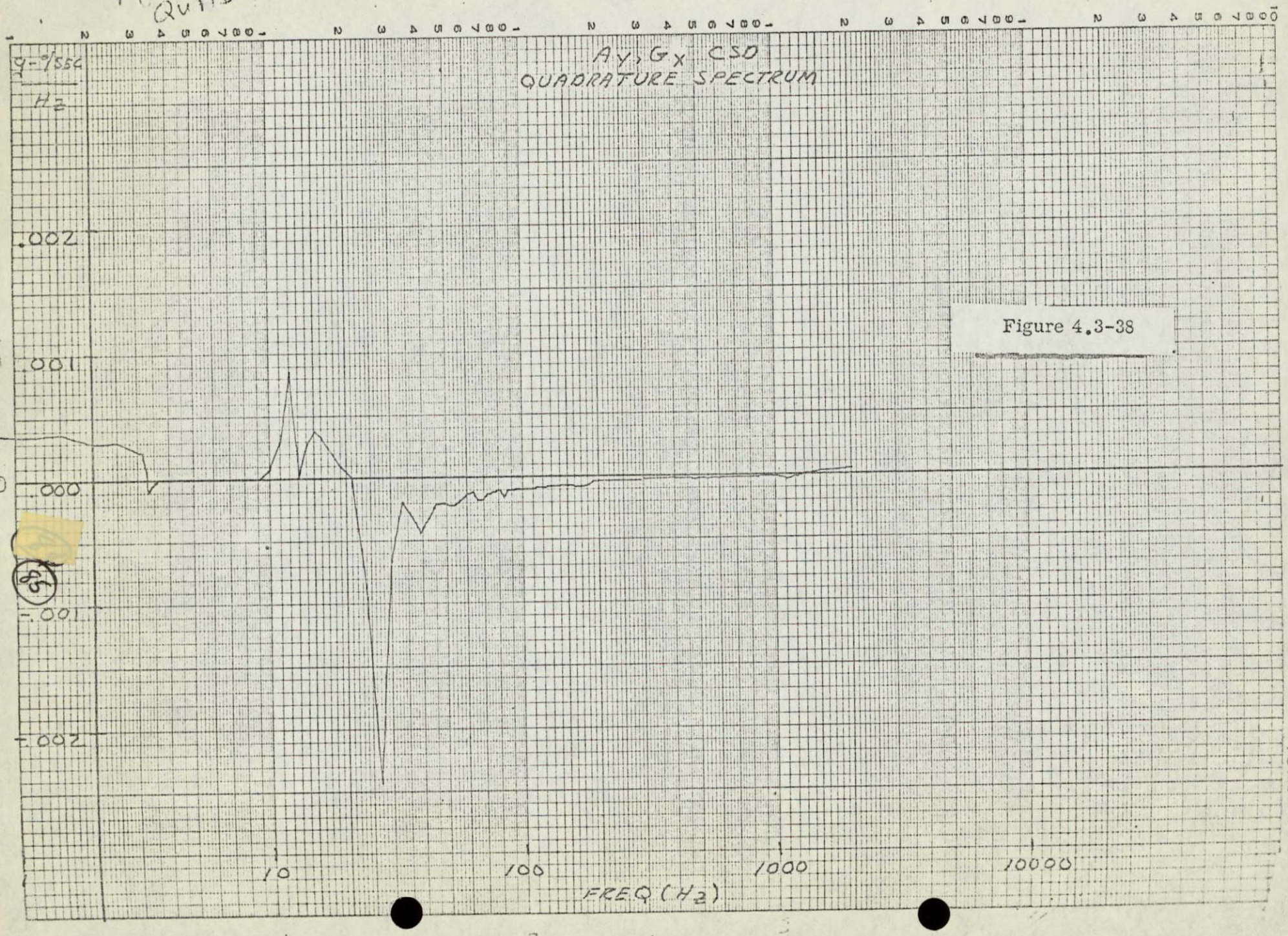

Figure 4.3-38

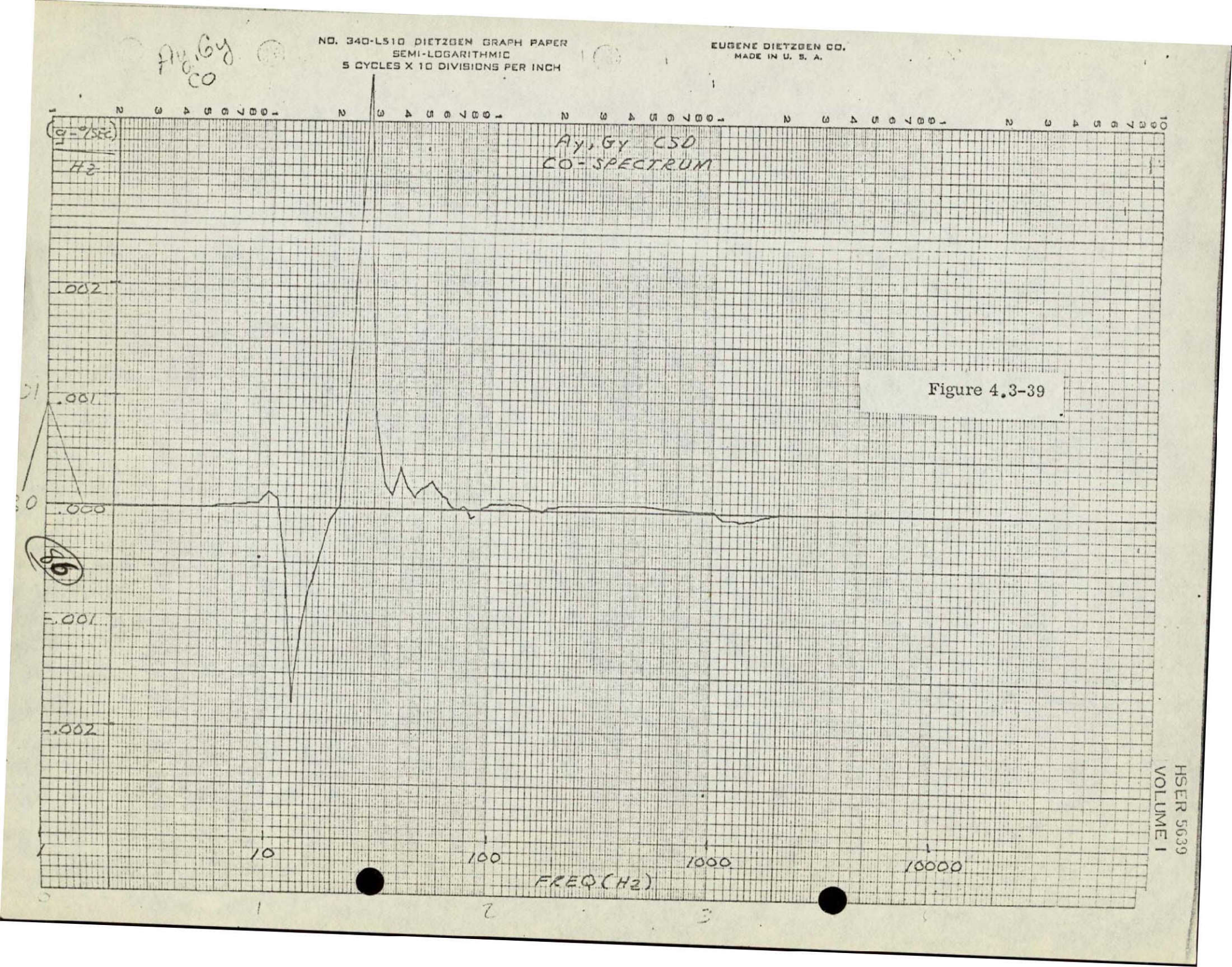
NO. 340-L510 DIETZGEN GRAPH PAPER
SEMI-LOGARITHMIC
5 CYCLES X 10 DIVISIONS PER INCH
EUGENE DIETZGEN CO.
MADE IN U. S. A.
Ay, Gy CSD
CO-SPECTRUM
.002
.001
.000
-.001
-.002
10
100
1000
10000
FREQ (Hz)

Figure 4.3-39

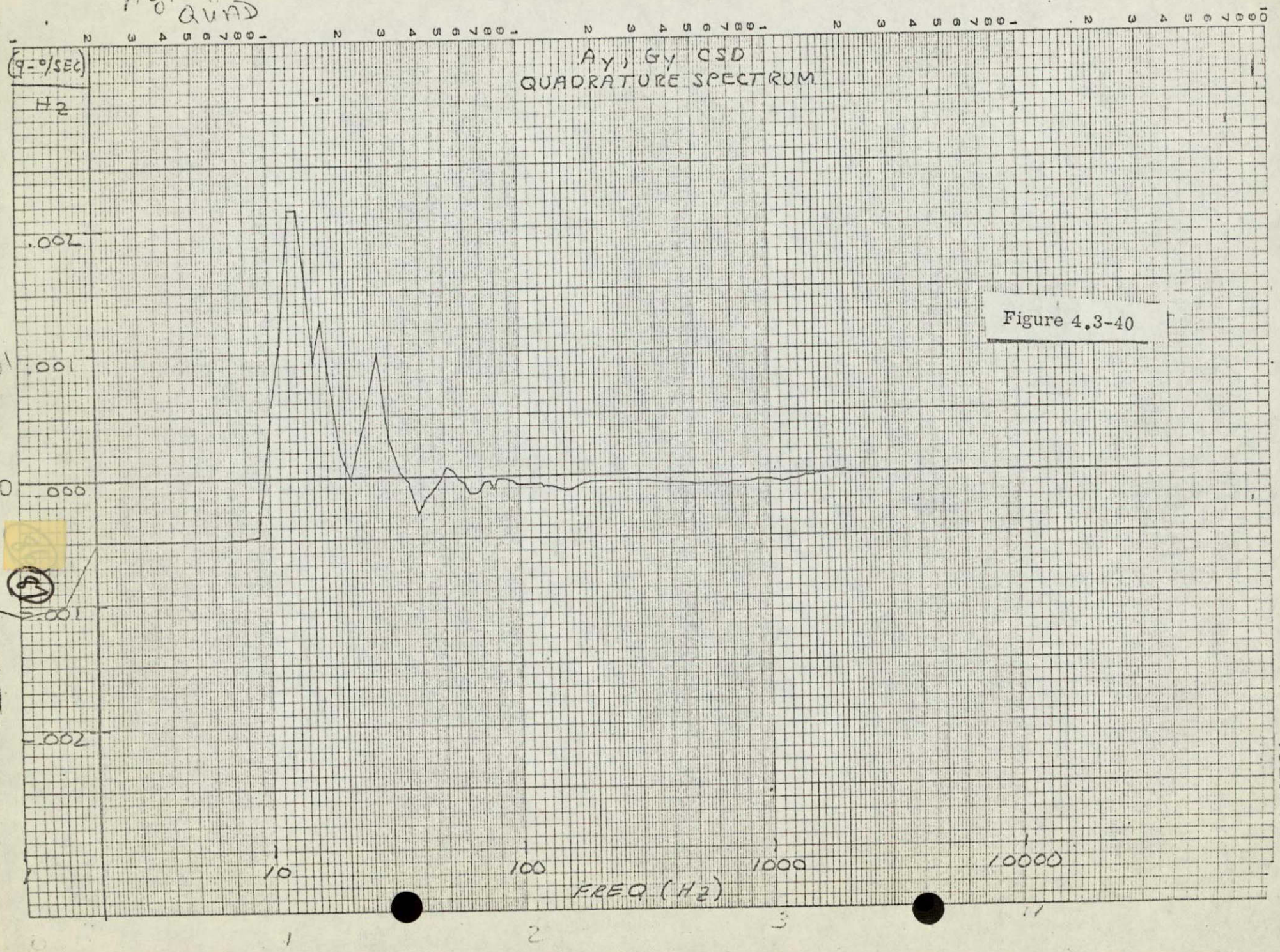

Figure 4.3-40

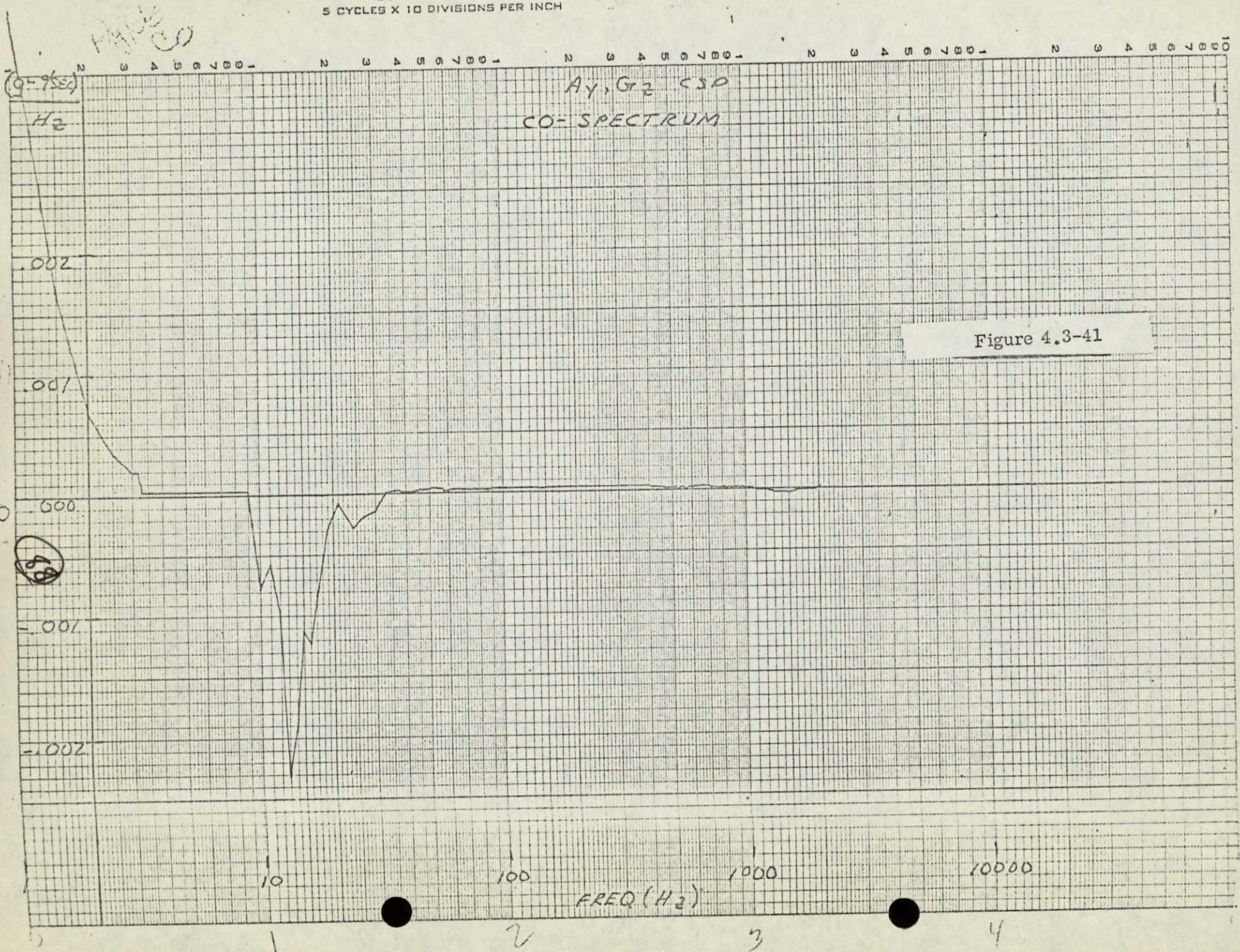

Figure 4.3-41

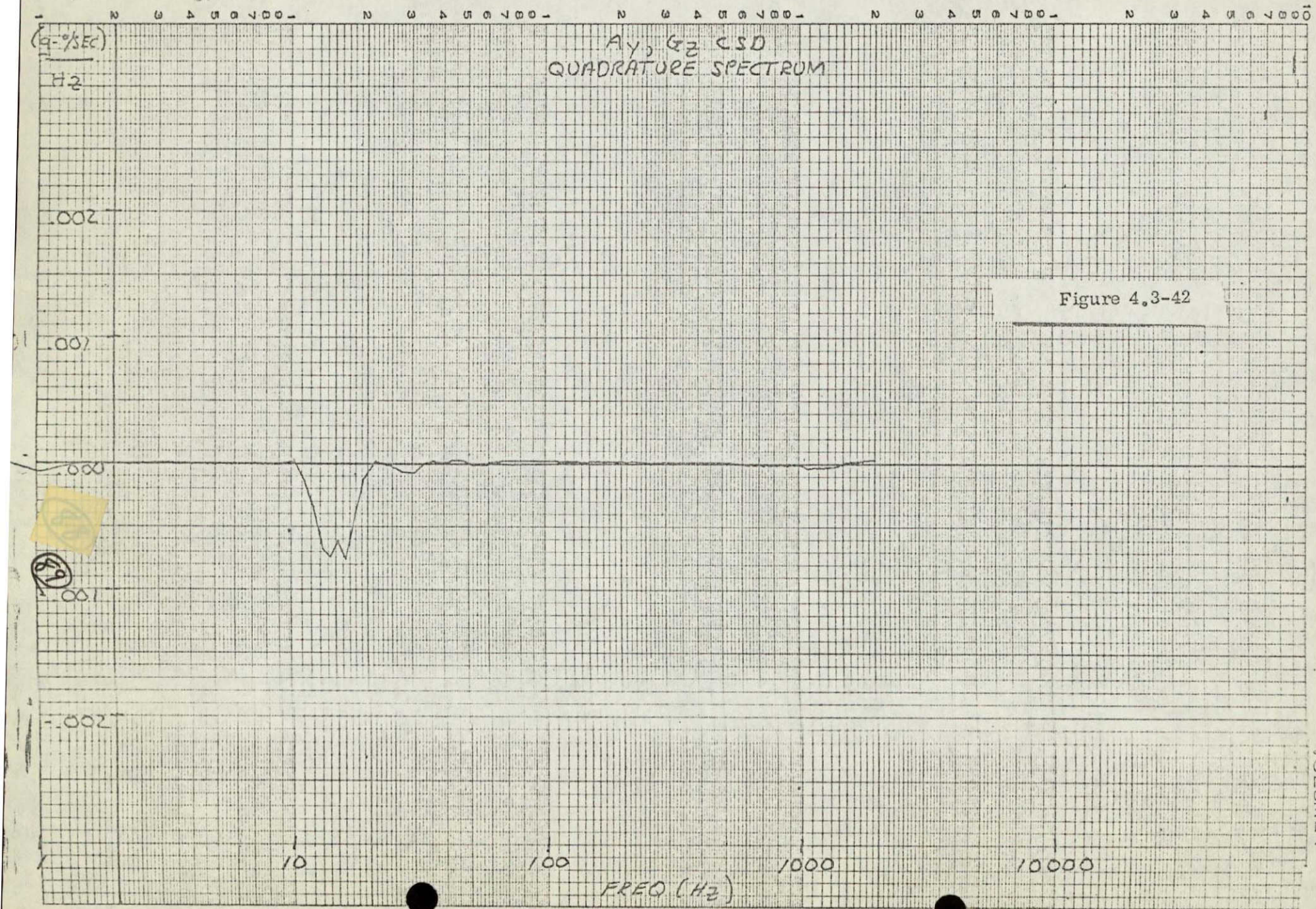

Figure 4.3-42

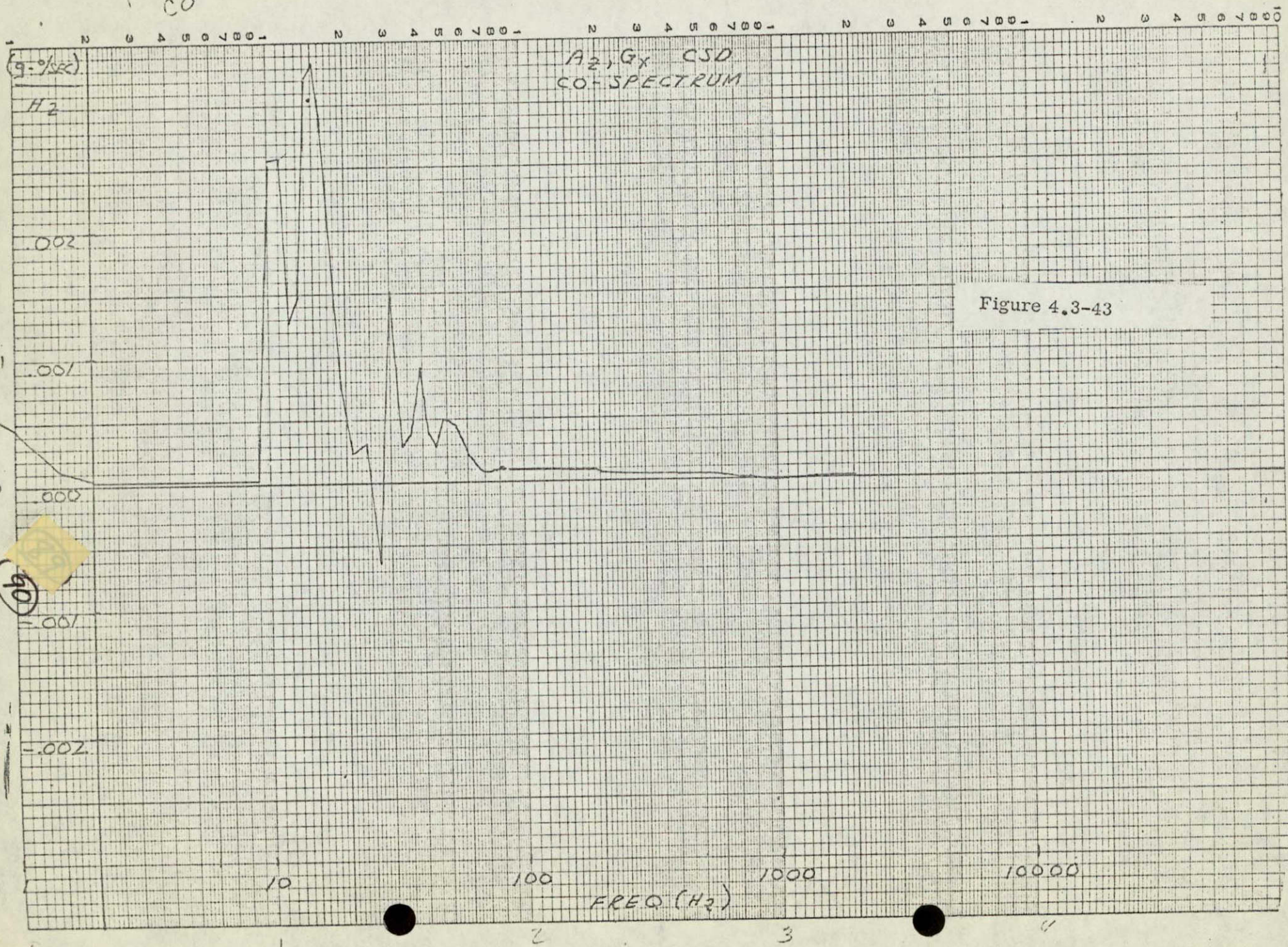

Figure 4.3-43

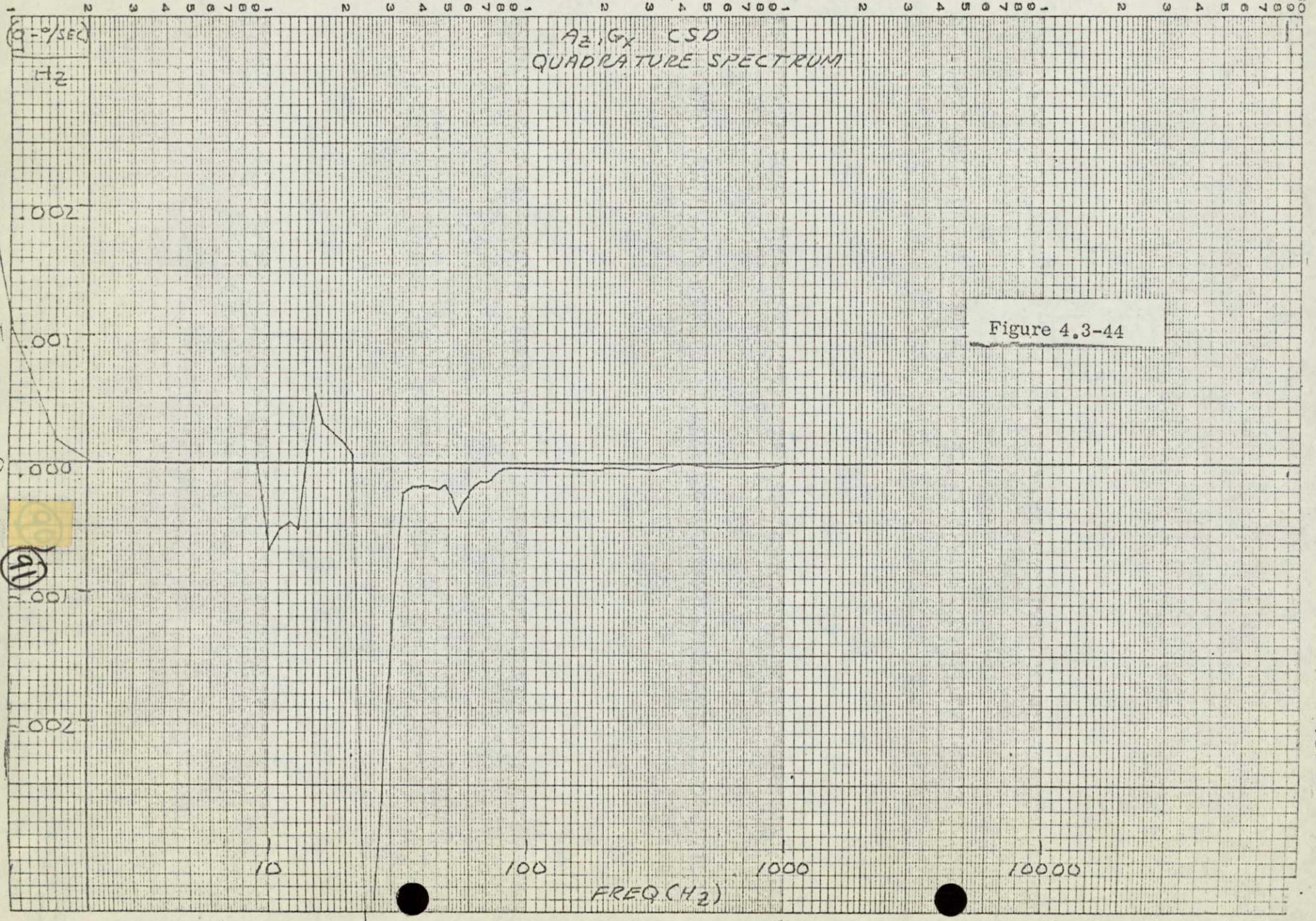

Figure 4.3-44

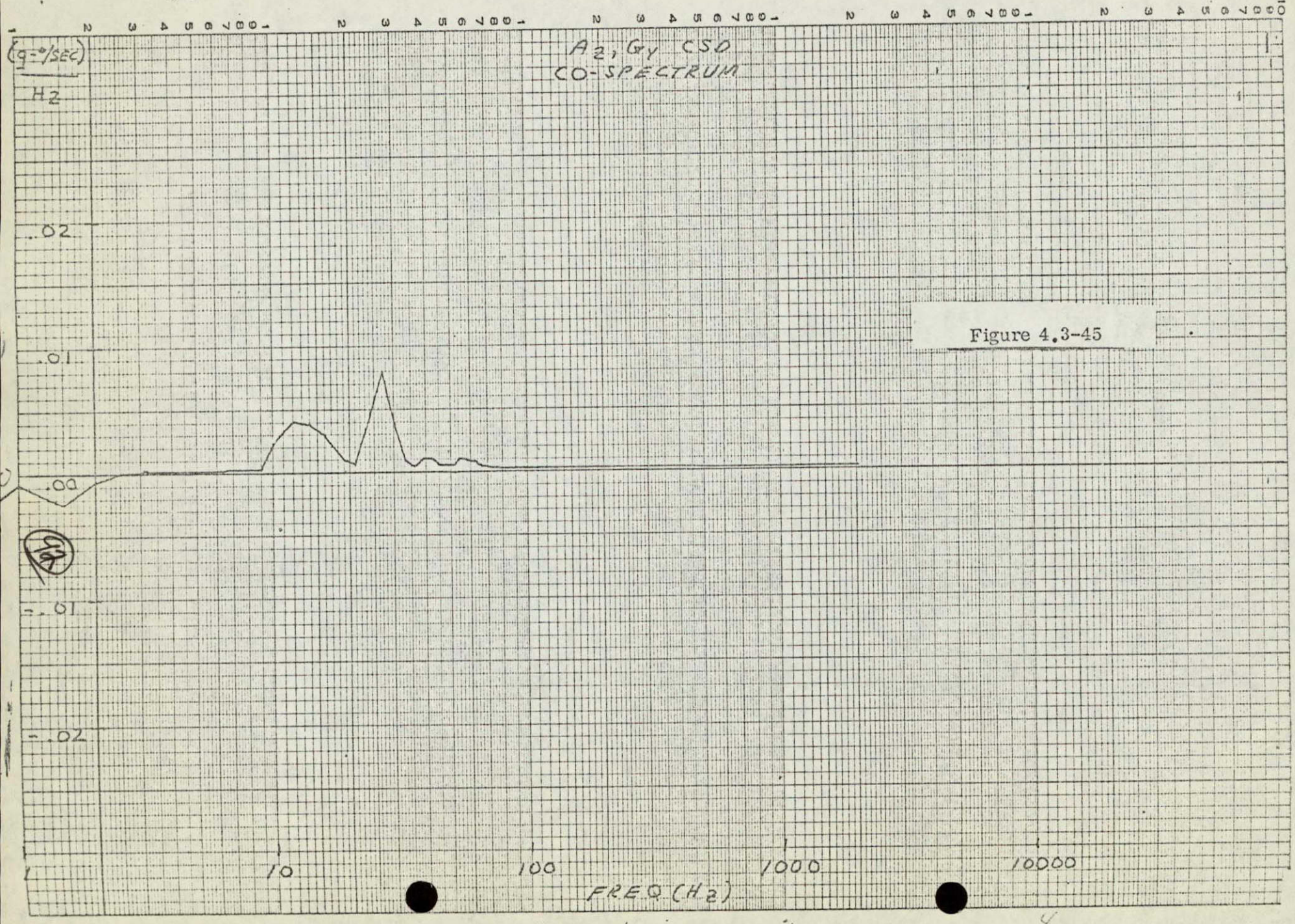

Figure 4.3-45

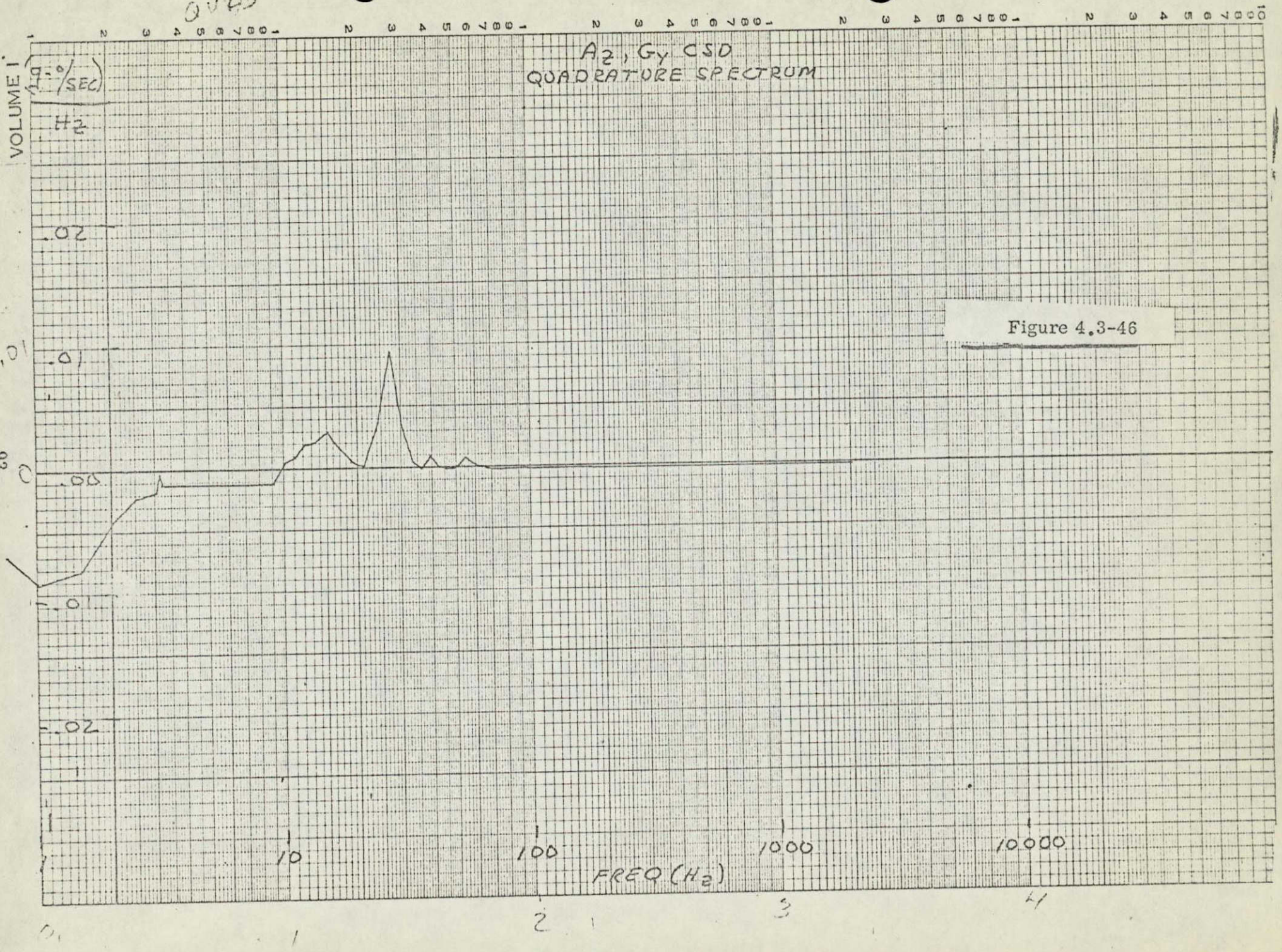

Figure 4.3-46

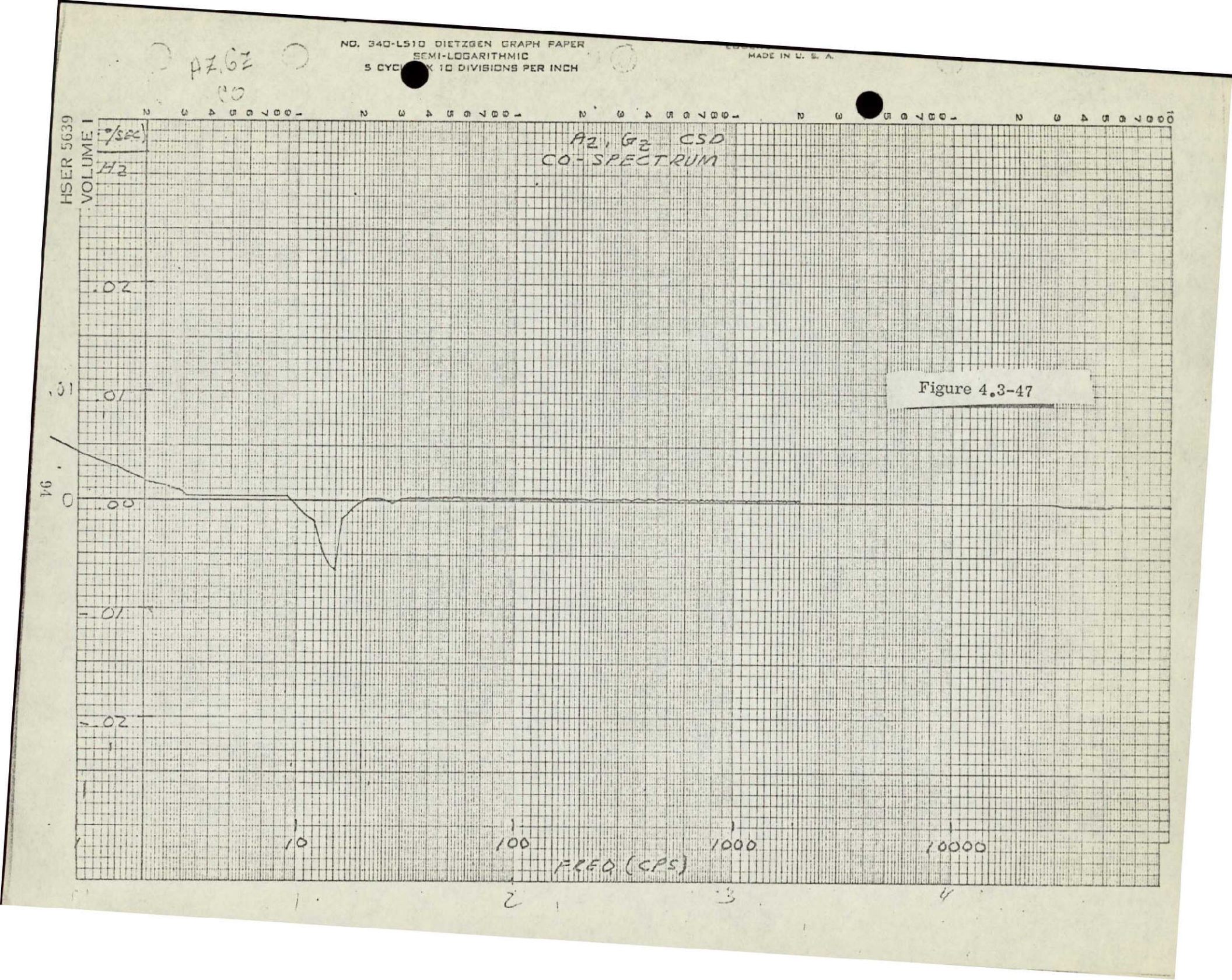
NO. 340-L510 DIETZGEN GRAPH PAPER
SEMI-LOGARITHMIC
MADE IN U. S. A.
HSER 5639
VOLUME I
A2, G2 CSD
CO-SPECTRUM
Figure 4.3-47
.02
.01
.00
-.01
-.02
10
100
1000
10000
FREQ (CPS)

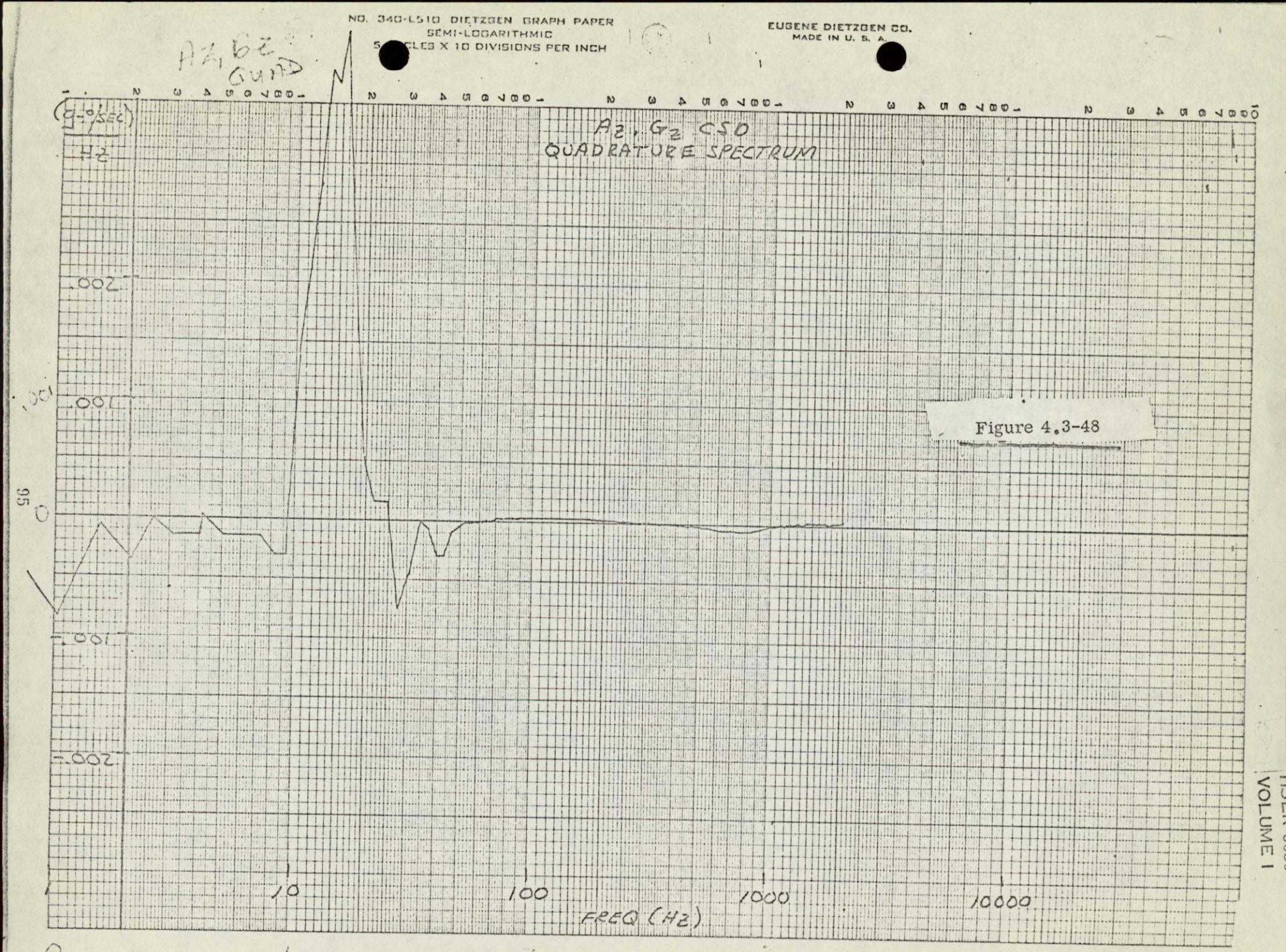
NO. 340-L510 DIETZGEN GRAPH PAPER
SEMI-LOGARITHMIC
EUGENE DIETZGEN CO.
MADE IN U. S. A.
A2, b2 GUARD
A2, G2 C50
QUADRATURE SPECTRUM
(g-o/sec)
Hz
.002
.001
0
-.001
-.002
10
100
1000
10000
FREQ (Hz)

Figure 4.3-48

DATA REDUCTION FLOW CHART

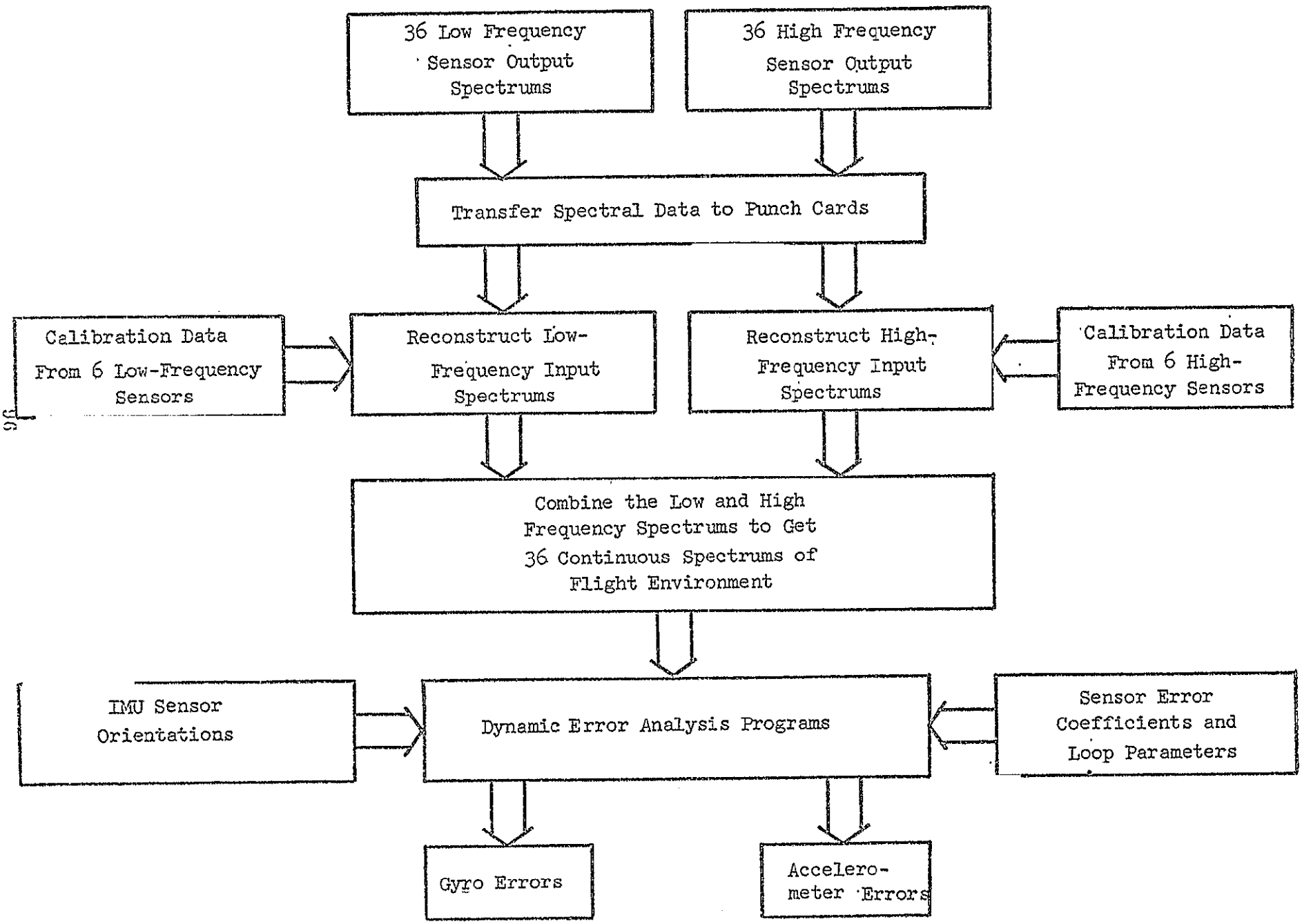

Figure 4.3-49

5.0 STRAPDOWN IMU DYNAMIC ERROR ANALYSIS

5.1 IMU Configuration

The evaluation of a strapdown IMU operating in the helicopter vibrational environment was accomplished by evaluating HSSC's Strapdown System for the forward flight condition. It is noted here that this IMU was not specifically designed for helicopter applications and thus, it does not reflect the optimum strapdown performance capability. Also, the errors presented here are applicable only to loops which exhibit linear operating characteristics for the environment, and are thus predictable for random-type vibrations.

The basic IMU sensor axes orientation relative to vehicle axes are shown in Figure 5.1-1. The individual sensor rebalance loops incorporate rate integrating gyros and pendulous accelerometers. Figure 5.1-2 presents the linearized block diagram for the complete sensor loop. Table 5.1-1 and 5.1-2 present the numerical values for the gyro and accelerometer loops, respectively, which will be used for this evaluation. Figures 5.1-3 and 5.1-4 present the closed loop frequency response characteristics for the gyro and accelerometer loops, respectively.

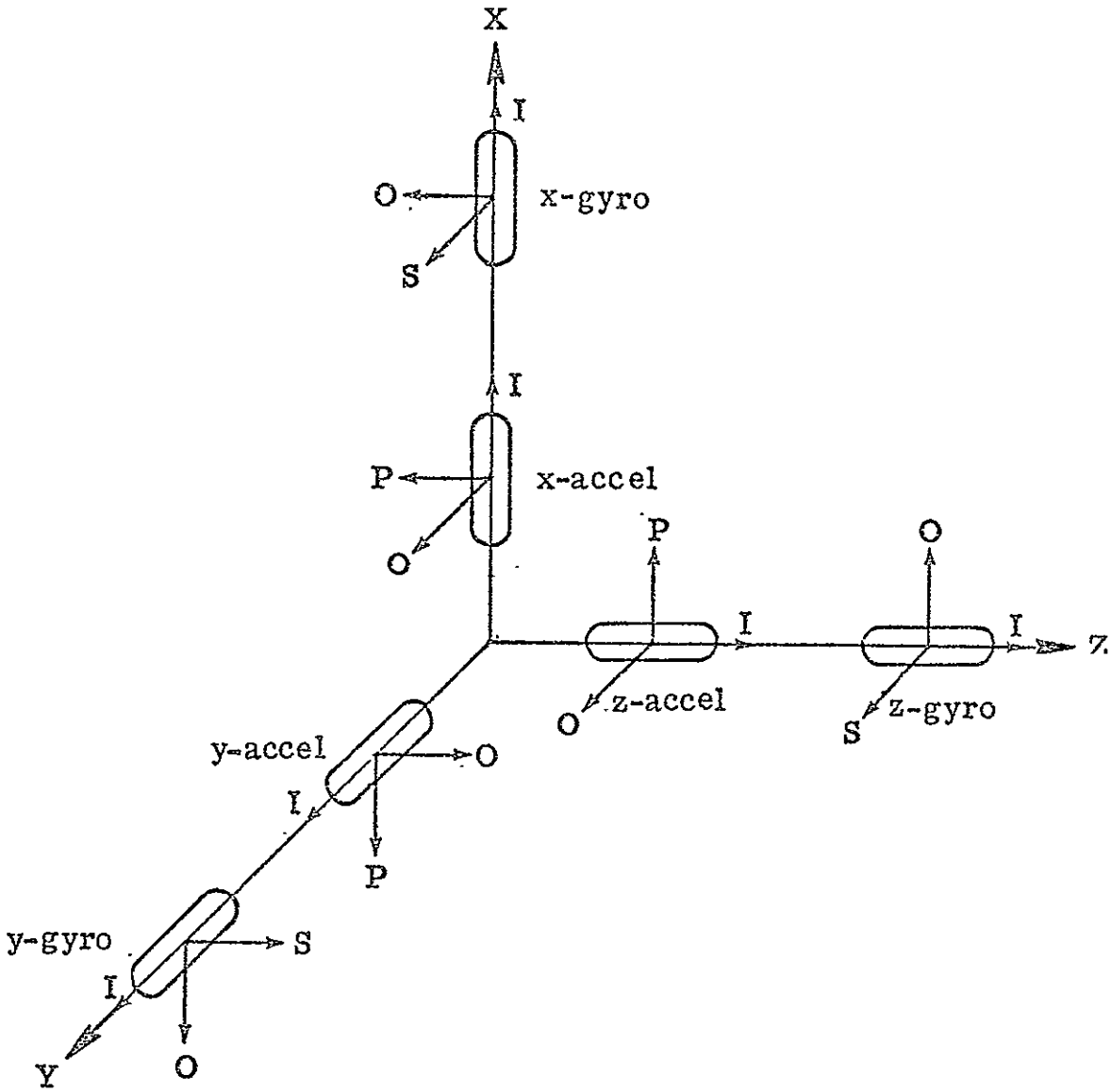

Fig 5.1-1

Gyro Design #15
Accelerometer Design #15

Sensor/Package Axes Orientation

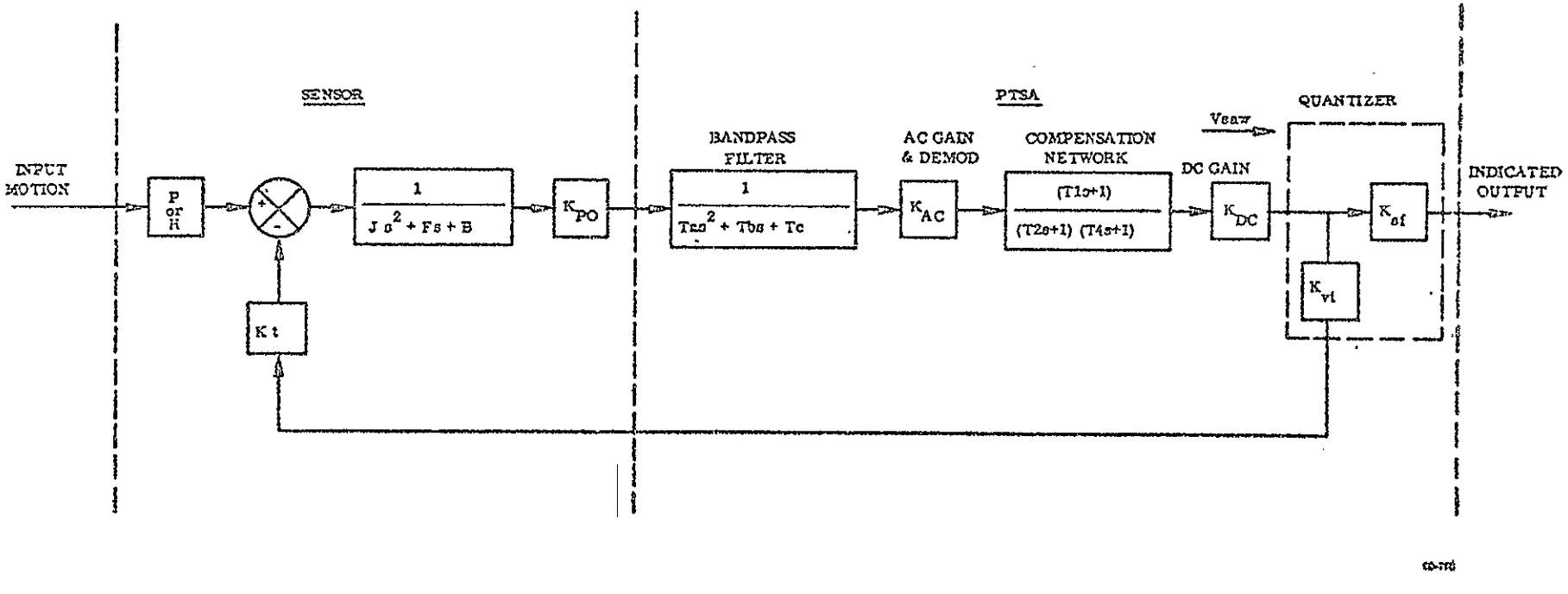

Figure 5.1-2 Linearized Sensor Loop Block Diagram

Table 5.1-1

LINEARIZED GYRO LOOP PARAMETERS

(Design No. 15)

Gyro			PTSA		
H	$= 2.5 \times 10^{+5}$	dy-cm/rad/sec.	Kac	= .442.	V DC/V_{rms}
J	= 399.	gm-cm^2	Kdc	= 33.	V DC/V DC
F	$= 1.38 \times 10^{+6}$	dy-cm-sec.	Ksf	= .098	$\frac{rad}{sec}$/V (max. range/V_{SAW})
B	= .1	dy-cm/rad.	Kvi	= 22.	ma/V (max. I/V_{SAW})
Kpo	= 70.	mv_{rms}/millirad.	V_{SAW}	= 5.0	V_{peak} (Effective)
Kt	= 1110.	dy-cm/ma.	Max. I	= 110.	ma
Max. Range	= 0.49	rad./sec.			

(Compensation Network)			(Bandpass Filter)	
T_1	= 0.0143	sec.	Center Frequency	=8.0 k Hz
T_2	= 1.0	sec.	Ta	$.634 \times 10^{-8}$ sec.2
T_4	= 0.00143	sec.	Tb	$.1125 \times 10^{-3}$sec.
T_6	= 0.0	sec.	Tc	= 1.0

Table 5.1-2

LINEARIZED ACCELEROMETER LOOP PARAMETERS

(Design No. 15)

Accelerometer			PTSA		
P = 1100.	dy-cm/g		Kac = 153.	V_{DC}/V_{rms}	
J = 14.	$gm\text{-}cm^2$		Kdc = 33.	V DC/V DC	
F = 96000.	dy-cm-sec.		Ksf = .62	g/V (max. range/V_{SAW})	
B = 1310.	dy-cm/rad.		Kvi = .62	ma/V (max. I/V_{SAW})	
Kpo = 10.	mv_{rms}/millirad.		V_{SAW} = 5.0	V_{peak} (Effective)	
Kt = 1100.	dy-cm/ma.		Max. I = 3.1	ma	
Max. Range = 3.1	g				

(Compensation Network)		(Bandpass Filter)
T_1 = 0.0	sec.	Center Frequency = 8.0 k Hz
T_2 = 0.00196	sec.	Ta ,634 x 10^{-8} $sec.^2$
T_4 = 0.0	sec.	T_b .1125 x 10^{-3} sec.
T_6 = 0.0	sec.	Tc = 1.0

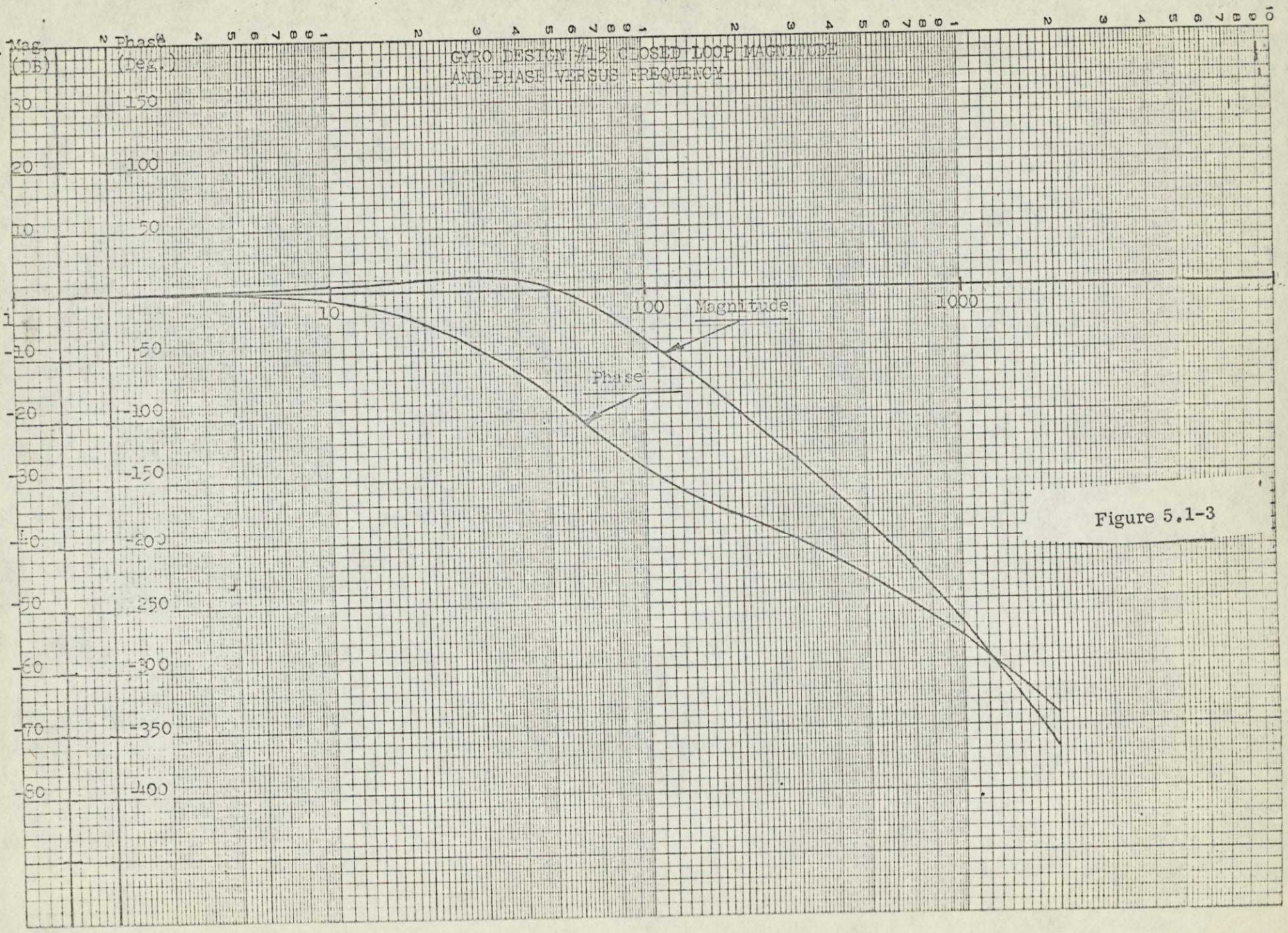

Figure 5.1-3

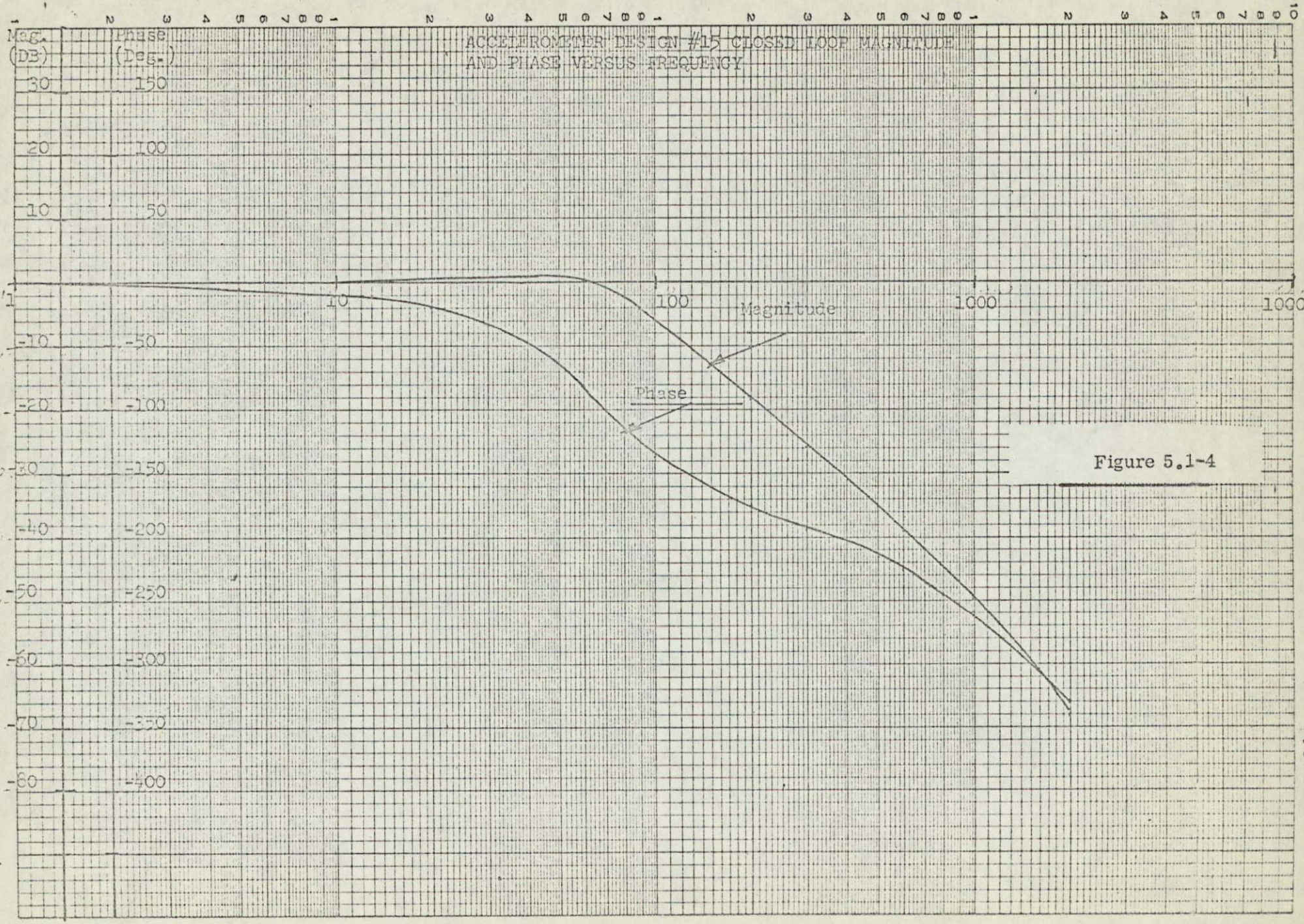

Figure 5.1-4

5.2 Dynamic Error Model

The strapdown IMU performance was predicted using HSSC's current error model. This model includes the following error sources:

Single Channel

Gyro - Spin Input Rectification
Spin Output Rectification
Anisoinertia
Anisoelastic
Scale Factor Asymmetry

Accel - Vibropendulous
Anisoinertia
Non-Linear g^2
Scale Factor Asymmetry

System

Coning
Sculling

The model also assumes a flight computer with a 50 Hz sampling rate with a (sin x/x) attenuation characteristic. An alternate evaluation using a quadratic characteristic was also made. Here $x = (2\pi f/f_c)^*$

Table 5.2-1 summarizes the figures and error coefficients which were used for the analysis. These are presented in Figures 5.2-1 through 5.2-14.

The detail description of the mechanism for each of the single channel error sources will not be presented here, since they are readily available in the current literature. Figure 5.2-15 is a block diagram for the system errors and is presented here to aid in the understanding of system errors.

The equations which were used to compute the dynamic errors in terms of the random environmental spectrum characteristics are presented in the following tables:

Table 5.2-2	Single Channel Gyro Errors
Table 5.2-3	Single Channel Accelerometer Errors
Table 5.2-4	System Errors

Table 5.2-5 presents the nomenclature used for the terms of the equations.

* f_c = The computer sampling frequency.

TABLE 5.2-1

Summary of Dynamic Error Coefficients

Gyro Design #15	
SIIP, Spin-Input Rectification (In-Phase)	Figure 5.2-1
SIOP, Spin-Input Rectification (Out-of-Phase)	Figure 5.2-2
σ $\bar{c}_{IS}$, Anisoinertia (In-Phase)	Figure 5.2-3
σ q_{I-S}, Anisoinertia (Out-of-Phase)	Figure 5.2-4
SOIP, Spin-Output Rectification (In-Phase)	Figure 5.2-5
SOOP, Spin-Output Rectification (Out-of-Phase)	Figure 5.2-6
σ SF^W, Non-Linear Scale Factor Rectification	0.143 ($^\circ$/hr)/deg/sec RMS out-of-loop
A_{IS}, Anisoelastic - Major	0.06 deg/hr/g^2 PK-IA-SA
A_{OS}, Anisoelastic - Minor	0.006 deg/hr/g^2 PK-OA-SA
AW_{I-O}, Input-Output Wheel Retainer Resonance	Figure 5.2-7
AW_{O-S}, Output-Spin Wheel Retainer Resonance	Figure 5.2-8
AW_{I-S}, Input-Spin Wheel Retainer Resonance	Figure 5.2-9
AW_{I-I}, Input-Input Wheel Retainer Resonance	Figure 5.2-10
AW_{S-S}, Spin-Spin Wheel Retainer Resonance	Figure 5.2-11
AW_{O-O}, Output-Output Wheel Retainer Resonance	Figure 5.2-12
Accelerometer Design #15	
VIP, Vibropendulous Rectification (In-Phase	Figure 5.2-13
VOP, Vibropendulous Rectification (Out-of-Phase)	Figure 5.2-14
σ IP, Accelerometer Anisoinertia	1.5 $\mu g/(deg/sec)^2$ PK-IA-PA
σ g^2, Non-Linear g^2	10 $\mu g/g^2$ RMS-IA
σ SF^A, Non-Linear Scale Factor Rectification	4.0 $\mu g/g$ RMS Out-of-loop

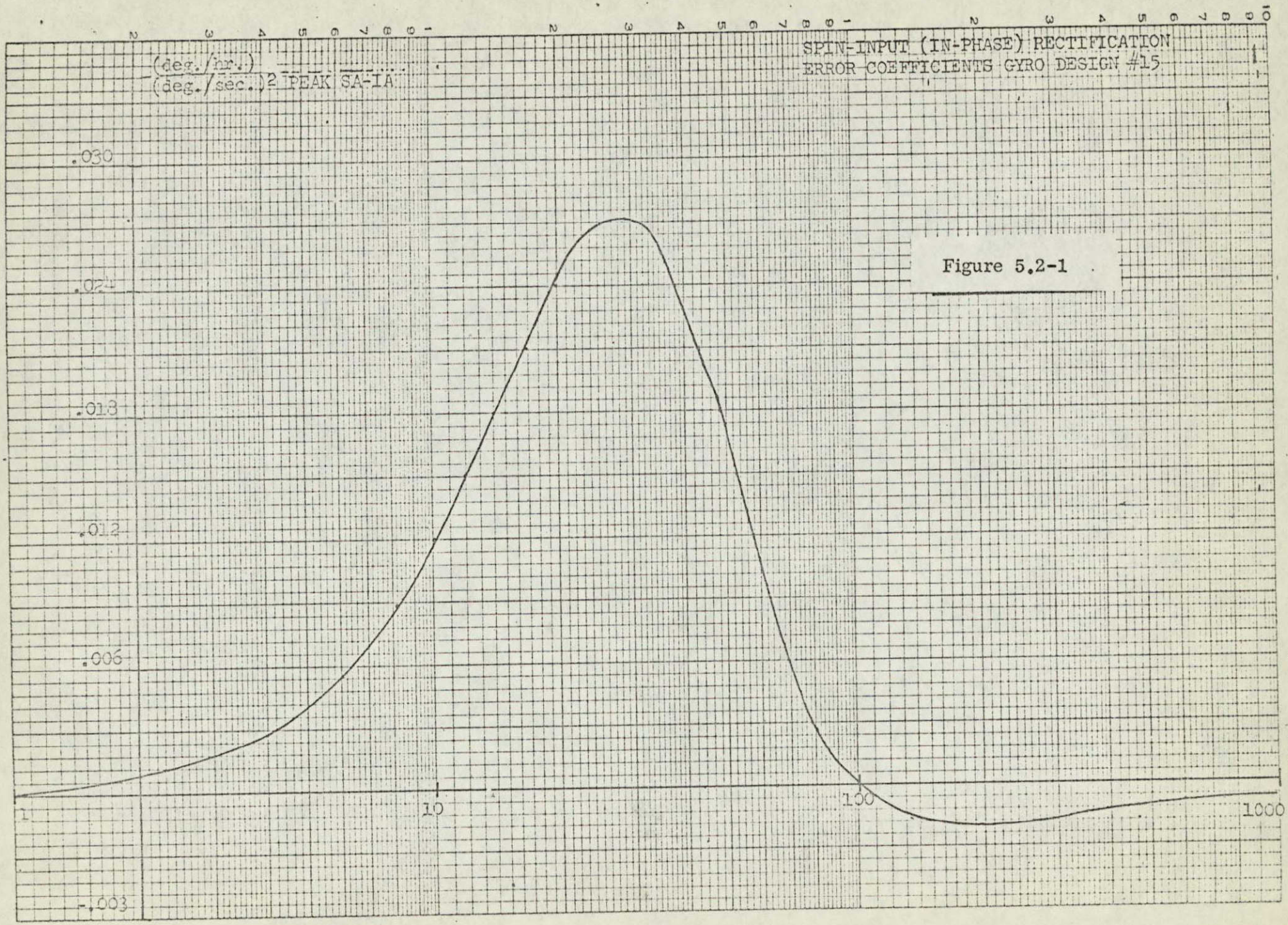

Figure 5.2-1

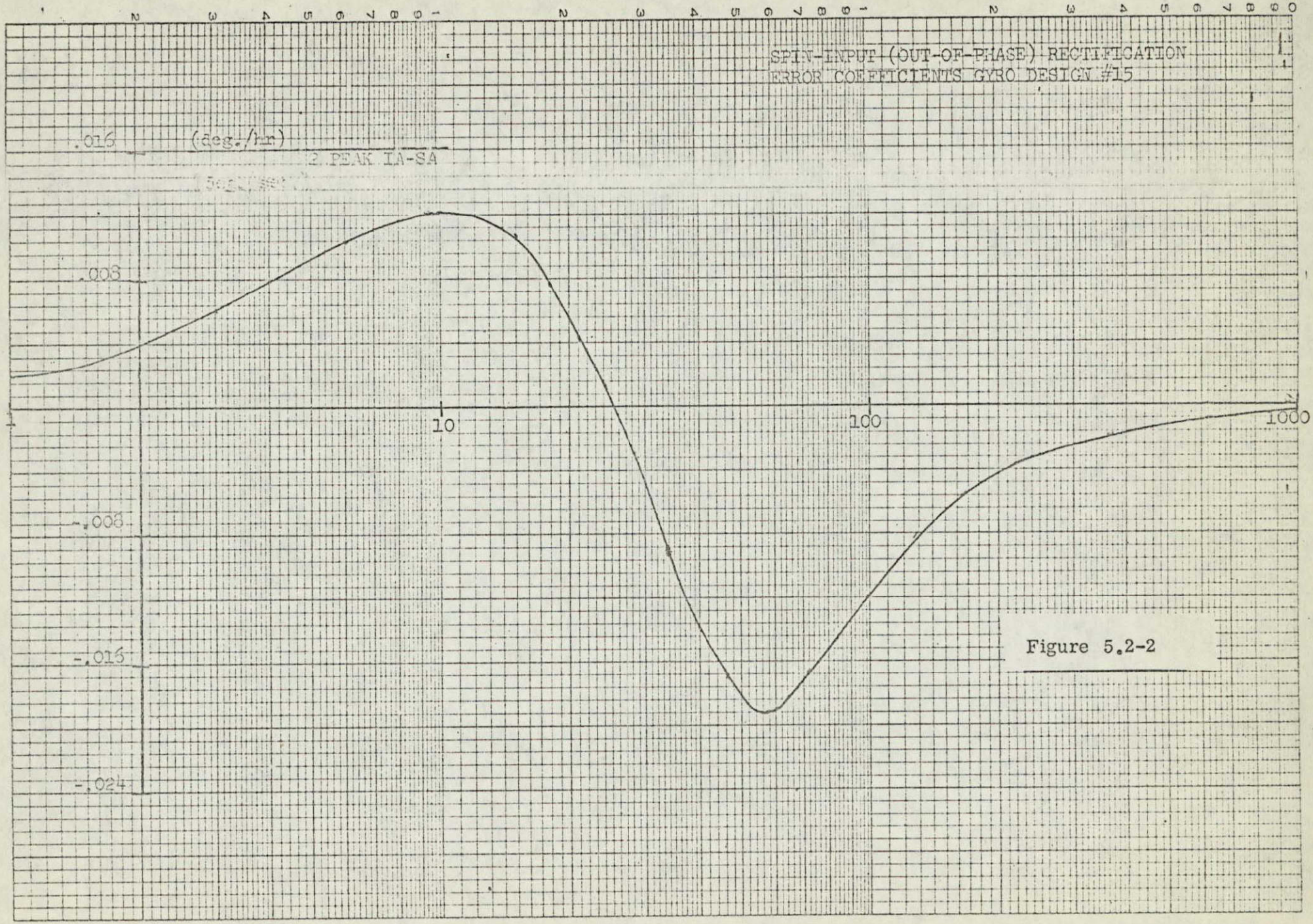

Figure 5.2-2

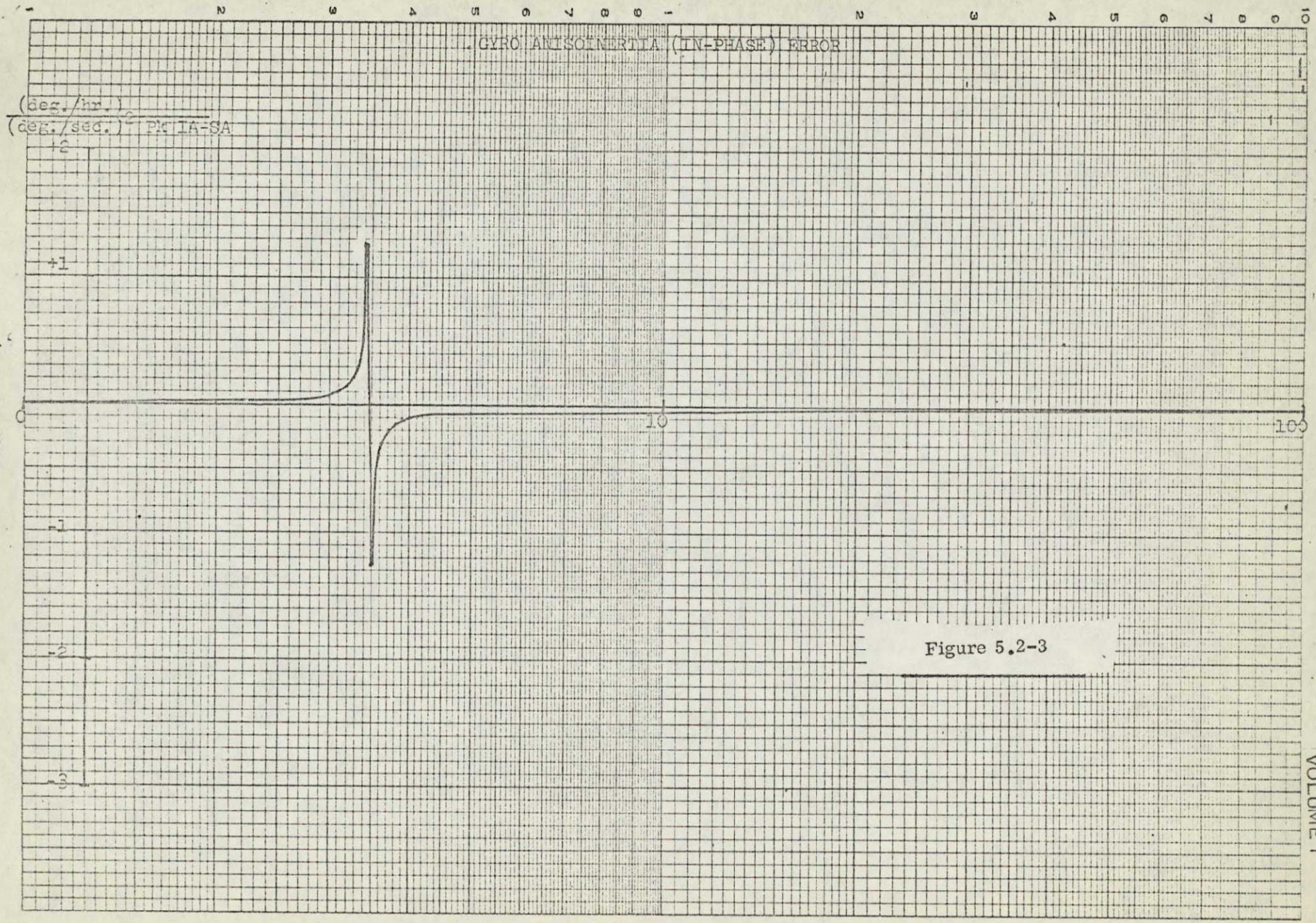

Figure 5.2-3

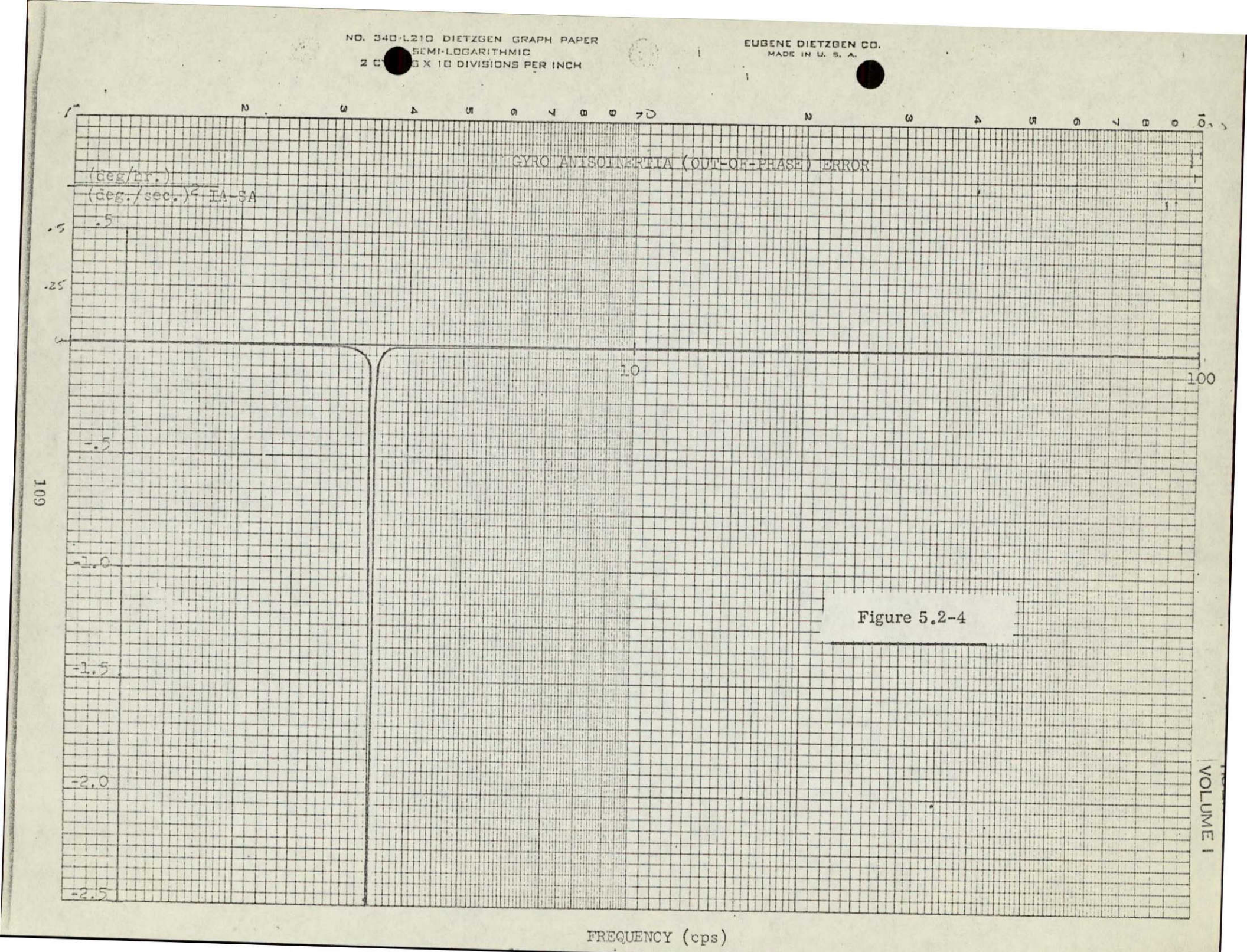
NO. 340-L210 DIETZGEN GRAPH PAPER
SEMI-LOGARITHMIC
X 10 DIVISIONS PER INCH
EUGENE DIETZGEN CO.
MADE IN U. S. A.
GYRO ANISOINERTIA (OUT-OF-PHASE) ERROR
(deg/hr.)
(deg./sec.)² IA-SA
.5
.25
0
-.5
-1.0
-1.5
-2.0
-2.5
10
100
FREQUENCY (cps)

Figure 5.2-4

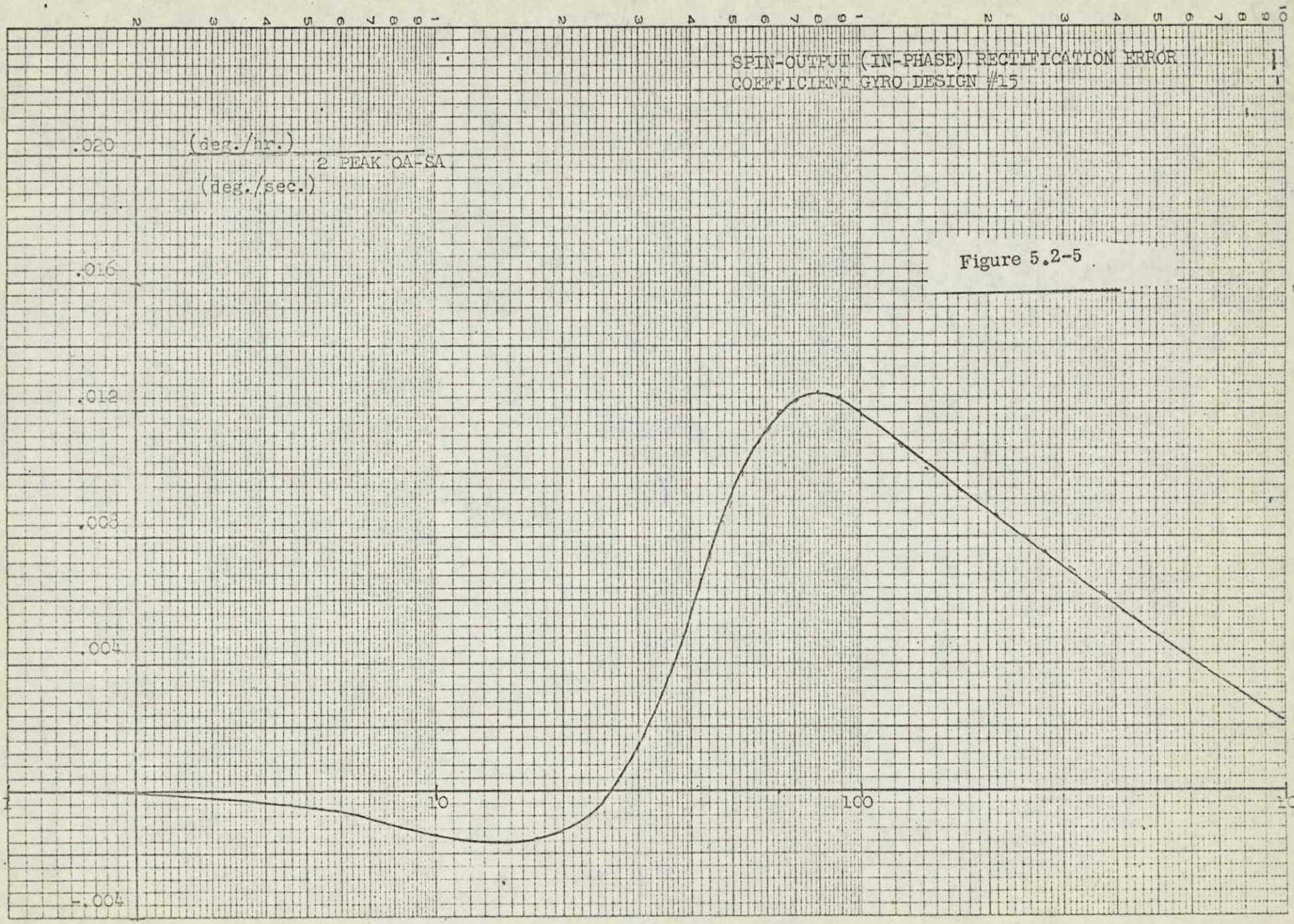

Figure 5.2-5

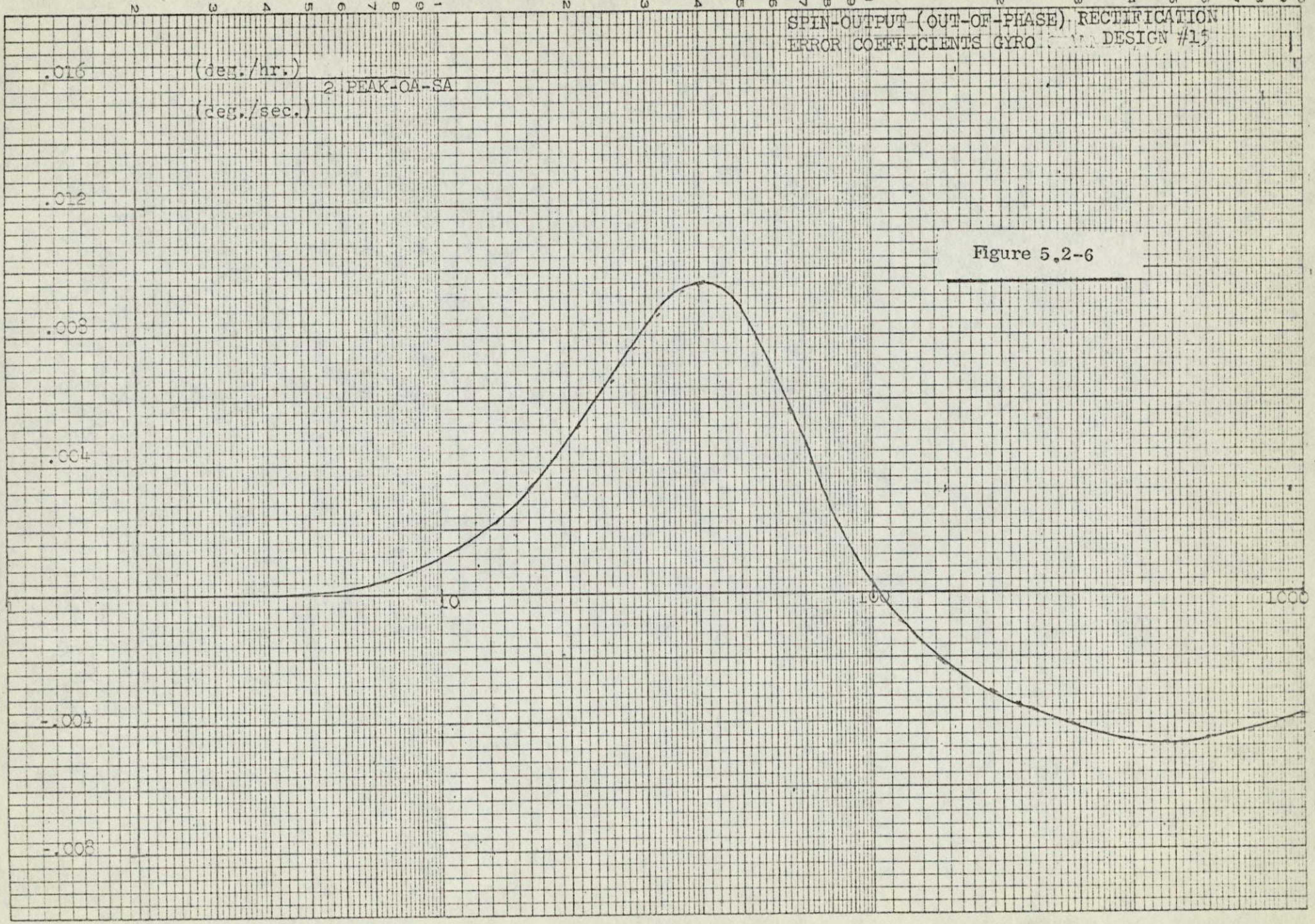

Figure 5.2-6

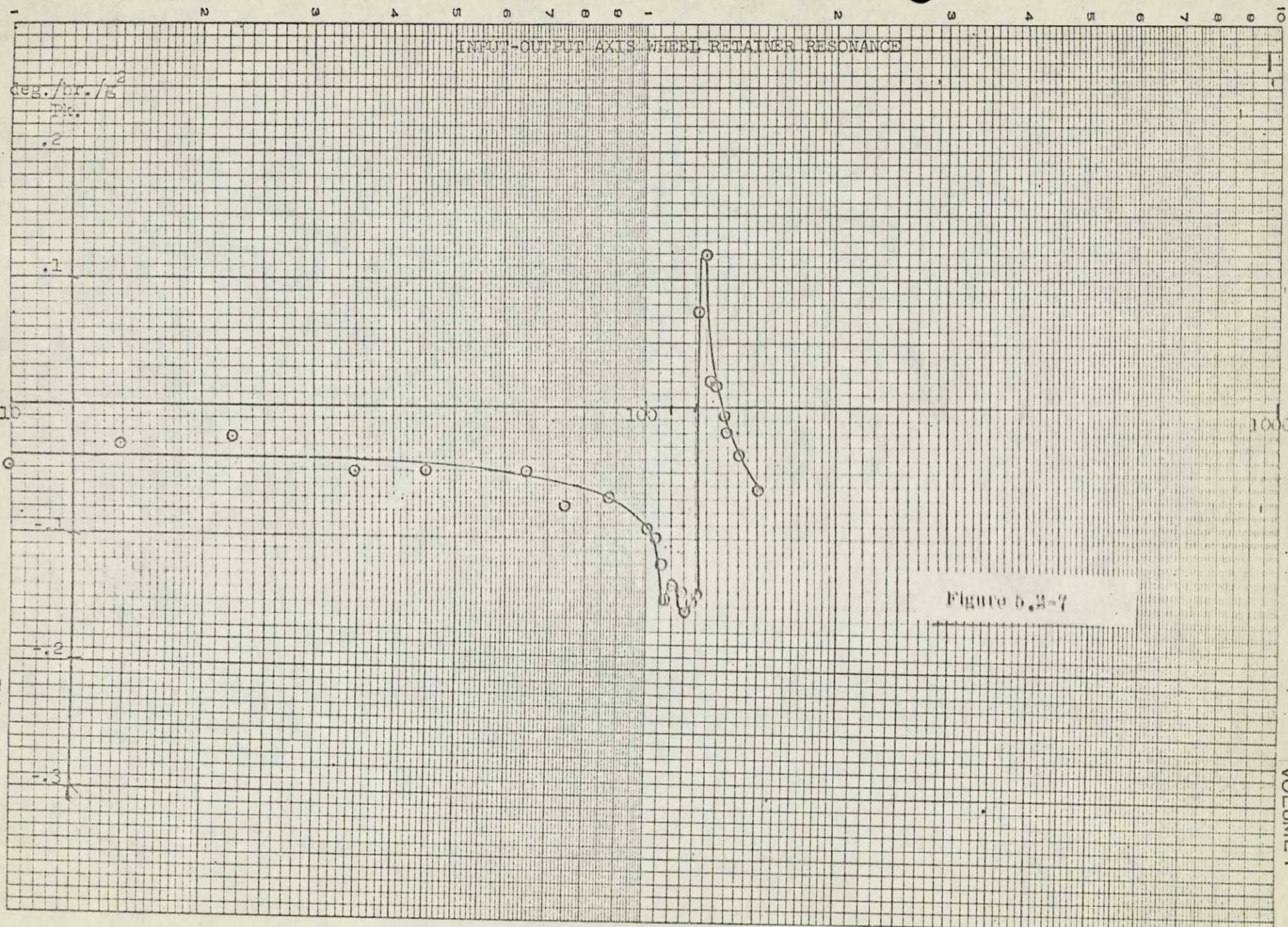

Figure 5.2-7

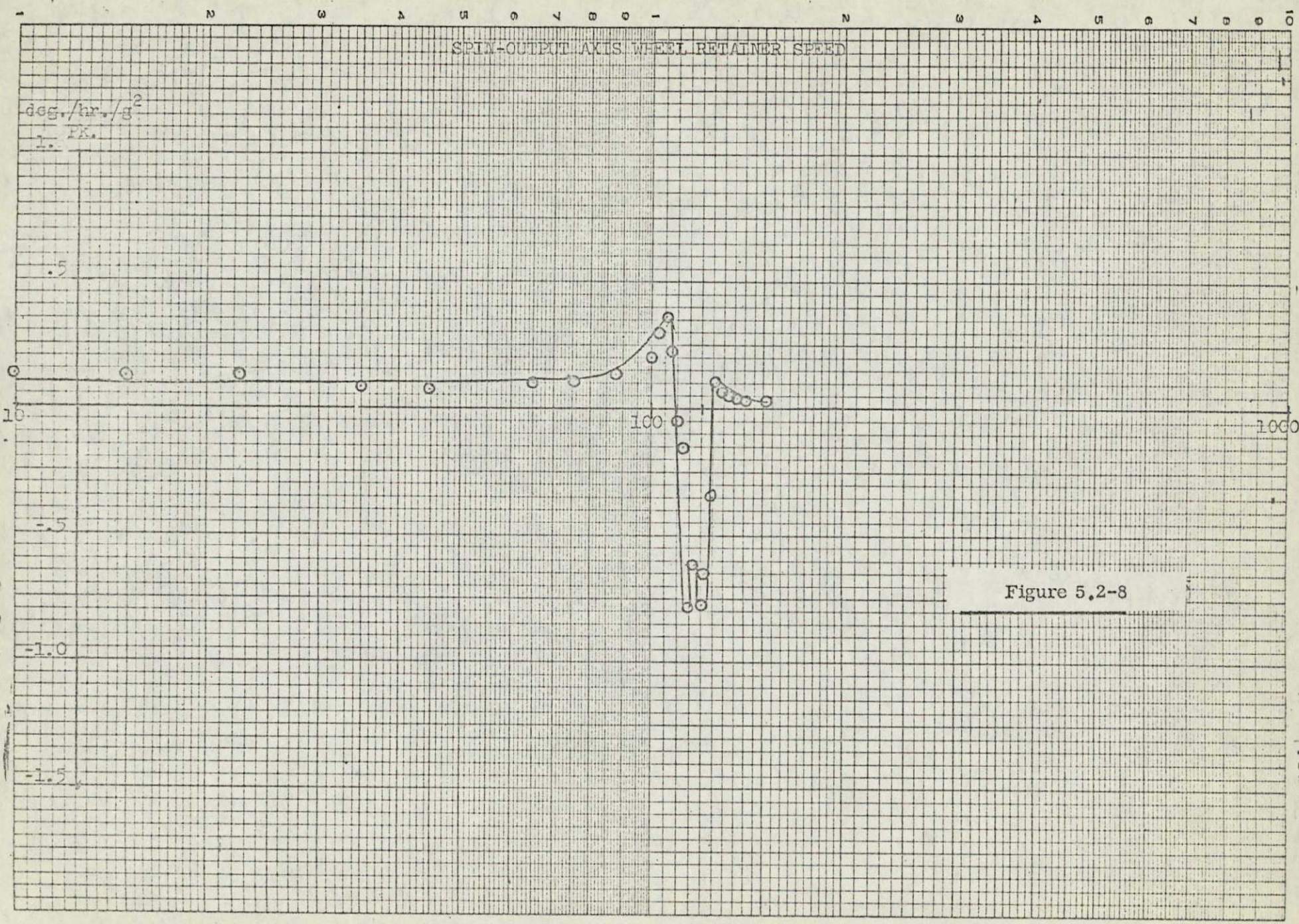

Figure 5.2-8

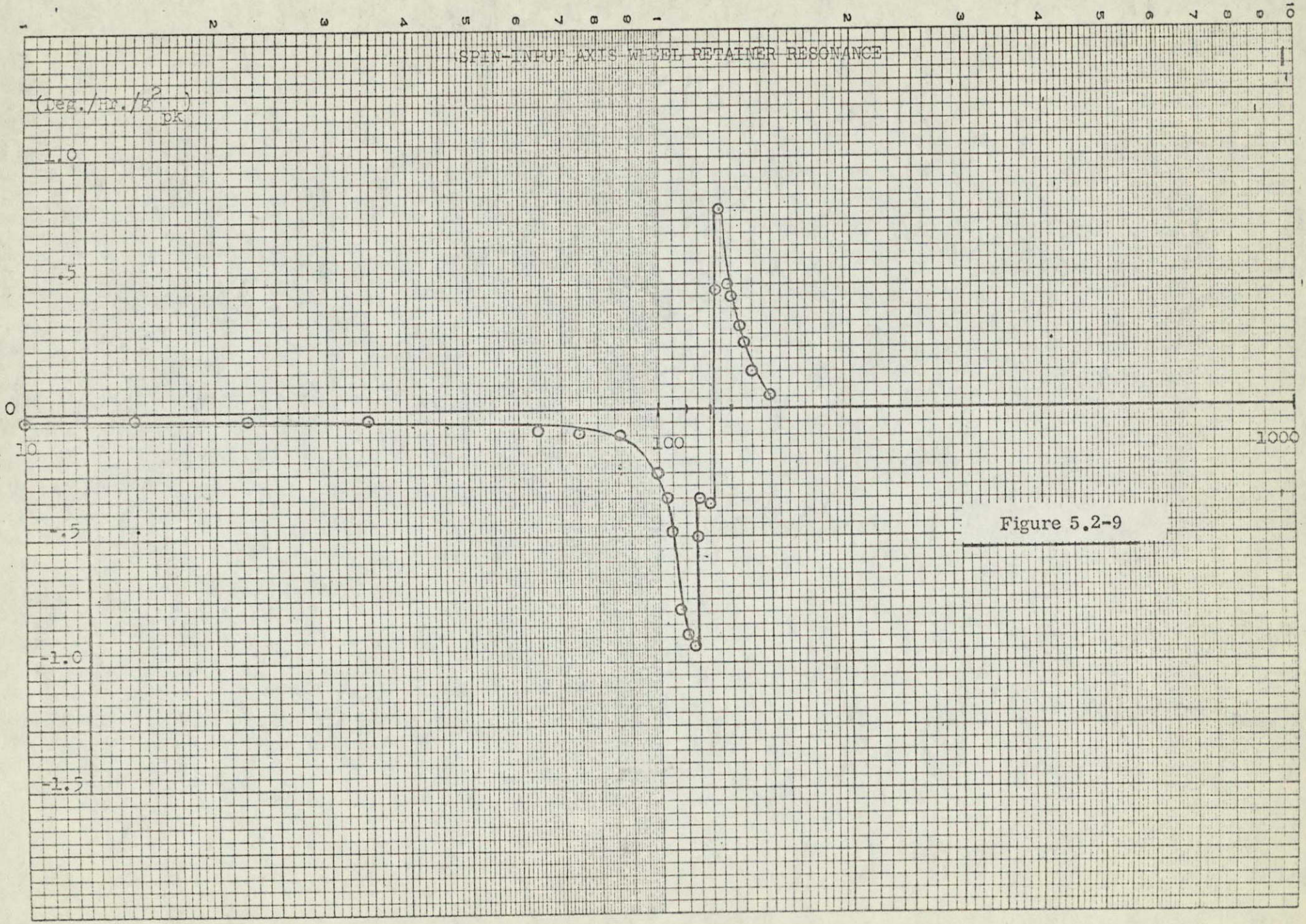

Figure 5.2-9

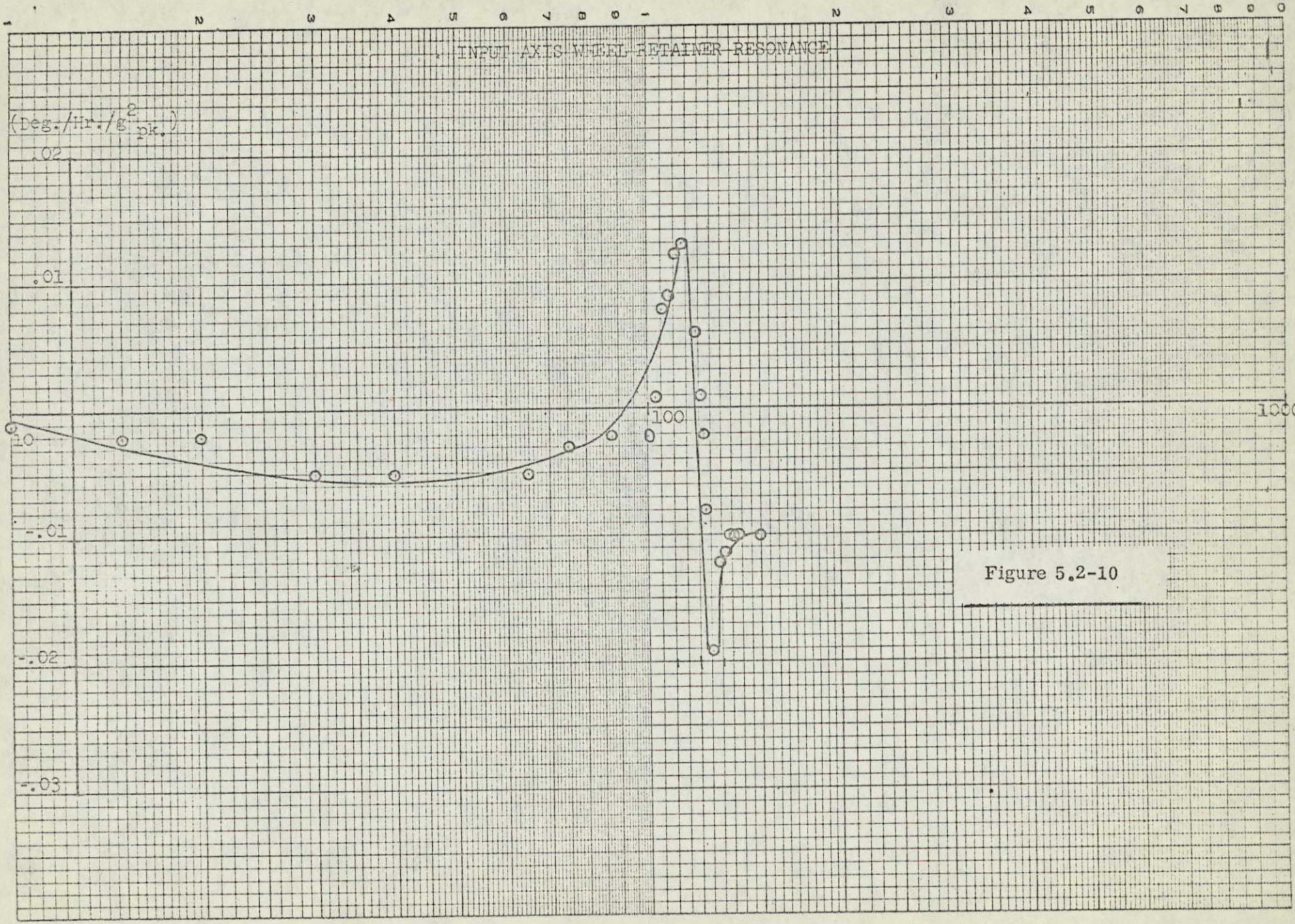

Figure 5.2-10

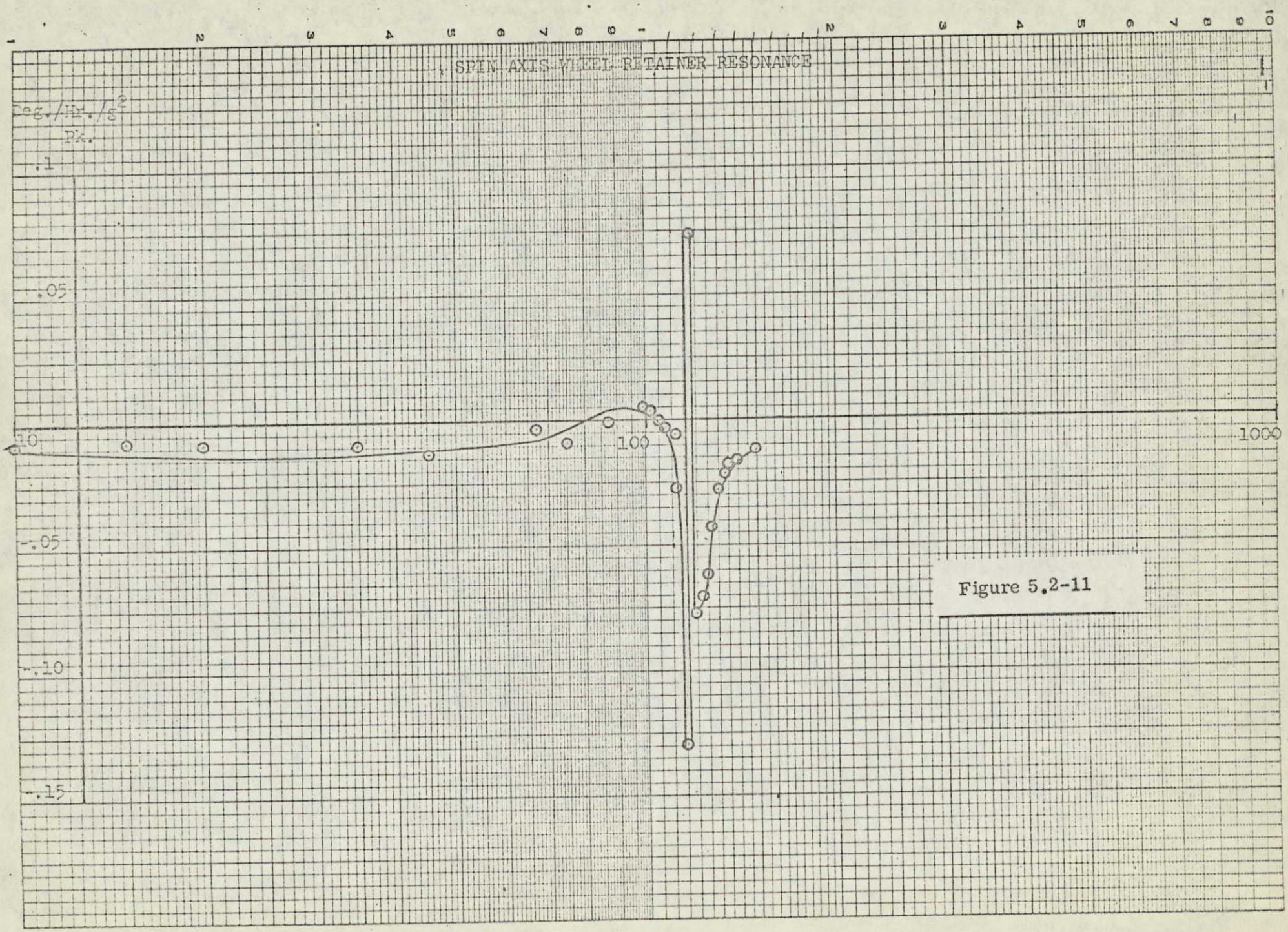

Figure 5.2-11

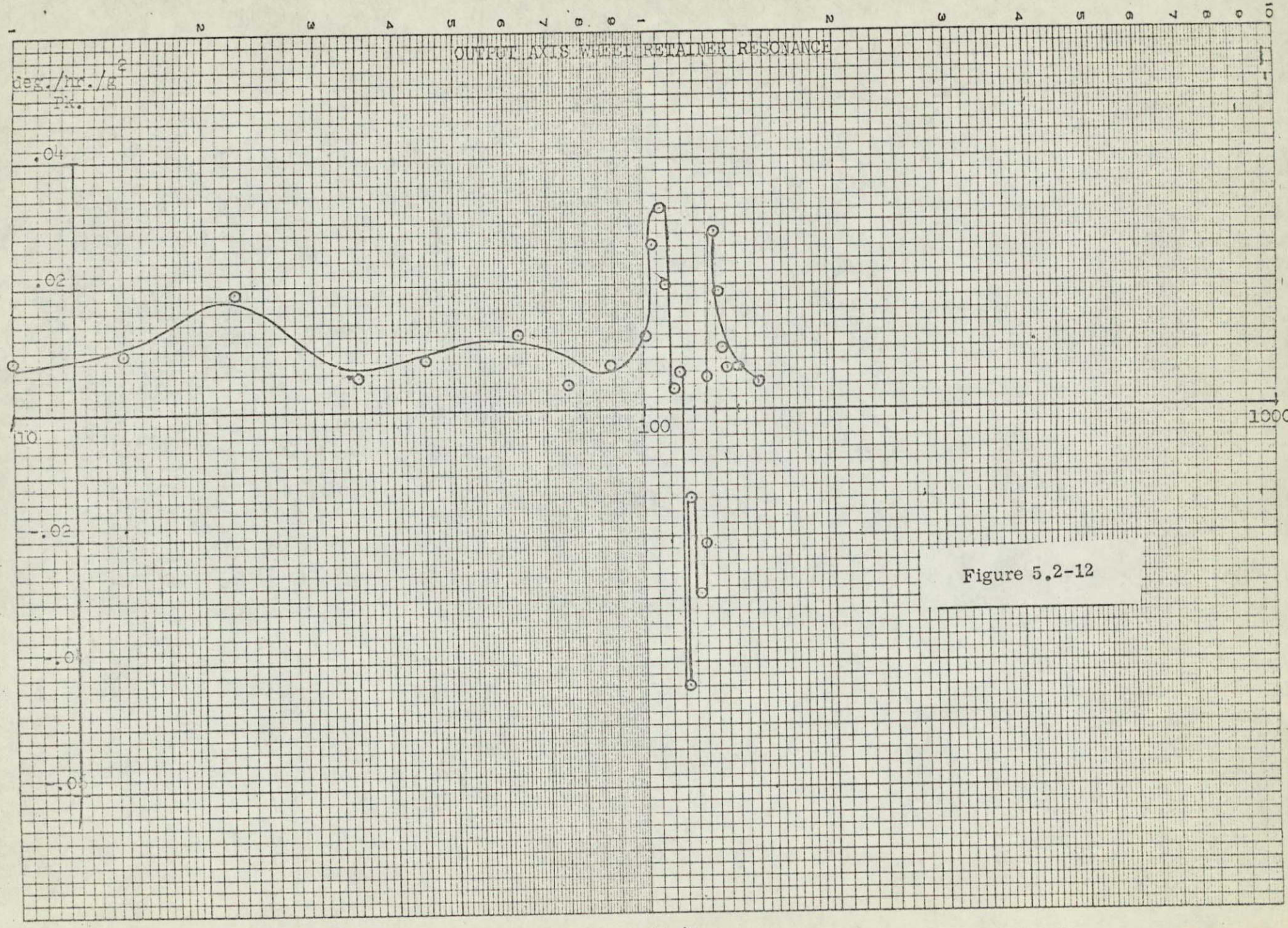

Figure 5.2-12

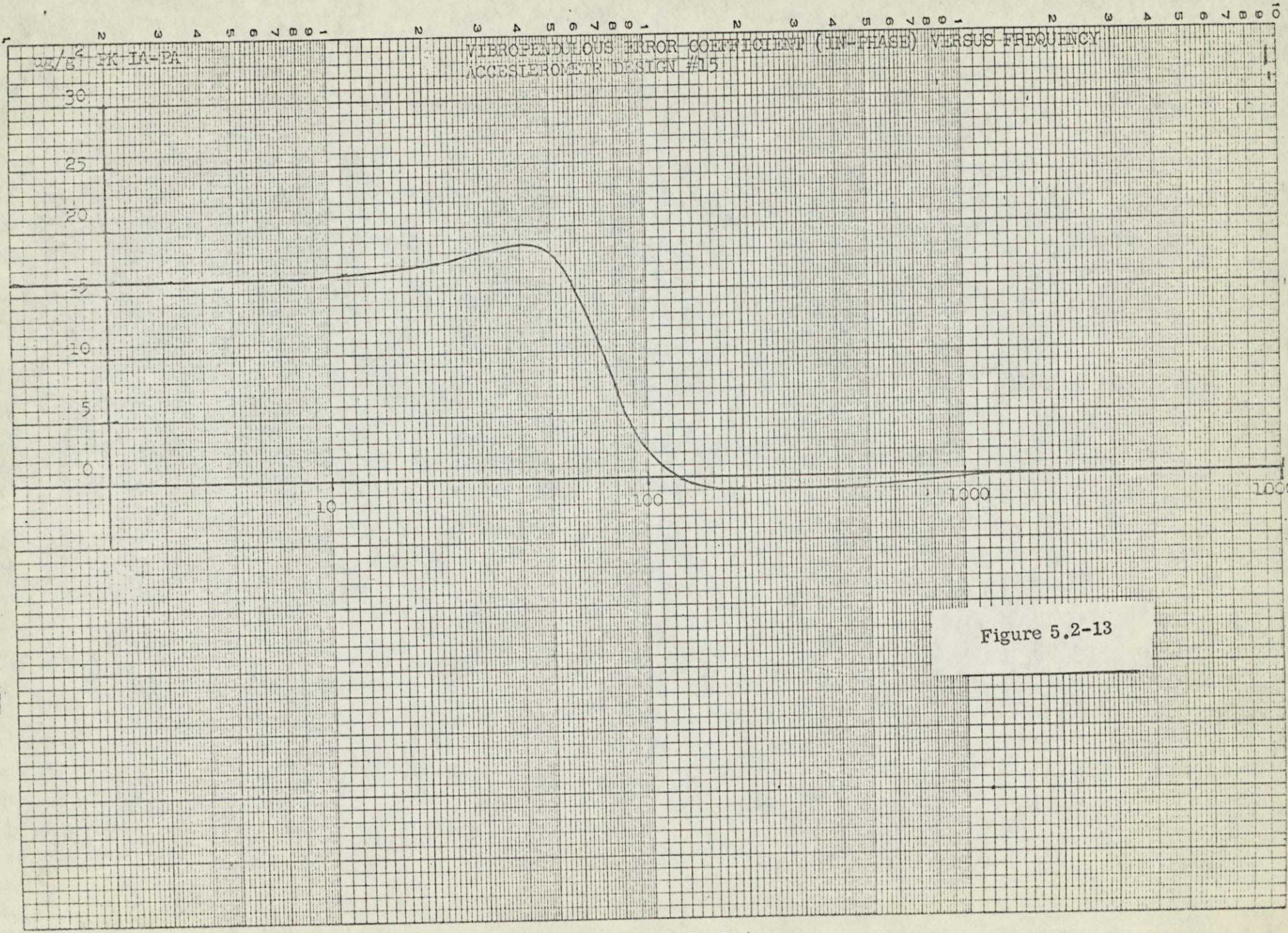

Figure 5.2-13

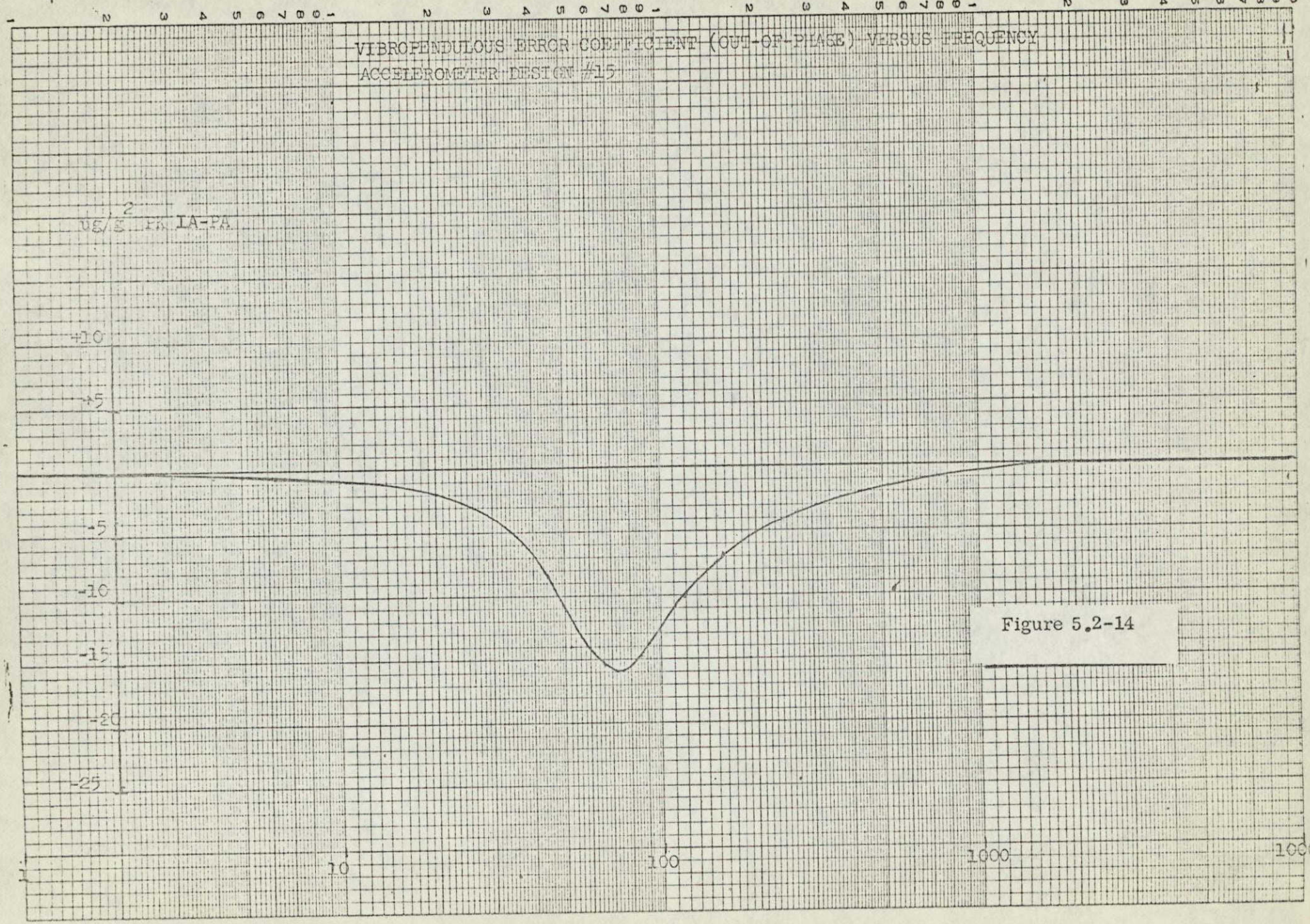

Figure 5.2-14

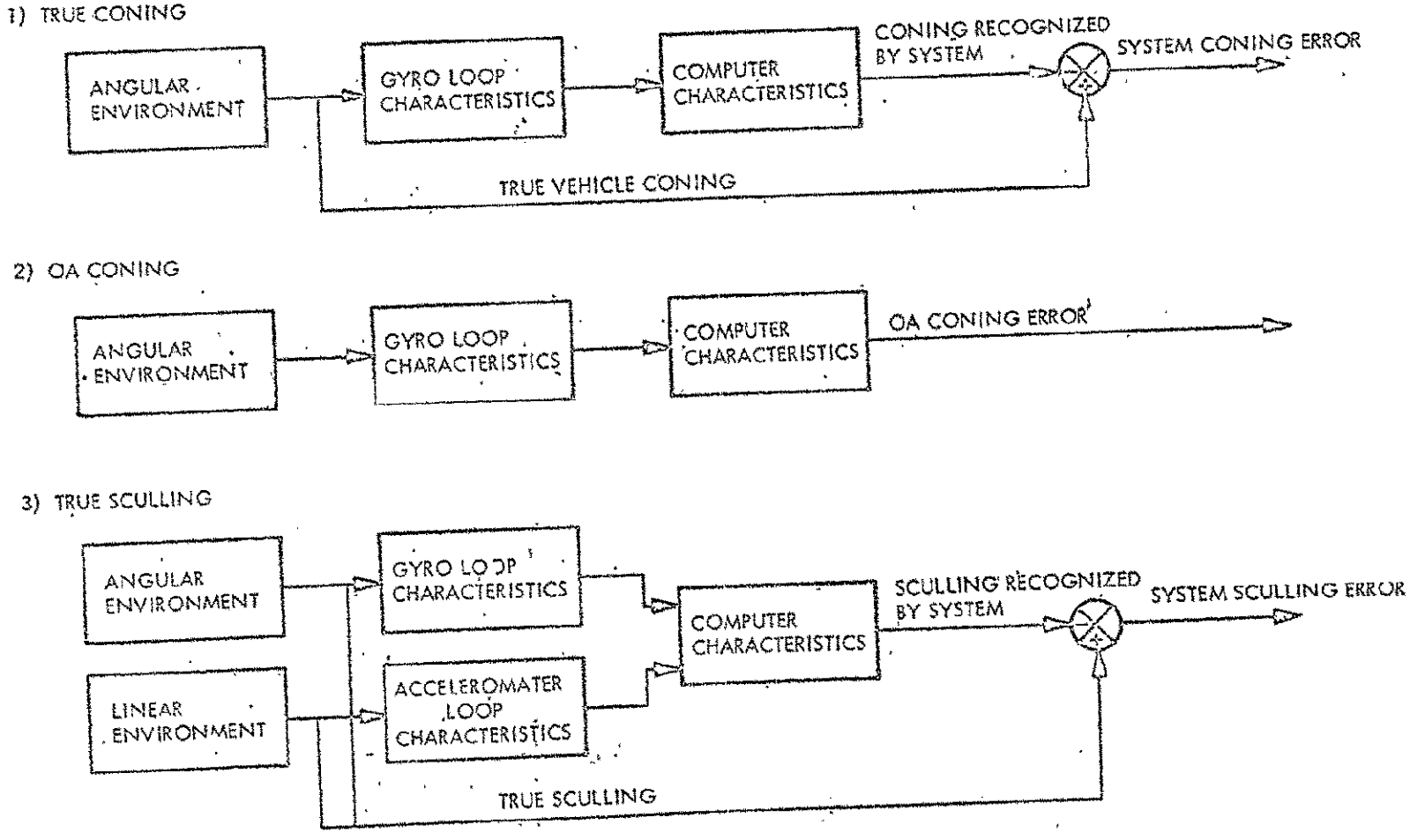

Figure 5.2-15 System Error Description

Table 5.2-2

SINGLE CHANNEL GYRO ERRORS:

SPIN INPUT RECTIFICATION $\left(°/HR/(°/SEC_{RMS})^2\right)$

$$BIAS = 2\left[\int_{f_0}^{f_m} SIIP(f) \times G_c{}^{WW}_{I-S}(f) \times df + \int_{f_0}^{f_m} SIOP(f) \times G_q{}^{WW}_{I-S}(f) \times df\right]$$

ANISOINERTIA $\left(°/HR/(°/SEC_{RMS})^2\right)$

$$BIAS = 2\left[\int_{f_0}^{f_m} \sigma_{c_{I-S}}(f) \times G_c{}^{WW}_{I-S}(f) \times df + \int_{f_0}^{f_m} \sigma_{q_{I-S}}(f) \times G_q{}^{WW}_{I-S}(f) \times df\right]$$

SPIN OUTPUT RECTIFICATION $\left(°/HR/(°/SEC_{RMS})^2\right)$

$$BIAS = 2\left[\int_{f_0}^{f_m} SOIP(f) \times G_c{}^{WW}_{S-O}(f) \times df + \int_{f_0}^{f_m} SOOP(f) \times G_q{}^{WW}_{S-O}(f) \times df\right]$$

NON-LINEAR SCALE FACTOR RECTIFICATION $\left(°/HR/(°/SEC_{RMS})^2\right)$

$$BIAS = \sigma_{SF}{}^{W}\left[\frac{4\pi J_{OA}}{H}\int_{f_0}^{f_m} f \times G_q{}^{WW}_{I-O}(f) \times T_L(f)^2 df + \int_{f_0}^{f_m} G^{WW}_{I-I}(f) \times T_L(f)^2 df + \left(\frac{2\pi J_{OA}}{H}\right)^2 \int_{f_0}^{f_m} f^2 \times G^{WW}_{O-O}(f) \times T_L(f)^2 \times df\right]^{1/2}$$

Table 5.2-2 (Cont.)

GYRO ANISOELASTIC $\left(°/HR/(g^2_{rms})\right)$

MAJOR

$$BIAS = 2\left[\int_{f_0}^{f_m} A_{I-S}(f) * Gc^{AA}_{I-S}(f) * df\right]$$

MINOR

$$BIAS = 2\left[\int_{f_0}^{f_m} A_{O-S}(f) * Gc^{AA}_{O-S}(f) * df\right]$$

WHEEL RETAINER RESONANCE $\left(°/HR/(g^2_{rms})\right)$

$$BIAS = 2\int_{f_0}^{f_m} AW_{I-O}(f) * Gc^{AA}_{I-O}(f) * df$$

$$BIAS = 2\int_{f_0}^{f_m} AW_{O-S}(f) * Gc^{AA}_{O-S}(f) * df$$

$$BIAS = 2\int_{f_0}^{f_m} AW_{I-S}(f) * Gc^{AA}_{I-S}(f) * df$$

$$BIAS = 2\int_{f_0}^{f_m} AW_{I-I}(f) * G^{AA}_{I-I}(f) * df$$

$$BIAS = 2\int_{f_0}^{f_m} AW_{S-S}(f) * G^{AA}_{S-S}(f) * df$$

$$BIAS = 2\int_{f_0}^{f_m} AW_{O-O}(f) * G^{AA}_{O-O}(f) * df$$

SUMMARY OF DYNAMIC ERROR EQUATIONS

SINGLE CHANNEL ACCELEROMETER ERRORS:

VIBROPENDULOUS RECTIFICATION $(\mu g's / g^2_{rms})$

$$BIAS = 2\left[\int_{f_0}^{f_m} VIP(f) \times G_{c_{I-P}}^{AA}(f) \times df + \int_{f_0}^{f_m} VOP(f) \times G_{b_{I-P}}^{AA}(f) \times df\right]$$

ANISOINERTIA $\left(\mu g's / (deg/sec_{rms})^2\right)$

$$BIAS = 2 \times \sigma_{I-P} \int_{f_0}^{f_m} G_{c_{x-P}}^{\omega\omega}(f) \times df$$

NON LINEAR g^2 $(\mu g's / g^2_{rms})$

$$BIAS = \sigma_{g^2} \times \int_{f_0}^{f_m} G_{I-I}^{AA}(f) \times df$$

NON-LINEAR SCALEFACTOR RECTIFICATION $(\mu g's/g_{rms})\left(\mu g's/\%_{SF_{rms}}\right)$

$$BIAS = \sigma_{SF}^{A}\left[\frac{4\pi^2 J_{OA}}{P(180)} \int_{f_0}^{f_m} f \times G_{q_{I-O}}^{AW}(f) \times T_L(f)^2 \times df + \int_{f_0}^{f_m} G_{I-I}^{AA}(f) \times T_L(f)^2 \times df + \left(\frac{\pi^2 J_{OA}}{P(90)}\right)^2 \times \int_{f_0}^{f_m} f^2 \times G_{O-O}^{WW}(f) \times T_L(f)^2 \times df\right]$$

Table 5.2-4

ERC V/STOL SUMMARY OF SYSTEM DYNAMIC ERRORS

Gyro Coning

$^{o}/hr./(deg./sec.\ rms)^{2}$

$$w\tilde{d}_X = -2\pi \int_0^\infty G_g \frac{{}^{W}_{YZ}(f)}{W} + T_Y(f) * T_Z(f) * T_C^2(f) * (\sin\gamma_Y * \sin\gamma_Z + \cos\gamma_Y * \cos\gamma_Z)$$

$$* \left[- G_g \frac{{}^{W}_{YZ}(f)}{W} + \frac{J_{gY}}{H} * G_C \, {}^{W}_{XZ}(f) + \frac{J_{gZ}}{H} * G_C \, {}^{W}_{XY}(f) \right] * df$$

$$w\tilde{d}_Y = 2\pi \int_0^\infty G_g \frac{{}^{W}_{XZ}(f)}{W} + T_X(f) * T_Z(f) * (\sin\gamma_X \sin\gamma_Z + \cos\gamma_X \cos\gamma_Z) * T_C^2(f)$$

$$* \left[- G_g \frac{{}^{W}_{XZ}(f)}{W} + \frac{J_{gX}}{H} * G \, {}^{W}_{ZZ}(f) + \frac{J_{gZ}}{H} * G \, {}^{W}_{XX}(f) - \frac{J_{gX} * J_{gZ}}{H^2} * W * G_g \, {}^{W}_{XZ}(f) \right] * df$$

$$w\tilde{d}_Z = -2\pi \int_0^\infty G_g \frac{{}^{W}_{XY}(f)}{W} + T_X(f) * T_Y(f) * T_C^2(f) * (\sin\gamma_X * \sin\gamma_Y + \cos\gamma_X * \cos\gamma_Y)$$

$$* \left[- G_g \frac{{}^{W}_{XY}(f)}{W} + \frac{J_{gX}}{H} * G_C \, {}^{W}_{YZ}(f) - \frac{J_{gY}}{H} * G \, {}^{W}_{XX}(f) + \frac{J_{gX} * J_{gY}}{H^2} * W * G_g \, {}^{W}_{XZ}(f) \right] * df$$

LM/ASA SYSTEM .

X Axis Sculling Error (ug's/(g rms - deg./sec. rms)); (ug's/(deg./sec./rms)^2)

$$\widetilde{ad}_X = \frac{\pi * 10^6}{180} \int_0^\infty \left\{ \left[\frac{Gg_{\frac{Y}{Z}}^{\frac{A}{W}}(f)}{W} - Ta_Y(f) * Tg_Z(f) * Tc^2(f) \right] \left\{ \left[\frac{Gg_{\frac{Y}{Z}}^{\frac{A}{W}}(f)}{W} - \frac{Jg_Z}{H} * Gc_{YX}^{AW}(f) + \frac{\pi}{180} * \frac{Ja_Y}{P} * G_{ZZ}^{WW}(f) - \frac{\pi}{180} * \frac{Ja_Y}{P} * \frac{Jg_Z}{H} * W * Gg_{XZ}^{WW}(f) \right] * \left[\cos\beta_Y(f) * \cos\gamma_Z(f) + \sin\beta_Y(f) * \sin\gamma_Z(f) \right] + \left[\frac{Gc_{\frac{Y}{Z}}^{\frac{A}{W}}(f)}{W} + \frac{Jg_Z}{H} * Gg_{YX}^{AW}(f) + \frac{\pi}{180} * \frac{Ja_Y}{P} * \frac{Jg_Z}{H} * W * Gc_{XZ}^{WW}(f) \right] * \left[\cos\beta_Y(f) * \sin\gamma_Z(f) - \sin\beta_Y(f) * \cos\gamma_Z(f) \right] \right\} - \frac{Gg_{\frac{Z}{Y}}^{\frac{A}{W}}(f)}{W} - Ta_Z(f) * Tg_Y(f) * Tc^2(f) \left\{ \left[- \frac{Gg_{\frac{Z}{Y}}^{\frac{A}{W}}(f)}{W} + \frac{Jg_Y}{H} * Gc_{ZX}^{AW}(f) - \frac{\pi}{180} * \frac{Ja_Z}{P} * \frac{Jg_Y}{H} * W * Gg_{XY}^{WW}(f) \right] * \left[\cos\beta_Z(f) * \cos\gamma_Y(f) + \sin\beta_Z(f) \sin\gamma_Y(f) \right] + \left[- \frac{Gc_{\frac{Z}{Y}}^{\frac{A}{W}}(f)}{W} + \frac{Jg_Y}{H} * Gg_{XZ}^{WA}(f) + \frac{\pi}{180} * \frac{Ja_Z}{P} * \frac{Jg_Y}{H} * W * Gc_{XY}^{WW}(f) \right] * \left[\cos\beta_Z(f) * \sin\gamma_Y(f) - \sin\beta_Z(f) * \cos\gamma_Y(f) \right] \right\} df$$

LM/ASA System
Y Axis Sculling Error (ug's/(g rms-deg./sec. rms)); (ug's/(deg./sec. rms)^2)

$$\tilde{ad}_y = \frac{\pi * 10^6}{180} * \int_0^\infty \left\{ \left[\frac{Gg_{zx}^{AW}(f)}{W} - Ta_z(f) * Tg_x(f) * Tc^2(f) \right] \left[\frac{Gg_{zx}^{TT}(f)}{W} - \frac{Jg_x}{H} * Gc_{zz}^{AW}(f) + \frac{\pi * Ja_z}{180 * P} * Gc_{xy}^{WW}(f) - \frac{\pi * Ja_z}{180 * P} * \frac{Jg_x}{H} * W * Gg_{yz}^{WW}(f) \right] * \right.$$

$$\left[Cos\beta_z(f) * Cos\gamma_x(f) + SIN\beta_z(f) * SIN\gamma_x(f) \right] + \left[\frac{Gc_{zx}^{AW}(f)}{W} - \frac{Jg_x}{H} * Gg_{zz}^{AW}(f) \right.$$

$$\left. \frac{\pi * Ja_z}{180 * P} * Gg_{xy}^{WW}(f) - \frac{\pi * Ja_z}{180 * P} * \frac{Jg_x}{H} * W * Gc_{yz}^{WW}(f) \right] *$$

$$\left. \left[Cos\beta_z(f) * SIN\gamma_x(f) - SIN\beta_z(f) Cos\gamma_x(f) \right] \right\} - \frac{Gg_{xz}^{AW}(f)}{W} + Ta_x(f) *$$

$$Tg_z(f) * Tc^2(f) \left\{ \left[\frac{Gg_{xz}^{AW}(f)}{W} - \frac{Jg_z}{H} * Gc_{xx}^{AW}(f) + \frac{\pi * Ja_x}{180 * P} * \right.\right.$$

$$Gc_{yz}^{WW}(f) - \frac{\pi * Ja_x}{180 * P} * \frac{Jg_z}{H} * W * Gg_{xy}^{WW}(f) \left. \right] * \left[Cos\beta_x(f) * \right.$$

$$Cos\gamma_z(f) + SIN\beta_x(f) * SIN\gamma_z(f) \left. \right] + \left[\frac{Gc_{xz}^{AW}(f)}{W} + \frac{Jg_z}{H} * Gg_{xx}^{AW}(f) - \right.$$

$$\left. \frac{\pi * Ja_x}{180 * P} * Gg_{yz}^{WW}(f) + \frac{\pi * Ja_x}{180 * P} * \frac{Jg_z}{H} * W * Gc_{xy}^{WW}(f) \right] *$$

$$\left. \left[Cos\beta_x(f) * SIN\gamma_z(f) - SIN\beta_x(f) Cos\gamma_z(f) \right] \right\} df$$

LM/ASA System
Z Axis Sculling Error (ug's/(g rms - deg./sec. rms)); (ug's/(deg./sec. rms)^c)

$$\tilde{a}_{dz} = \frac{\pi}{180} * 10^6 \int_0^\infty \frac{G_q{}^{AW}_{XY}(f) - \tilde{T}_{aX}(f) * T_{gY}(f) * \tilde{T}_c{}^2(f)}{W} \left\{ \left[\frac{G_q{}^{AW}_{XY}(f)}{W} + \frac{J_{gY}}{H} * G_c{}^{AW}_{XX}(f) + \frac{\pi}{180} * \frac{J_{aX}}{\rho} * G^{WW}_{YY}(f) + \frac{\pi}{180} * \frac{J_{aX}}{\rho} * \frac{J_{gY}}{H} * W * G_q{}^{WW}_{XY}(f) \right] * \left[\cos\beta_X(f) \cos\gamma_Y(f) + \sin\beta_X(f) \sin\gamma_Y(f) \right] + \left[\frac{G_c{}^{AW}_{XY}(f)}{W} - \frac{J_{gY}}{H} * G_q{}^{AW}_{XX}(f) + \frac{\pi}{180} * \frac{J_{aX}}{\rho} * \frac{J_{gY}}{H} * W * G_c{}^{WW}_{XY}(f) \right] \left[\cos\beta_X(f) \sin\gamma_Y(f) - \sin\beta_X(f) \cos\gamma_Y(f) \right] \right\}$$

$$\frac{G_q{}^{AW}_{YX}(f)}{W} + \tilde{T}_c{}^2(f) * \tilde{T}_{aY}(f) * T_{gX}(f) \left\{ \left[\frac{G_q{}^{AW}_{YX}(f)}{W} + \frac{J_{gX}}{H} * G_c{}^{AW}_{YZ}(f) + \frac{\pi}{180} * \frac{J_{aY}}{\rho} * G_c{}^{WW}_{XZ}(f) \right] \left[\cos\beta_Y(f) \cos\gamma_X(f) + \sin\beta_Y(f) \sin\gamma_X(f) \right] + \left[\frac{G_c{}^{AW}_{YX}(f)}{W} - \frac{J_{gX}}{H} * G_q{}^{AW}_{YZ}(f) + \frac{\pi}{180} * \frac{J_{aY}}{\rho} * G_q{}^{WW}_{XZ}(f) - \frac{\pi}{180} * \frac{J_{aY}}{\rho} * \frac{J_{gX}}{H} * W * G^{WW}_{ZZ}(f) \right] \left[\cos\beta_Y(f) * \sin\gamma_X(f) - \sin\beta_Y(f) \cos\gamma_X(f) \right] \right\} df$$

TABLE 5.2-5

Nomenclature

VIP(f)	Vibropendulous In-Phase Coefficient ($\mu g's/g^2$ pk)
VOP(f)	Vibropendulous Out-of-Phase Coefficient ($\mu g's/g^2$ pk)
σ $\bar{I}$-P	Accelerometer Anisoinertia Coefficient ($\mu g's/(°/sec)^2$ pk)
σ g^2	Accelerometer Non-Linear g^2 Coefficient ($\mu g's/g^2$ RMS)
σ SF^A	Accelerometer Non-Linear Scale Factor Coefficient ($\mu g's/g$ RMS)
SIIP(f)	Spin Input In-Phase Rectification Coefficient $(°/hr)/(°/sec)^2$ pk
SIOP(f)	Spin Input Out-of-Phase Rectification Coefficient $(°/hr)/(°/sec)^2$ pk
σ $C_{I-S}(f)$	Gyro Anisoinertia In-Phase Coefficient $(°/hr)/(°/sec)^2$ pk
σ $q_{I-S}(f)$	Gyro Anisoinertia Out-of-Phase Coefficient $(°/hr)/(°/sec)^2$ pk
SOIP(f)	Gyro Spin Output In-Phase Rectification Coefficient $(°/hr)/(°/sec)^2$ pk
SOOP(f)	Gyro Spin Output Out-of-Phase Rectification Coefficient $(°/hr)/(°/sec)^2$ pk
σ SF^W	Gyro Non-Linear Scale Factor Coefficient $(°/hr)/(°/sec)$ RMS
$A_{I-S}(f)$	Major Anisoelastic Coefficient $(°/hr)/g^2$ pk
$A_{O-S}(f)$	Minor Anisoelastic Coefficient $(°/hr)/g^2$ pk
AW_{I-O}	Wheel Retainer Resonance Input-Output $(°/hr)/g^2$ pk
AW_{O-S}	Wheel Retainer Resonance Output-Spin $(°/hr)/g^2$ pk
AW_{I-S}	Wheel Retainer Resonance Input-Spin $(°/hr)/g^2$ pk
AW_{I-I}	Wheel Retainer Resonance Input^2 $(°/hr)/g^2$ pk
AW_{S-S}	Wheel Retainer Resonance Spin^2 $(°/hr)/g^2$ pk
AW_{O-O}	Wheel Retainer Resonance Output^2 $(°/hr)/g^2$ pk

TABLE 5.2-5 (continued)

JOA	Inertia of Sensitive Axis About Output Axis (dyn-cm/RAD/sec^2)
P	Accelerometer Pendulosity (dyn-cm/g)
H	Gyro Angular Momentum (dyn-cm/RAD/sec)
fo	Lowest Frequency of Spectral Density (cps)
fm	Highest Frequency of Spectral Density (cps)
f	Frequency (cps)
$T_L(f)$	Input/Output Loop Transfer Function
$G_{ii}^{WW}(f)$	Angular Rate PSD of ith Axis in (^{o}/sec RMS)^2/Hz
$G_{ii}^{AA}(f)$	Acceleration PSD of ith Axis in (g rms)^2/Hz
$G_{cij}^{AA}(f)$	Acceleration Co Spectrum Between ith and jth Axes in (g rms)^2/Hz
$G_{qij}^{AA}(f)$	Acceleration Quad Spectrum Between ith and jth Axes in (g rms)^2/Hz
$G_{cij}^{WW}(f)$	Angular Rate Co Spectrum Between ith and jth Axes in (^{o}/sec rms)^2/Hz
$G_{qij}^{WW}(f)$	Angular Rate Quad Spectrum Between ith and jth Axes in (^{o}/sec rms)^2/Hz
$G_{cij}^{AW}(f)$	Angular Rate Acceleration Co Spectrum Between ith and jth Axes in (g ^{o}/sec rms)/Hz
$G_{qij}^{AW}(f)$	Angular Rate Acceleration Quad Spectrum Between ith and jth Axes in (g ^{o}/sec rms)/Hz
Jgi	ith Channel Gyro Output Axis Inertia in (dyn-cm/RAD/sec^2)
Jai	ith Channel Accelerometer Output Axis Inertia in (dyn-cm/RAD/sec^2)
Tgi	ith Gyro Channel Magnitude Gain at Frequency f
Tai	ith Accelerometer Channel Magnitude Gain at Frequency f

TABLE 5.2-5 (Continued)

$Tc(f)$	Computer Magnitude Amplification at Frequency f
$\gamma_i(f)$	ith Gyro Channel Phase Shift at Frequency f
$\beta_i(f)$	ith Accelerometer Channel Phase Shift at Frequency f

5.3 Dynamic Error Results

The total IMU dynamic performance was predicted using the environment from Flight 3 (forward flight) and the error model presented in the previous sections. By utilizing the proper environments which take into account the IMU/Sensor Axes relationship for each error source, the total error for each axis was computed. These results are presented in Tables 5.3-1 and 5.3-2 for the angular and linear errors, respectively. The total error for each axis is the linear sum of the individual errors. The only error which is not completely deterministic is that due to scale factor asymmetry, and thus, leads to a predicted maximum and minimum, depending on the sign and size of this error source. These results show the maximum linear and angular error expected for HSSC's IMU operating in the helicopter environment to be 9 μg and 0.28°/hr, respectively. These results were obtained with a (sin x/x) computer characteristic for attenuation. These errors could be significantly reduced by compensation in the computer for the major error terms which, for this environment, turned out to result from OA coning and scale factor asymmetry. Table 5.3-3 presents the system errors for an alternate model for the computer which has a quadratic characteristic.

In addition to errors presented in the previous tables, the following tables summarize the resulting dynamic errors for different combinations of environments to enable ERC to predict errors for other IMU configurations.

TABLE 5.3-4	Summary of Environmental RMS Levels
TABLE 5.3-5.	Summary of All Possible Scale Factor Asymmetry Errors
TABLE 5.3-6	Summary of All Possible Wheel Retainer Resonance Errors
TABLE 5.3-7	Summary of All Possible Loop Dependent Rectification Errors
TABLE 5.3-8	Steady State Error Coefficients

ANGULAR ERROR BUDGET (deg./hr.)

Error Source		Channel X	Channel Y	Channel Z
Single Channel:				
Spin-Input (In-Phase)		-.0001	.0010	.0010
Spin-Input (Out-of-Phase)		.0017	-.0015	-.0015
Anisoinertia (In-Phase)		.0099	.0105	.0105
Anisoinertia (Out-of-Phase)		.0014	.0001	-.0001
Spin-Output (In-Phase)		-.0013	-.0004	.0009
Spin-Output (Out-of-Phase		-.0007	-.0003	.0005
Scale Factor Asymmetry		±.1510	±.1560	±.0710
Anisoelastic-Major		-.0075	.0017	.0017
Anisoelastic-Minor		-.0002	-.0001	-.0008
Retainer Resonance:				
Input-Spin		-.0004	-.0010	-.001(
Input-Output		.0012	.0001	-.001
Spin-Output		-.0024	-.0028	.000
Input		-.0001	-.0001	-.000
Spin		-.0004	-.0019	-.000
Output		.0018	.0002	.000
Total Single Channel Error:		+.1539 -.1481	+.1615 -.1505	+.083 -.0588
System:				
True Coning		-.2834	.3350	.3364
Computer Estimate of True Coning		-.2441	.3202	.3625
OA Coning by Computer		.0028	-.1089	-.0928
Total Coning Error:		-.0420	.1236	.0667
Total Error	Max.	+.1119	+.2851	+.1503
	Min.	-.1901	-.0269	-.0079

Table 5.3-2

LINEAR ERROR BUDGET (μg)

Error Source		Channel X	Channel Y	Channel Z
Single Channel:				
Vibropendulous (In-Phase)		-.501	-.069	.501
Vibropendulous (Out-of-Phase)		-.001	.117	-.001
Anisoinertia		.474	.474	-.438
Non-Linear g^2		.199	.172	.700
Scale Factor Asymmetry		±.425	±.387	±1.199
Total Single Channel Error:		.596	1.081	1.961
		-.254	.307	-.437
System:				
True Sculling		15.834	-3.463	-5.125
Computer Estimate of True Sculling		24.482	1.501	-9.134
OA Sculling by Computer		.251	.265	1.912
Non-Symmetric Loop IA Sculling		.212	.027	-.035
Non-Symmetric Loop OA Sculling		.004	-.014	.001
Total Sculling Error:		-9.115	-5.243	2.131
Total Error	Max.	-8.519	-4.162	4.092
	Min.	-9.369	-4.936	1.694

Table 5.3-3

SYSTEM ERRORS USING AN ALTERNATE COMPUTER MODEL

$$T(s) = \frac{1}{(Ts+1)^2} \qquad T = 1/50\pi$$

	Units	CHANNEL X	Y	Z
True Coning	deg./hr.	-.2834	.3350	.3364
Computer Estimate of True Coning	deg./hr.	-.2692	.3303	.3574
OA Coning by Computer	deg./hr.	.0008	-.1174	-.0982
Total Coning Error	deg./hr.	-.0150	.1220	.0772
True Sculling	μg	15.834	-3.462	-5.125
Computer Estimate of True Sculling	μg	21.689	- .308	-8.495
OA Sculling by Computer	μg	.146	.632	2.622
Non-symmetric Loop IA Sculling	μg	.407	.021	- .087
Non-symmetric Loop OA Sculling	μg	.056	- .038	- .002
Total Sculling Error	μg	-6.465	-3.769	.837

SUMMARY OF ENVIRONMENTAL RMS LEVELS

Case #	Environmental Axis	Vibration Level CO(RMS)	Vibration Level Quad (RMS)
1.	Ax-Ax	.141 g	-
2.	Ax-Ay	-.250 g	-.059 g
3.	Ax-Az	.070 g	-.109 g
4.	Ax-Gx	.100 (g-deg./sec.)$^{1/2}$	.119 (g-deg./sec.)$^{1/2}$
5.	Ax-Gy	.167 "	.209 "
6.	Ax-Gz	-.038 "	.128 "
7.	Ay-AY	.131 g	-
8.	Ay-Az	-.120 g	-.198 g
9.	Ay-Gx	-.256 (g-deg./sec.)$^{1/2}$	-.140 (g-deg./sec.)$^{1/2}$
10.	Ay-Gy	-.217 "	-.101 "
11.	Ay-Gz	-.210 "	-.097 "
12.	Az-Az	.265 g	
13.	Az-Gx	.183 (g-deg./sec.)$^{1/2}$	-.186 (g-deg./sec.)$^{1/2}$
14.	Az-Gy	.246 "	.243 "
15.	Az-Gz	-.135 "	.150 "
16.	Gx-Gx	1.037 deg./sec.	--
17.	Gx-Gy	.398 "	.229 deg./sec.
18.	Gx-Gz	.383 "	.280 "
19.	Gy-Gy	.952 "	-- "
20.	Gy-Gz	.456 "	.530 "
21.	Gz-Gz	.520 "	--

SUMMARY OF ALL POSSIBLE SCALE FACTOR ASYMMETRY ERRORS

Case #	Sensor	Input Axis Env.	Output Axis Env.	Output Axis Phase	Resulting Error
1.	Gyro	X	Y	Negative	.00149 deg./hr./PPM
2.	Gyro	X	Y	Positive	.00158 "
3.	Gyro	X	Z	Negative	.00151 "
4.	Gyro	X	Z	Positive	.00154 "
5.	Gyro	Y	Z	Negative	.00149 "
6.	Gyro	Y	Z	Positive	.00155 "
7.	Accel.	X	Y	Negative	.02573 µg/PPM
8.	Accel.	X	Y	Positive	.04253 "
9.	Accel.	X	Z	Negative	.03380 "
10.	Accel.	X	Z	Positive	.03599 "
11.	Accel.	Y	X	Negative	.04421 "
12.	Accel.	Y	X	Positive	.03275 "
13.	Accel.	Y	Z	Negative	.03896 "
14.	Accel.	Y	Z	Positive	.03872 "
15.	Accel.	Z	X	Negative	.11700 "
16.	Accel.	Z	X	Positive	.11195 "
17.	Accel.	Z	Y	Negative	.10895 "
18.	Accel.	Z	Y	Positive	.11988 "
19.	Gyro	Y	X	Negative	.00148 deg./hr./PPM
20.	Gyro	Y	X	Positive	.00156 "
21.	Gyro	Z	X	Negative	.00071 "
22.	Gyro	Z	X	Positive	.00076 "
23.	Gyro	Z	Y	Negative	.00069 "
24.	Gyro	Z	Y	Positive	.00081 "

Table 5.3-6

SUMMARY OF ALL POSSIBLE WHEEL RETAINER RESONANCE ERRORS

Case #	Axis of Linear Vibration	Type Error Coefficient	Resulting Error (deg./hr.
1.	X	Input Axis	-.00006
2.	X	Spin Axis	-.00020
3.	X	Output Axis	.00017
4.	Y	InputAxis	-.00007
5.	Y	Spin Axis	-.00036
6.	Y	Output Axis	.00022
7.	Z	Input Axis	-.00067
8.	Z	Spin Axis	-.00191
9.	Z	OutputAxis	.00176
10.	X and Y	Spin and Input Axis	-.00039
11.	X and Y	Spin and Output Axis	.00013
12.	X and Y	Input and Output Axis	-.00004
13.	X and Z	Spin and Input Axis	.00119
14.	X and Z	Spin and Output Axis	.00282
15.	X and Z	Input and Output Axis	-.00118
16.	Y and Z	Spin and Input Axis	-.00101
17.	Y and Z	Spin and Output Axis	.00238
18.	Y and Z	Input and Output Axis	-.00096

Table 5.3-7

SUMMARY OF ALL POSSIBLE LOOP DEPENDENT RECTIFICATION ERRORS

Case	Envr. Axis	(Spin-Input, Spin-Output, and Anisoinertia Error -Deg./hr.) SI-CO	SI-QU	AI-CO	AI-QU	Total SI	SO-CO	SO-QU	Total SO
1.	X and Y	-.00012	.00174	.00987	.00139	.01289	.00094	.00053	00040
2.	X and Z	.00164	.00052	.01088	.00004	.01204	.00037	.00032	00004
3.	Y and Z	.00102	.00147	.01054	.00004	.01014	.00131	00073	00204

		(Vibropendulous Error - μg) V-CO	V-QU	Total V
1.	X and Y	.0692	.1167	.1860
2.	X and Z	.5006	.0012	.5019
	Y and Z	.4056	.2806	.6863

TABLE 5.3-8

Steady State Error Coefficients

GYRO LOOP			
1)	Spin-Input Coupling	-0.0006	$(deg/hr)/(deg/sec)^2_{IA-SA}$
2)	Anisoinertia	-0.0012	$(deg/hr)/(deg/sec)^2_{IA-SA}$
3)	Anisoelastic - Major	0.12	$(deg/hr)/(g)^2_{IA-SA}$
4)	Anisoelastic - Minor	0.01	$(deg/hr)/(g)^2_{OA-SA}$
ACCELEROMETER LOOP			
1)	Input - Pendulcus Coupling	32	$(\mu g)/(g)^2_{IA-PA}$
2)	Anisoinertia	3	$(\mu g)/(deg/sec)^2_{IA-PA}$
3)	Non-Linear g^2	10	$(\mu g)/(g)^2_{IA}$